PhD-FSTM-2025-097

Faculty of Science, Technology and Medicine

DISSERTATION

Defence held on 19 September 2025 in Luxembourg

to obtain the degree of

DOCTEUR DE L'UNIVERSITÉ DU LUXEMBOURG
EN INFORMATIQUE

by

Teweldebrhan Mezgebo Kebedew
Born on 21 April 1987 in Bizet (Ethiopia)

QUALITY OF EXPERIENCE AWARE DYNAMIC RESOURCE ALLOCATION FOR NEXT GENERATION SATELLITE NETWORKS

Dissertation defence committee

Dr. Eva Lagunas, Dissertation Supervisor
Assistant Professor, University of Luxembourg
Dr. Björn Ottersten, Chairman
Professor, University of Luxembourg
Dr. Symeon Chatzinotas, Member
Professor, University of Luxembourg
Dr. Mauro De Sanctis, Member
Professor, University Tor Vergata, Rome, Italy
Dr. Joel Grotz, Member
Senior Manager, SES S.A., Luxembourg

Quality of Experience Aware Dynamic Resource Allocation for Next Generation Satellite Networks

Teweldebrhan Mezgebo Kebedew

Abstract

With the growing integration of 5G technologies, satellite communication (SatCom) networks, particularly next-generation geostationary (GEO) multi-beam systems, have been increasingly designed to support a wide range of 5G applications and services. This evolution, often based on High-Throughput Satellite (HTS) architectures and increasingly incorporating AI-enabled dynamic management strategies, is driven not only by the technical potential of SatCom to extend connectivity but also by intense market competition. In such a competitive landscape, it is often economically impractical for service providers to deploy their own dedicated satellites for each service category. Consequently, they rely on renting capacity (Mbts) from satellite operators, which introduces the need for efficient and responsive resource allocation mechanisms. In this context, dynamic, Quality of Experience (QoE) aware allocation strategies are critical to manage the limited satellite capacity across heterogeneous service demands efficiently. This approach seeks a well-balanced outcome: maximizing operator revenue, minimizing service provider costs, and enhancing end-user QoE.

However, this model is constrained by limited satellite capacity and the stringent QoE requirements of end users, which vary significantly across services. Accurate modeling of QoE remains a fundamental challenge, especially in the face of dynamic, time-varying traffic patterns that are unpredictable and not known in advance. Different services exhibit diverse packet inter-arrival time distributions, further complicating resource allocation. Furthermore, multiple services often coexist and compete for resources within the same satellite beam, generating fluctuating and conflicting demands. These challenges underscore the critical need for online, adaptive, and QoE-aware capacity allocation strategies that can operate effectively under uncertainty.

To address capacity limitations more effectively, satellite operators need to enhance their available capacity by exploiting various options, including utilizing Extremely High-Frequency (EHF) bands. However, resource allocation, traffic steering, and load balancing in multi-

gateway, multi-beam SatCom networks, particularly in the EHF bands (Ka, Q, and V) face critical challenges due to unpredictable rain attenuation, dynamic traffic variations, and stringent QoE requirements.

In response to these challenges, this thesis develops QoE-aware dynamic capacity management strategies for multi-beam, multi-service SatCom networks. The aim is to design flexible and proactive policies for online capacity and traffic management, accounting for the diverse service requirements, stochastic traffic behavior, and environmental uncertainties. To this end, we incorporate traffic demand forecasting and rain attenuation prediction techniques to enable intelligent traffic steering, load balancing, and resource provisioning across beams and gateways.

Chapter 2 presents a QoE-aware, cost-minimizing dynamic capacity renting framework tailored for Satellite-as-a-Service (SaaS) enabled multi-beam SatCom systems. This model is designed to minimize the rental costs of satellite service providers, considering the time-varying traffic demand while simultaneously ensuring the QoE and blocking probability requirements of diverse services. Our study models the QoE stochastically based on the transmission waiting time of data packets in the system buffer, with a defined target threshold and an allowable violation probability.

In Chapter 3, we address the limitation of uniform traffic models by developing a more general, flexible capacity allocation policy that accommodates multiple services with varying packet inter-arrival distributions and QoE expectations. In addition, to prioritize critical services, our model includes service prioritization during congestion. This model utilizes advanced Deep Reinforcement Learning (DRL) techniques to learn and adapt optimal policies in real time.

Finally, Chapter 4 addresses the challenges of traffic and feeder link capacity management in EHF bands. We propose a predictive framework for proactive beam traffic to gateway matching, incorporating both traffic demand forecasting and rain attenuation prediction to enable robust load balancing and improved resource utilization.

Preface

This Ph.D. thesis has been conducted from December, 2021 to September, 2025 at the Interdisciplinary Centre for Security, Reliability and Trust (SnT), University of Luxembourg, Luxembourg, under the supervision of Prof. Eva Lagunas at SnT, University of Luxembourg, Luxembourg. Additionally, the Ph.D. thesis was co-supervised by Dr. Vu Nguyen Ha, and Prof. Symeon Chatzinotas at SnT, University of Luxembourg, Luxembourg. Furthermore, this thesis was carried out in collaboration with Dr. Joel Grotz from Société Européenne des Satellites (SES S.A.), Luxembourg.

Contents

This Ph.D. thesis, titled "QoE-Aware Dynamic Resource Allocation in Next Generation Satellite Networks", is structured into five chapters. Chapter 1 provides an introduction and background on satellite networks, time-varying traffic demand, QoE modeling, and resource allocation. It also outlines the motivation for the research and formulates the key research questions. Chapter 2 proposes a QoE-aware, cost-minimizing dynamic capacity allocation framework for multi-beam, multi-service SatCom systems. Chapter 3 builds on the work in Chapter 2 by incorporating multiple services with different inter-arrival time distributions and distinct QoE requirements, while also introducing service prioritization. Chapter 4 presents a proactive beam traffic-to-gateway matching approach with load balancing for EHF bands, taking into account both traffic demand forecasting and rain attenuation prediction. Finally, Chapter 5 offers concluding remarks, a summary of the contributions, and potential directions for future research.

Collaborations

This work was done through collaboration with SES S.A. However, the views expressed in this work are those of the author and do not necessarily reflect those of SES S.A.

Support of the Thesis

This work has been supported by the Luxembourg National Research Fund (FNR) under the project INSTRUCT (IPBG19/14016225/INSTRUCT). Additionally, the substantial support from SIGCOM is gratefully acknowledged.

Declaration

Except where acknowledged, the work presented in this thesis is entirely original and has not been submitted, either in whole or in part, for a degree at any other university.

Publication List

Journals

- T. Mezgebo-Kebedew, V.N. Ha, E. Lagunas, J. Grotz, S. Chatzinotas, "QoE-Aware Cost-Minimizing Bandwidth Renting for Satellite-as-a-Service enabled Multiple-Beam SATCOM Systems", IEEE Transactions on Communications, Nov 2023.
- T. Mezgebo-Kebedew, D.D. Tran, V.N. Ha, E. Lagunas, J. Grotz, S. Chatzinotas, "QoE-Aware Flexible Capacity Allocation Planning for Multi-Service Satellite Communication Systems", IEEE Transactions on Vehicular Technology, Aug 2025.
- T. Mezgebo-Kebedew, V.N. Ha, E. Lagunas, D.D. Tran, J. Grotz, J.B. Mariotte, S. Chatzinotas, "Data-Driven Beam-to-Gateway Matching and Adaptive Load Balancing for Multi-beam GEO Satellite Systems", submitted to Open Journal of Communication (IEEE OJCOM).

Conferences/Workshops

- T. Mezgebo-Kebedew, V.N. Ha, E. Lagunas, J. Grotz, S. Chatzinotas, "QoE-Oriented Resource Allocation Design Coping with Time Varying Demands in Wireless Communication Networks", IEEE Vehicular Technology Conference (VTC2022-Fall), Beijing/London, Sept. 2022.

- T. Mezgebo-Kebedew, V.N. Ha, E. Lagunas, D. Dung-Tran, J. Grotz, S. Chatzinotas, "Reinforcement Learning for QoE-Oriented Flexible Bandwidth Allocation Design in Wireless Communication Networks", IEEE Globecom Workshops (GC Wkshps): Workshop on Cellular UAV and Satellite Communications 2023, 4-8 December, Malaysia.

Acknowledgments

Firstly, I would like to thank my supervisor, Prof. Eva Lagunas, for her exceptional guidance, unwavering support, and invaluable assistance throughout my research journey. Her insightful advice, motivation, and dedication have been instrumental in shaping this work. I am profoundly grateful for the time and effort she invested in mentoring me, and for her encouragement during the challenging times I have faced. I also need to extend my heartfelt thanks to Dr.Vu Nguyen Ha for his invaluable technical assistance. His expertise and support were crucial in overcoming challenges during my PhD journey. Without this help, this research would have been significantly more difficult. I deeply appreciate his time, guidance, and the knowledge he shared, which greatly contributed to the success of this work. I would also like to express my deepest gratitude to Prof. Symeon Chatzinotas, Dr. Joel Grotz, and Dr. Duc Dung Tran for their collaborative efforts and invaluable contributions to the research presented in this thesis. Their expertise and insights have been instrumental in enhancing the quality of this work.

Teweldebrhan Mezgebo Kebedew

Luxembourg, October 11, 2025

Contents

List of Figures

List of Tables

Abbreviations

5G	Fifth Generation
6G	Sixth Generation
ACO	Ant Colony Optimization
AGA	Adaptive Genetic Algorithm
BP	Blocking Probability
B2G	Beam to gateway Matching
CA	Capacity Allocation
CDF	Cumulative Distribution Function
CTMC	Continuous Time Markov Chain
D3QN	Dueling Double Deep Q-Network
dB	Decibel
DCA	Dynamic Capacity Allocation
DDQN	Double Deep Q-Network
DQN	Deep Q-Network
DRL	Deep Reinforcement Learning
EHF	Extremely High Frequency
FCFS	First-come-first-served
GA	Genetic Algorithm
GEO	Geostationary Earth Orbit
MILP	Mixed Integer Linear Programming Problem
IAT	Inter-arrival Time
ISA	Iterative Staffing Algorithm
ISL	Inter Satellite Link
ISTN	Integrated Satellite-Terrestrial Networks
ITU	International Telecommunication Union

IoT	Internet of Thing
LB	Load Balance
LEO	Low Earth Orbit
LSTM	Long Short Term Memory
MAC	Medium Access Control
MILP	Mixed-Integer Linear Programming
ML	Machine Learning
MEO	Medium Earth Orbit
MOS	Mean Opinion Score
NMC	Network Management Center
NGSO	Non-geostationary Satellite Systems
NN	Neural Networks
OPEX	Operational Expenditure
PDCP	Packet Data Convergence Protocol
PMF	Probability Mass Function
QL	Queuing Length
QoE	Quality of Experience
QoS	Quality of Service
RL	Reinforcement Learning
RNN	Recurrent Neural Networks
RQ	Research Question
RRC	Radio Resource Control
RLC	Radio Link Control
SaaS	Satellite-as-a-Service
SatCom	Satellite Communication
SDAP	Service Data Adaptation Protocol
SLA	Service Level Agreement
SNR	Signal to Noise Ratio
SOTA	State-of-the-Art
SP	Satellite Service Providers
TS	Time Slot

Notations

$\log(z)$	The natural logarithm of z.
$\arg\max Z$	Index of the maximum values of a vector Z.
e^z	Exponential function of z.
$\mathbb{E}[\cdot]$	Expected value.
$\lceil \cdot \rceil$	Ceiling function.
$\boldsymbol{b}^{\mathbf{T}}, \boldsymbol{B}^{\mathbf{T}}$	Transpose of vector $\boldsymbol{b}$, transpose of matrix $\boldsymbol{B}$.
$\lvert z \rvert$	The absolute value of z.
$\lVert \boldsymbol{b} \rVert$	The norm of vector $\boldsymbol{b}$.
max	Maximum operation.
min	Minimum operation.
$z \in \mathcal{Z}$	Element z belongs to set $\mathcal{Z}$.
$\frac{\partial Z(t)}{\partial t}$	Partial derivative of $Z(t)$ with respect to t.

Chapter 1

Introduction

In today's hyper-connected world, SatCom systems play a critical role in enabling global connectivity and supporting diverse applications that demand high availability, resilience, and service quality, especially in remote and underserved regions. The demand for satellite services is growing rapidly and becoming increasingly dynamic due to a surge in users and the diversity of service types [1], [2]. To meet these evolving needs, satellites across all orbital regimes, such as GEO, MEO, and LEO, are increasingly being integrated into the 5G ecosystem to extend coverage and support next-generation applications and services.

1.1 Satellite Networks Architecture

The SatCom network architecture can be broadly classified into transparent and regenerative satellite systems, each with distinct roles in data processing, protocol handling, and traffic management [3]. As illustrated in Fig. 1.1, when a user requests a service (downlink), the requested data typically originates from the Internet or a centralized core network. This content is routed through the satellite network, where it is delivered via a feeder link to the satellite and then forwarded to the user terminal over the user link. The specific handling of this data—whether processed onboard the satellite or managed entirely on the ground—depends on the underlying satellite architecture.

Transparent satellites act as passive relays: they amplify and forward RF signals between the user terminal and the ground segment. Consequently, all protocol processing, including Radio Resource Control (RRC), Packet Data Convergence Protocol (PDCP), Radio Link Control (RLC), and Medium Access Control (MAC), is performed at the terrestrial gateway

(GW), where packet queues are maintained, resource allocation decisions are made, and traffic is prioritized based on operator policies [4]. In contrast, regenerative satellites incorporate onboard processing capabilities [4]. This enables the satellite to act as an intelligent network node, such as an onboard gNB, with the ability to locally schedule resources, maintain packet queues, and dynamically allocate capacity based on real-time traffic demands and user priorities. As a result, regenerative satellites can achieve lower latency and more flexible bandwidth utilization, particularly in highly dynamic or delay-sensitive scenarios. However, they are also constrained by limited onboard computational and energy resources, which can affect their ability to scale or support complex scheduling algorithms. In addition, both architectures must cope with challenges such as time-varying traffic demand, limited and shared spectrum resources, the need for real-time adaptation, and the need to maintain consistent and uninterrupted QoE.

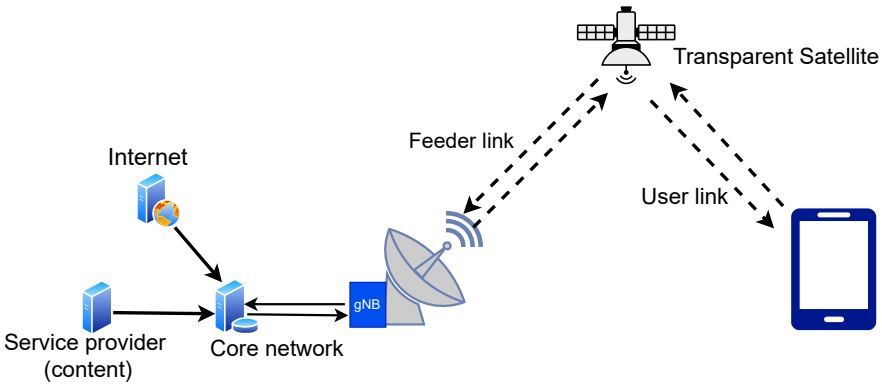

(a) Transparent satellite.

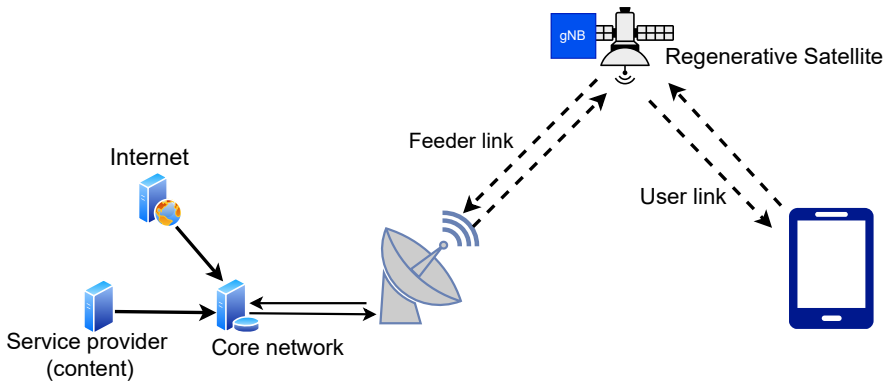

(b) Regenerative satellite.

Figure 1.1: Generic satellite architecture.

Therefore, regardless of the architecture, the deployment of an intelligent, QoE-aware

dynamic resource allocation mechanism is critical to optimize traffic flow, prevent congestion, and ensure service quality under heterogeneous and unpredictable network conditions.

1.2 Time-varying Traffic Demand

With the advancements of 5G and next generation SatCom networks and the continuous evolution of their application scenarios, massive traffic data is being generated from different applications and services [5,6]. Different services induce significantly different traffic volumes and temporal characteristics. For example, video streaming applications typically produce sustained high-throughput traffic, while massive machine-type communications (MTC) or IoT devices generate short, intermittent bursts. Moreover, the number of concurrently active users accessing these services fluctuates over time, influenced by diurnal patterns, user mobility, and regional demands. This variation in user access leads to time-varying traffic, which can exhibit highly volatile characteristics over different intervals. Traffic demand can be conceptualized as a flow of packets transmitted over time. Each service typically generates a sequence of packets with service-specific characteristics such as packet size, inter-arrival times, and burstiness. When the same service is accessed by multiple users simultaneously, the resulting traffic can be aggregated into a flow of packets with an effective arrival rate.

The temporal distribution of traffic—particularly the diversity in packet arrival patterns reflected by varying inter-arrival time distributions—plays a critical role in modeling demand variability. For example, certain services follow a Poisson arrival process, while others exhibit heavy-tailed or bursty behavior, which is better modeled using distributions such as the Weibull or Pareto distributions. The heterogeneity in these distributions across different services complicates the modeling of traffic variability and burstiness [7, 8].

Additionally, the spatial distribution of traffic across satellite beam coverage regions is far from uniform. Traffic demand differs significantly between beams, driven by variations in population density, user activity patterns, and service subscriptions. This spatial disparity is particularly pronounced in GEO satellite systems due to their fixed coverage areas and limited beam reconfiguration capability. In contrast, non-geostationary (NGSO) constellations—with their moving beams and dynamic footprint tend to experience more evenly distributed traffic patterns, although still subject to regional hot-spots [10].

As shown in Fig. 1.2, the heterogeneous nature of 5G service traffic, characterized by

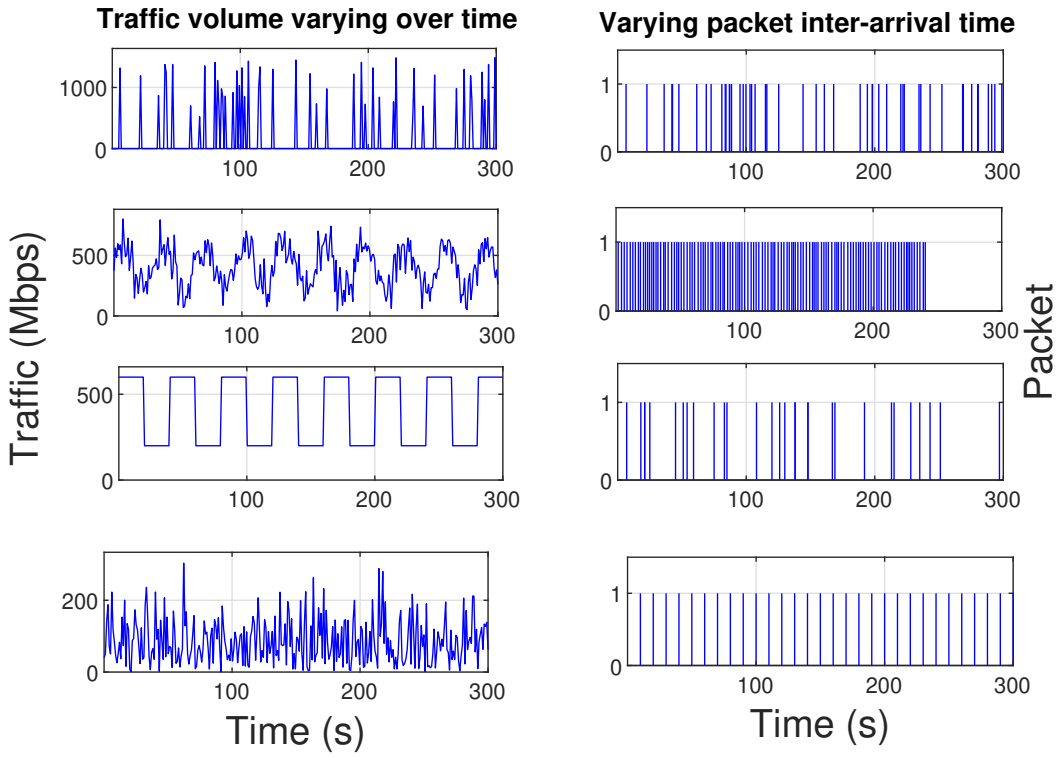

Figure 1.2: Demand over time and inter-arrival distribution variation demonstration plot [9].

varying volumes and diverse inter-arrival distributions, necessitates precise modeling of traffic variability, which is essential for maintaining and accurately estimating QoE.

1.3 Quality of Experience

The emergence of various services has introduced new challenges, intensified competition among network satellite operators, and heightened user expectations for network services. As a result, QoE has become a primary design objective in next-generation satellite networks, serving as a critical metric for quantifying user satisfaction [11–13]. In practice, QoE is often incorporated within Service Level Agreements (SLAs), which formally define the minimum service quality that must be ensured.

In the context of multi-service networks, relying on aggregate or average QoE across services can obscure critical performance bottlenecks. Since different applications have distinct QoE sensitivity, it is essential to fulfill QoE in a service-specific manner [13]. To meet the performance demands of these advanced applications, QoE must be accurately estimated.

1.3.1 QoE Estimation

Traditionally, QoE estimation was conducted through user surveys, where users are asked about their satisfaction with the application or service they use. They indicate their satisfaction on a scale of 1 to 5. The opinions are then averaged to obtain a mean opinion score (MOS) [13], [14].

State-of-the-art methods commonly use the MOS as a standard metric for QoE estimation. However, the basic MOS approach may not accurately capture QoE, as it relies on users' subjective expectations of fulfilling certain requirements [11, 15]. It is also costly, time-consuming, and impractical for large-scale environments due to the extensive number of participants required for the experiment [16].

MOS, primarily designed for human-centric services like voice and video, is insufficient for emerging 5G use cases such as massive MTC, where the end-users are often machines rather than humans. These applications necessitate a redefined QoE paradigm that accurately reflects the performance and reliability expectations of both human and machine users. Consequently, network design and performance evaluation must evolve to incorporate these new QoE assessment models, ensuring that future networks can effectively support the diverse and stringent requirements of next-generation applications.

Alternatively, for continuous, consistent, and large-scale monitoring without the need for constant human input, objective QoE estimation is applied [17]. The objective QoE estimation is more important in 5G and beyond networks to enable real-time monitoring and dynamic adaptation of network resources. Furthermore, the time-varying and uncertain traffic demand and available resources necessitate the consideration of advanced QoE estimation techniques [12, 15].

1.4 Satellite Stackholders

Satellite stakeholders are entities that have a direct or indirect interest, investment, or role in the operation, development, or use of satellite resources. Although there are several stakeholders [18], they can be broadly categorized as follows,

- Satellite Operators: These are the infrastructure owners who manage and control the satellites in orbit and the satellite resources in general.

- Service Providers (SPs): These entities utilize the satellite infrastructure to deliver communication services to their customers.
- Customers: These are the beneficiaries of services for various applications.

Each of these stakeholders has distinct interests. Satellite operators aim to maximize their revenue by renting their available resources to as many SPs as possible. Conversely, SPs seek to minimize rental costs, and customers prioritize obtaining a high QoE [19].

Traditionally, satellite operators managed both the infrastructure and service delivery, providing direct services to end-users. For SPs to extend their reach and adapt to rapidly changing markets due to the rising number of services, they are expected to make substantial investments in network infrastructure and advanced satellite technology. However, the escalating costs associated with launching and maintaining satellite infrastructure have prompted a shift in this business model. Satellite SPs, facing prohibitive infrastructure expenses, have found it unfeasible to deploy their own satellites for each service offered to customers. This economic challenge has led to the emergence of the Satellite-as-a-Service (SaaS) model [20,21]. Under this paradigm, satellite operators lease resources to SPs based on predefined SLAs. SaaS is increasingly seen as the future for major operators like SES and Eutelsat. This model allows for more flexible, efficient, and cost-effective use of resources, allowing operators to better meet the growing and dynamic traffic demands of users in the market [20], [22]. unless the static renting contracts that involve fixed bandwidth allocations and regular payments, the SaaS enabled dynamic renting contracts require operators to adapt to varying traffic volumes and QoE requirements, complicating resource planning. Dynamic contracts necessitate estimating resource needs, risking either wasted resources or unmet commitments if overbooking is used.

1.5 Satellite Capacity Allocation

In early satellite systems, capacity allocation (CA) was static, with resources such as bandwidth and power pre-assigned to specific users or services and remaining fixed. However, as the number of users and traffic demand vary, this static allocation results in under-utilization of capacity during low-demand periods and congestion during peak hours.

To address these inefficiencies, Dynamic CA (DCA) has emerged as a key mechanism in modern SatCom systems. DCA enables the adaptive allocation of satellite capacity based on

real-time traffic demands, QoS, and QoE requirements. Given the inherently time-varying nature of traffic, satellite systems must contend with periods of underload (off-peak traffic) as well as overload (peak-traffic), where demand exceeds available capacity. During peak traffic, operators prioritize services based on business criteria and may not admit all traffic requests at a time.

The responsiveness of the DCA mechanism is critical. Faster adaptation allows the system to allocate resources more effectively, thereby improving capacity utilization. Conversely, slower adaptation leads to inefficiencies in CA and possible degradation in service quality [10]. Therefore, designing effective admission and adaptation policies is crucial for optimizing satellite resource use and enhancing network performance. Critical design parameters influencing CA decisions include:

- Rate of Capacity Adaptation: Determining the frequency of capacity adjustments (e.g., every 5 minutes, 10 minutes, hourly, or daily) involves a trade-off between monitoring complexity and resource allocation efficiency.
- Target QoE Requirements: Ensuring that QoE metrics are met and managing the trade-off between capacity and target QoE requirements involves continuously monitoring network conditions and dynamically adjusting capacity.
- Target Blocking Probability (BP): Setting acceptable levels of BP ensures that the system can handle incoming traffic without excessive packet loss, thereby maintaining service reliability.

Operators must design their CA models with these performance indicators in mind to optimize resource utilization and ensure service quality, ultimately contributing to revenue optimization. Additionally, the advancement of key enabling technologies such as digital transparent payload systems lead to a dynamic and adaptable CA.

1.5.1 Data Packets Queuing Techniques

When users request access to a particular service, they are effectively initiating a demand for a specific volume of data to be transmitted either from the internet or a content server through the satellite GW. To minimize the transmission overhead and ensure efficient handling, data from various applications is aggregated into flows of packets. These flows are managed by the network to support smooth and reliable delivery. However, due to limited transmission

capacity, incoming packets cannot always be processed and forwarded immediately upon arrival. As a result, packets are temporarily stored in a queue within the satellite's buffer system, awaiting transmission.

(a) Static queue model. (b) Time-varying queue model.

Figure 1.3: Static versus time-varying queuing.

Queue Length (QL) is a widely adopted measure of congestion and queuing delay, which directly impacts perceived latency and throughput, both critical components of overall system performance and QoE [23]. In general, a longer QL returns a higher network congestion probability and a longer service time that the users may suffer because the data spends more time in the buffer before being processed and transmitted. As the QL approaches the system's maximum buffer size, the QoE deteriorates due to increased waiting times. In critical scenarios, this may lead to buffer overflow, resulting in packet blocking and potential packet loss. To cope with such an issue and conserve the required QoE, one demands a higher allocated resource to increase the service rate. On another hand, letting the system operate with very short queuing lengths may imply that an over-needed amount of resources is allocated.

There exists a wide range of queuing techniques in the literature. Due to the highly dynamic nature of 5G traffic that can vary significantly due to factors like user mobility, diverse service requirements, and varying network conditions, the commonly used queuing models like $M/M/1$ and $G/G/1$ can not fully capture the complexities of the queuing analysis [24], [25]. To estimate the congestion and queuing delay more accurately, we need to consider advanced queuing models that could be suitable for time-varying arrival and service rates.

1.5.2 Optimization Techniques

Optimization techniques play a central role in enabling objective-driven decision-making in dynamic resource allocation. They offer mathematically rigorous and systematic frameworks to make efficient, fair, and reliable resource allocation under multiple system-level constraints. These techniques are particularly effective at handling complex constraints, such as capacity limits, QoE requirements, traffic dynamics, and environmental impairments.

Conventional optimization approaches, such as linear programming, convex optimization, and integer programming, often come with provable guarantees of optimality and convergence, making them highly reliable for structured and well-defined problems [26]. Additionally, Lagrangian duality—discussed in detail in Chapter 2—is a powerful technique for handling large-scale optimization problems with coupling constraints. When the underlying problem is convex, this method enables distributed solution of decomposed subproblems while ensuring global optimality under strong duality.

For non-convex problems, especially those involving integer or combinatorial variables, global optimality is harder to achieve due to the presence of multiple local minima. However, exact methods such as the Branch and Bound (B&B) algorithm can still guarantee globally optimal solutions by systematically exploring the solution space while pruning suboptimal branches. As detailed in Chapter 4 of this thesis, while B&B is a powerful method for solving non-convex mixed-integer linear (MILP) programs, it becomes computationally prohibitive for large-scale problems due to its exhaustive search nature. In such cases, heuristic and metaheuristic techniques, such as genetic algorithms and ant colony optimization, can offer near-optimal solutions with significantly lower computational overhead [27], [28].

However, these conventional techniques may become less effective when dealing with:

- Very large or high-dimensional solution spaces.
- Highly dynamic systems with time-varying conditions.
- Poorly modeled or uncertain constraints.

In such cases, optimization problems become difficult to formulate explicitly or solve in real time. Artificial Intelligence (AI) and Machine Learning (ML) models are well-suited for these scenarios [29–31].

1.5.3 Artificial Intelligence and Machine Learning

The rapid advancement of 5G networks, along with the growing complexity of management, traffic handling, and dynamic service demands, highlights the need for more intelligent resource optimization techniques. AI, particularly ML techniques, is becoming indispensable to advance resource optimization and facilitate smarter, adaptive decisions in resource allocation [29]. Unlike traditional mathematical model-based approaches, AI utilizes a data-driven

framework to dynamically allocate resources by continuously learning from the network environment. This approach provides insights into demand and available capacity over time, enabling more efficient and adaptive resource management.

Data-Driven Models

Resource allocation becomes more efficient when guided by accurate traffic and channel condition predictions [32], [33]. To achieve this, operators must anticipate user traffic demands and environmental impairments such as rain attenuation. This requires maintaining spatio-temporal historical data, including traffic patterns and weather events, which can support predictive models for future resource planning. As detailed in Chapter 4 of the thesis, techniques such as time series forecasting, including LSTM networks, are commonly used for this purpose.

Nevertheless, prediction alone is not sufficient for optimal performance in highly dynamic and uncertain environments. Satellite systems must also be able to respond rapidly to unanticipated fluctuations. The next section explores how Deep Reinforcement Learning (DRL) can be leveraged to enable such adaptive and QoE-aware resource allocation policies.

Deep Reinforcement Learning

RL is a ML approach that allows an agent to reach a specific objective by maximizing long-term rewards through trial-and-error interactions with its environment [34, 35]. The agent is the resource manager that can be located at the satellite GW or onboard the satellite, depending on the satellite architecture. It interacts with the network environment by choosing actions from its available action space based on its current state. Each action results in a corresponding reward and a transition to a new state. This process is repeated until the agent's learning process converges to an optimal policy, maximizing the average reward [35, 36]. In the context of multi-beam SatCom systems, DRL offers a powerful solution for DCA by learning to adaptively allocate resources based on fluctuating user demand, environmental conditions, and service-level QoE requirements. Unlike rule-based or static optimization approaches, DRL can operate in real-time, handle high-dimensional state-action spaces, and generalize across different network scenarios [29]. This makes it well-suited to address the inherent uncertainties and heterogeneity in traffic patterns and service types, ultimately enabling efficient and QoE-centric resource management. Several efficient DRL algorithms

exist, among which Deep Q-Networks (DQN), Double DQN (DDQN), and Dueling Double DQN (D3QN) have been widely adopted and demonstrated to be particularly effective. The detailed implementation is discussed in Chapter 3 of this thesis.

1.6 Motivation

The SatCom industry is undergoing rapid transformation. Well-known satellite operators such as SES, Intelsat, Inmarsat, Airbus, and Viasat are now competing with emerging broadband SPs like SpaceX and Eutelsat for global market share [18]. Despite a 29% increase in overall satellite broadband revenue and a 46% growth in subscriptions in 2024 [37], several operators reported revenue declines. This apparent paradox is driven by intensifying market competition, the rising influence of Over-the-Top (OTT) streaming platforms, and the commoditization of satellite capacity through wholesale business models [38, 39].

Concurrently, the SaaS market is projected to expand significantly, from USD $5.87 billion in 2025 to USD $21.42 billion by 2034 [40]. This growth is fueled by increased demand for satellite connectivity across industries such as agriculture, disaster management, remote sensing, and maritime operations. In this evolving ecosystem, satellite operators face growing pressure to deliver high QoE while minimizing operational costs and responding to dynamic, heterogeneous traffic demands.

Traditional CA techniques, often based on static provisioning, are insufficient in this context. Satellite networks are inherently constrained by limited spectrum, high latency, and susceptibility to environmental disturbances like rain attenuation. These challenges are further compounded by the unpredictable and time-varying nature of user traffic. Moreover, accurately modeling QoE remains difficult due to the complexity of user behavior and diverse application requirements.

To remain competitive and profitable, satcom SPs must adopt intelligent resource allocation frameworks that strike an optimal balance among capacity utilization, capacity leasing costs, and user-perceived quality (see Fig. 1.4). This necessitates novel, QoE-aware approaches that can dynamically allocate network capacity while adapting to fluctuating traffic patterns and uncertain channel conditions.

This thesis is motivated by the urgent need to develop a dynamic, QoE-centric CA framework that can handle the inherent uncertainties of traffic demand and environmen-

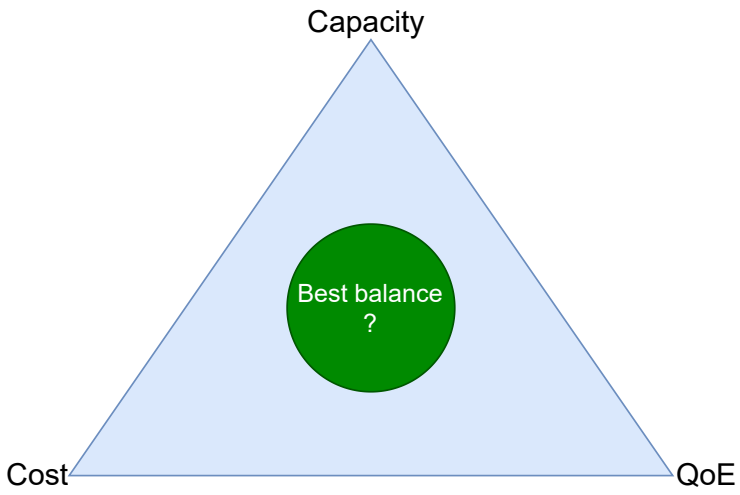

Figure 1.4: Capacity, cost, and QoE tradeoff in satellite networks.

tal impairments in satellite networks. Specifically, we aim to design scalable optimization techniques that incorporate predictive QoE modeling, environmental awareness, and cost-efficiency, thereby supporting sustainable satellite operations in a highly competitive and service-oriented market.

1.7 Research Questions

Building on a detailed understanding of the limitations of current dynamic resource allocation techniques, as well as the challenges posed by HTS communications and the transmission of large, time-varying volumes of data to users, this thesis explores the following research questions to develop novel methods for QoE-aware DCA in multi-beam, multi-service SatCom systems.

Question 1: How can we design a cost-minimizing DCA method for next-generation HTS systems, aimed at minimizing the capacity required to meet target QoE and BP requirements?

Satellite operators need to develop a flexible, cost-efficient CA strategy that allows them to maximize revenue by leasing their available capacity to as many SPs as possible. This can be achieved through a cost-effective (cost-minimizing) capacity renting mechanism that ensures the QoE requirements of end-users. Finding the optimal balance between operators' revenue, SPs' rental costs, and users' QoE requirements is a crucial research

question.

Question 2: How can we design a flexible CA policy for multiple services, each characterized by distinct inter-arrival distributions and unique QoE requirements?

Operators must design a QoE-aware DCA policy capable of accommodating the demands of multiple services, each with different QoE requirements and distinct packet inter-arrival patterns. In cases of limited capacity, the allocation strategy must prioritize services based on their priority levels. Designing a DCA policy that accommodates multiple services, each with distinct QoE requirements and different packet arrival times, is an interesting research question that needs to be addressed.

Question 3: How can we design a proactive beam traffic-to-GW (B2G) matching strategy when traffic demand and rain attenuation are not known in advance?

The utilization of EHF band SatCom systems is complicated by the unpredictability of both traffic demand and rain attenuation levels, as these factors directly affect the capacity of the GW to satellite feeder links. Therefore, satellite operators must develop a proactive and optimal B2G matching mechanism to minimize service outages and packet loss.

1.8 Contributions

The main contribution of this PhD thesis is distributed among the chapters 2, 3, and 4 that are given below:

1. Chapter 2: Traditional satellite capacity leasing lacks the flexibility needed to efficiently support 5G-NTN networks, which involve multiple services with highly dynamic traffic demands. Satellite operators not only face the challenge of adapting to this variability but must also minimize the costs incurred by SPs renting their capacity, all while meeting stringent QoE requirements. Existing QoE models, often based on subjective user opinions, are not scalable or reliable for such environments. To overcome these limitations, we propose a dynamic, QoE-aware CA model that minimizes rental cost while objectively estimating QoE based on buffer queue lengths. The model ensures

that both stochastic QoE targets and BP constraints are satisfied, benefiting satellite operators, SPs, and end users alike.

2. Chapter 3: In modern satellite and 5G-enabled networks, CA must account for the diverse and dynamic nature of service demands. The primary challenges stem from the need for real-time decision-making under uncertain and rapidly changing traffic conditions, service-specific QoE requirements that are difficult to quantify, and the presence of heterogeneous packet inter-arrival patterns across services. Traditional optimization approaches struggle in such environments due to their static nature and reliance on prior knowledge of traffic patterns. To address these challenges, we propose a DRL-based approach for dynamic and intelligent CA. Specifically, we leverage DDQN to flexibly allocate capacity among multiple services with varying inter-arrival time distributions and distinct QoE expectations. Our model prioritizes more critical flows during congestion, ensuring responsiveness to real-time conditions.

3. Chapter 4: Satellite operators are increasingly turning to EHF bands to expand available capacity [41], [42], [43]. However, these bands are highly susceptible to rain fading, which is both severe and unpredictable—making it a major contributor to service outages. In addition, the time-varying nature of traffic demand, with future demands unknown in advance, often leads to load imbalances across feeder links and quality degradation during peak periods. To address these limitations, we propose a proactive and dynamic B2G traffic matching framework that balances load among feeder links by predicting both rain attenuation and traffic demand in advance.

1.9 Scope and Limitations

This thesis investigates a QoE-aware DCA framework tailored for next-generation satellite networks, with a primary focus on GEO satellites supporting multiple coexisting services with service-specific QoE requirements. The scope is confined to forward link transmission under unpredictably time-varying traffic demands and environmental impairments such as rain fading. The study does not address non-GEO constellations or uplink resource management.

The research methodology includes a comprehensive state-of-the-art review, system modeling, problem formulation, solution design, and performance evaluation. All evaluations are

carried out through analytical modeling and extensive simulations; no real-world satellite experiments or hardware implementations are included.

Chapter 2

QoE-Aware Cost-minimizing Dynamic Capacity Renting

*This chapter is based on work published in **IEEE Transactions on Communications**, vol. 73, no. 3, pp. 1773 - 1789, March 2024.*

2.1 Introduction

SatCom systems are becoming important to provide global connectivity with a wide range of applications requiring high availability and resilience to critical areas that are unreachable by the current terrestrial networks [44, 45]. The growing attention on the dynamic SatCom systems supporting service-aware communications and seamless coverage, as well as its associated implementation costs, has inspired a number of big names in the industry to develop new SaaS business platforms [20,21]. Such a platform comprises satellite operators - the owners of the SatCom systems, and the service SPs which may rent certain satellite capacity from the operators to provide different services to their end users [20,46,47]. This novel paradigm can enable the operators to access new markets and it can release the SPs from investing a huge amount of money in order to build dedicated satellites [48]. Given the unpredictable and time-varying nature of traffic generated by diverse services, the development of flexible and adaptive capacity renting mechanisms is becoming essential for SPs to optimize resource usage while ensuring service-level QoE. This mechanism is expected to allow the SPs to obtain capacity as needed rather than committing to a fixed amount. Such flexibility can boost network utilization, enhance revenue for the operators, and help the SPs save the costs while

ensuring the user QoE [49]. However, to establish such an optimal capacity renting framework between the operators and SPs, one should carefully manage and analyze a vast number of simultaneous data flows, each with distinct QoE requirements [50]. Specifically, the SPs must swiftly make provisions on the required capacity while still guaranteeing the desired QoE for their users. On the SatCom operators side, to realize the DCA mechanism, the advanced digital transparent payloads (DTP) using *"defacto"* platform can be deployed [10,51]. Based on this, the satellites can assign capacity across beams effectively and route traffic of various types efficiently.

To ensure effective network resources renting from the operators, the SPs have to cope with multiple challenges in maximizing their profit [48, 52]. Herein, the business problems at the SPs include (but are not limited to) capacity estimation accommodating the irregular and unpredictable *"time-varying"* data traffic from heterogeneous apps/services, and efficient management of rented resources during both peak and off-peak periods to reduce costs [53,54]. Additionally, maintaining or expanding the customer base is a significant business challenge for both the operators and SPs, and satisfying the diverse QoE requirements of customers is a key point of resource management that should be addressed carefully. Furthermore, the operators and SPs should also establish an agreement detailing the speed of capacity adjustments and the maximum capacity SPs are allowed to use [46, 52].

Consequently, the development of a dynamic, cost-effective, QoE-aware network resource renting mechanism in SatCom systems has emerged as an interesting and compelling research topic for both operators and SPs. Facilitated by the challenging problem, this paper focuses on designing a new QoE-aware cost-minimizing capacity-renting framework in SaaS-enabled multi-beam SatCom systems.

In the realm of wireless communication, the QoE at users can be affected by a variety of factors, ranging from signal strength, data rate consistency, and connection reliability, to service interruptions [55]. Among these aspects, a critical determinant of QoE in the SatCom schemes is the end-to-end latency where extended delay can significantly compromise a user's overall experience. While all QoE issues are essential, reducing the latent period is paramount [55]. It is worth noting that the end-to-end data transmission latency encompasses both the signal propagation delay and the waiting time during which data resides in the system buffer before transmission [56, 57]. However, in SatCom schemes, mitigating the propagation delay poses a formidable challenge due to the Line-of-Sight (LoS) connection

and almost-fixed distances between the satellite and user terminals. This inherent physical limitation demands innovative solutions to ensure consistent and efficient communication, enhancing the overall user experience.

In light of this challenge, our study focuses on addressing the QoE issue by modeling it in terms of the waiting time of data packets in the system buffer. This approach underscores the significance of minimizing delays to improve overall user satisfaction. At a specific time instance, the waiting time of one beam is related to the stochastic queuing length, which can be managed by dynamically allocating the capacity for the data transmission corresponding to this beam when the data arrival rates vary. Then, our work aims to propose a novel dynamic capacity planning model that minimizes the total renting cost of SPs while maintaining a target BP of the system and a target queuing delay requirement of customers.

2.1.1 Related Works

The majority of existing frameworks for SatCom resource allocation have primarily focused on maximizing overall power and spectrum utilization efficiency. Different techniques have been used, such as non-convex optimization for flexible power and capacity assignment [58], beam illumination and selective precoding [59], and joint beam selection and precoding [60]. The work in [58] focused on satellite–user association-oriented to minimize the total uplink transmit power for integrated satellite-terrestrial networks (ISTN). Research on QoE-aware DCA to maximize user satisfaction in Orthogonal Frequency Division Multiple Access (OFDMA) terrestrial networks considering time-varying channels has been conducted [61, 62]. These approaches aim to satisfy the overall demand by improving power, capacity, or both utilization efficiency. However, all previous works consider average beam demand which does not change over time. In addition, the cost of satisfying this demand, the QoE of users, and the amount of system capacity that remains unused is not well-documented in the literature. Other studies have discussed profit opportunities associated with 5G infrastructure dynamic leasing [52] and revenue management in SatCom systems [63].

Previous research has also applied different queue models for end-to-end latency estimation, packet loss minimization, and buffer bloat prevention in various wireless communication systems. For example, the $M/G/1$ queue model has been used to estimate transient QL [64], latency estimation [65–67], the $D/D/K$ queue model for dynamic buffer sizing [68], the $G/G/1$ queuing model for Quality of Service (QoS) analysis [69], and the $M/G/\infty$ queue

model to estimate the minimum required system capacity [70]. While these studies use different queue models to maintain QoS in different wireless systems, they fail to consider the QoE of users and the time-varying nature of average arrival rates.

In other areas, time-varying queue model-based resource allocation has been explored [71]. For example, in [72, 73] the application of different time-varying queue models in large-scale service systems such as customer contact centers and hospital emergency departments is discussed. In these works, iterative staffing algorithms (ISA) are developed to optimize the staff levels at the customer center to satisfy the stochastic waiting time requirement of customers. Herein, the state-of-the-art $M_t/M/S(t)$ queue model is exploited where the M_t indicates time-varying Poisson arrivals, and the $S(t)$ indicates time-varying servers and the M indicates a constant serving capacity of the servers in every staffing interval. Then, an efficient time-varying human-resource-management framework is established by iteratively determining the staff level at a specific time. Similarly, the authors in [24] also employed $M_t/M/S(t)$ to develop a *Deep-Reinforcement-Learning* based framework to optimize the beam-hopping strategy adapting with time-varying data traffic flows coming to the multiple-beam SatCom systems. Next, [25] describes how time-varying $M_t/G/\infty$ queue models can be applied to staffing and capacity planning of cloud services and protective equipment management in hospitals during the outbreak of a disease. All works given in [25, 72, 73] focus on a fixed processing rate at one serve (staff). On a different approach, the changeable processing rate mechanism is studied in [74] where the $M_t/M_t/1$ queue model is used for efficient resource allocation in industrial production by estimating the stochastic probability of the system QL. However, this work mainly focuses on developing the admission control strategy for network-slicing systems. Consequently, there is a very limited number of works considering multiple traffic flows accessing satellite systems as time-varying queue models and exploiting this to develop a QoE-aware dynamic capacity renting and allocation mechanism for the SPs to in multiple-beam SatCom systems. Therefore, the work in this paper aims to fill this gap in the literature.

2.1.2 Contributions

Our paper aims to propose a novel QoE-aware flexible capacity renting framework for SaaS-enabled multiple-beam SatCom systems to effectively manage the renting costs at the SPs. By employing the stochastic queuing theory, we first formulate the problem as a stochastic

optimization problem. This allows us to examine the impact of system and user requirements on the rent cost and the trade-off between them, thereby assisting SPs in predicting the capacity they need to request operators to maintain a satisfied customer base while minimizing rent costs. Our key technical contributions in this article can be summarized as follows:

- First, we express the traffic flows using a time-varying $(M_t/M_t/1)$ queuing model and estimate the stochastic QL of packets waiting in the system by using the continuous-time Markov chain (CTMC). The analysis results are then employed to formulate a stochastic optimization problem for QoE-aware DCA that includes queue status-based dynamic spectrum sharing among adjacent beams of the same cluster to minimize cost. The problem aims to help SPs to be able to efficiently allocate capacity and reduce un-utilized capacity as well as their rent costs.

- Next, we estimate the stochastic BP and the probability of violating the waiting-time requirement over the observation period, which allows SPs to predict the impact of decisions on user experience. We further analyze the trade-off between maintaining user satisfaction and capacity rent cost in SatCom systems will assist SPs in determining the optimal balance between these two objectives, based on which we provide a closed-form solution based on Lagrangian duality making use of the estimated BP.

- For comparison purposes, we introduce a greedy algorithm and modify the ISA frameworks in [72,73] to suit our design requirements. The proposed algorithms are validated through numerical results and Monte Carlo simulations using practical simulation parameters. The numerical and simulation outcomes have effectively confirmed the theoretical soundness of our proposed frameworks.

In summary, our proposed approach is based on the stochastic queuing theory and aims to assist satellite SPs in predicting the capacity they need to maintain a satisfied customer base while minimizing rent costs by using a QoE-aware DCA model.

2.2 System Model and Problem Formulation

We examine a SaaS platform in a multi-beam GEO communication system where the overall available capacity of a GEO satellite is owned by an operator that can be rented by SPs. The

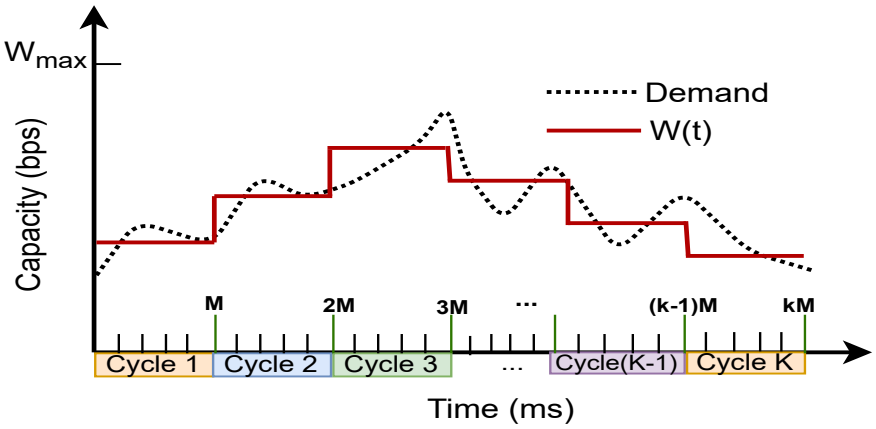

Figure 2.1: Capacity allocation for time-varying demand.

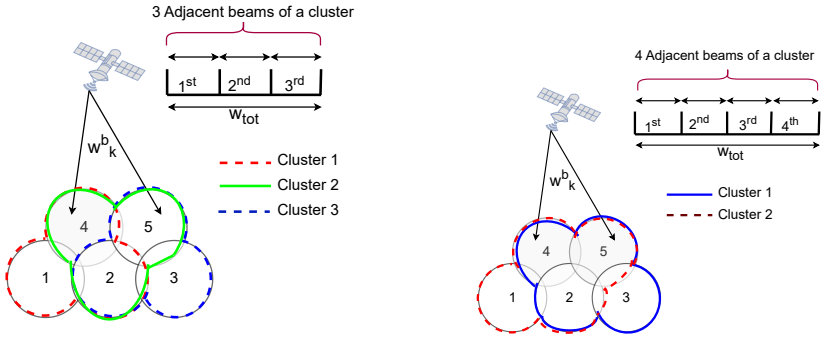

(a) 3 beams per cluster. (b) 4 beams per cluster.

Figure 2.2: The footprints of clusters containing J adjacent beams with non-overlapping frequency.

study focuses on a scenario where a specific SP[1] rents a time-varying amount of capacity from the operator to provide broadband services to multiple users randomly distributed across B beams. Let $W(t)$ (bps) represent the total capacity rented by the SP from operator to serve all traffic flows across all beams. Each beam is assigned a portion of this capacity, denoted by $W^b(t)$, which can range from 0 to $W(t)$, i.e. $0 \leq W^b(t) \leq W(t)$. The network operates in a time-slot manner, with each time slot having a duration of T_{TS} as the transmission time. Due to possible processing speed capability limitations of DTP reconfiguration combined with the consequent signaling through the tracking, telemetry, and command system (TT&C) links [10], it is assumed that $W^b(t)$ remains constant for a cycle duration of M time slots. $W^b(t)$ can only be reset at time-slot indices $t_c \in \{0, M, 2M, ..., kM, ...\}$ and $W^b(t) = W^b(kM)$ if $t \in ((k-1)MT_{\mathsf{TS}}, kMT_{\mathsf{TS}}]$ where $k = 1, 2, ..., K$. We refer to $W^b(kM)$ as W^b_k, which represents the allocated capacity of beam b in cycle k. The design framework considers a

[1]The work can be efficiently scaled up for a general scheme consisting of multiple SPs as well.

monitoring period of K cycles, equivalent to a total operation time of $T = KMT_{\mathsf{TS}}$ (seconds).

Let $f(X)$ stand for the cost function corresponding to X (bps) that the SP rents from operator. Normally, $f(X)$ is a monotonic increasing function with respect to X which reflects the idea that renting more capacity incurs more rental cost. Then, the total renting cost that the SPs have to pay to the operator during T seconds can be expressed as,

$$F_{SP} = f\left(\int_0^T W(t)dt\right) = f\left(\sum_{b=0}^{B}\sum_{k=0}^{K-1} MT_{\mathsf{TS}}W_k^b\right). \tag{2.1}$$

2.2.1 Capacity Allocation and Frequency Reuse

To address the strong cross-beam interference between adjacent beams, a dynamic multi-color policy is employed in this multi-beam transmission system. This differs from traditional color-reuse schemes, where the spectrum is equally distributed. Here, the spectrum is freely allocated to beams, ensuring that different and non-overlapping frequency bands are assigned to two arbitrary adjacent beams. It follows that the sum of capacity assigned to any cluster of J adjacent beams must not exceed the maximum available spectrum band capacity. For instance, Figs. 2.2a and 2.2b demonstrate settings of 3 and 4 adjacent-beam clusters with non-overlapping spectrum.

For a specific beam pattern, let C be the number of available J-adjacent-beam clusters and $\mathbf{U} \in \{0,1\}^{C\times B}$ be the adjacency matrix. In the c^{th} row of $\mathbf{U}$, only J elements corresponding to the indices of J adjacent beams of cluster c are set to one, while the others are set to zero. The dynamic multi-color reuse requirement can then be described by the following constraint:

$$\mathbf{U}\mathbf{W}_k \leq W^{\mathsf{max}}\mathbf{1}_{C\times 1}, \tag{2.2}$$

where $\mathbf{W}_k = \left[W_k^1, ..., W_k^b, ..., W_k^B\right]^T$, W^{max} (bps) indicates the maximum reusable capacity available per cluster, and $\mathbf{1}_{C\times 1}$ stands for a one-vector with size of $C \times 1$.

2.2.2 Queuing Model

From user perspective, a single device can generate multiple data packets that correspond to various applications operating on it concurrently. It's assumed that packets corresponding to a specific application type have identical packet sizes. Consequently, the number of packets resulting from a particular application, which is run by several devices concurrently, can be

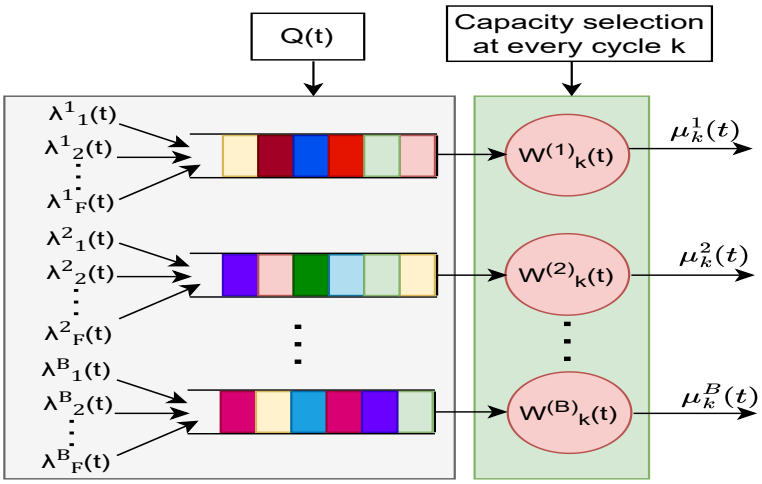

Figure 2.3: Capacity allocation for a queued flow of packets in multiple beam satellite networks.

consolidated into a traffic flow with a projected arrival rate. This number of packets adheres to a random process, with the estimated arrival rate serving as the mean value [75–77]. This work deals with heterogeneous time-varying traffic rates generated by different applications such as voice, video streams, and web browsing. To handle this, the demands from end users are modeled as multiple queues accessing each beam. The data flows are classified based on their corresponding statistical parameters, such as arrival rates and packet lengths. In this model, the arrived packets are processed based on the basic first-come first-served strategy.

Consider F data-flows corresponding to F services tending to access each of B beams as shown in Figure 2.3. We further assume that the flow f carrying data packets of L_f-bit length comes to beam b at a time t following an independent Poison process[2] [75–78] with a time-varying arrival rate of $\lambda_f^b(t)$, i.e., $\lambda_f^b(t)$ is the number of packets that changes over time.

The total arrival rate in bits per second to a beam becomes

$$\Lambda^b(t) = \sum_{f=1}^{F} \lambda_f^b(t) L_f. \tag{2.3}$$

Suppose that a packet of L bits is a normalized processing unit in this SatCom system. As a result, the arrived data can be divided into packets of L bits for transmission. Consequently,

[2]The traffic-flow arrival rates of some typical use cases for the next-generation communication services, such as Internet of Things with small packets and virtual-image communication, have been reported to follow the Poisson process [75–78].

the total arrival rate in terms of the number of packets at beam b can be determined as

$$\lambda^b(t) = \Lambda^b(t)/L. \tag{2.4}$$

Additionally, the service rate for all flows entering beam b at any time t, which is estimated as the number of packets based on the corresponding allocated capacity, can be expressed as,

$$\mu^b(t) = W^b(t)T_{\mathsf{TS}}/L. \tag{2.5}$$

Remark 1. *The users' demands in terms of QoS can be captured by the traffic flow model. For instance, a higher transmission rate can be equated to an elevated arrival rate ($\lambda_f^b(t)$ is scaled-up) or an extended packet size (L_f is set to a larger value). Moreover, rapid time-varying requirements can be depicted by a more fluctuating function of the time-varying arrival rate setting, $\lambda_f^b(t)$.*

2.2.3 QoE Requirement and Problem Formulation

In this section, we aim to ensure that the allocated capacity for every beam does not become a bottleneck violating the required QoE. Here, we probabilistically model the QoE requirements in the manner of transmission delay (waiting time) for the users in each beam with the queuing length of packets available in the data buffer corresponding to that beam transmission.

Specifically, let $q^b(t)$ denote the queuing length of data packets stored in the buffer of beam b at time t. Then, one denotes $P_{n,b}(t) = Pr(q^b(t) = n)$ as the probability that there are n packets in the buffer of beam b at time t. As discussed in [71], due to the time-varying arrival rate models, $P_{n,b}(t)$ can be expressed as a function of t. Assuming that users in all beams have the same waiting time tolerance which corresponds to a QoE threshold of queuing length q_{QoE}. The experience of network utilization is considered "acceptable" by the users if the probability of that such threshold is violated is less than a commitment factor $\bar{P}_{\mathsf{QoE}}$, i.e., $0 < \bar{P}_{\mathsf{QoE}} < 1$. Therefore, the design in this work focuses on keeping the probability that the QL surpasses q_{QoE} packets[3] over the window time of $[0, T]$ less than $\bar{P}_{\mathsf{QoE}}$ for all the beams, which can be expressed as

$$\frac{1}{T}\int_0^T Pr\{q^b(t) \geq q_{\mathsf{QoE}}\}dt \leq \bar{P}_{\mathsf{QoE}}, \forall b. \tag{2.6}$$

[3]Service specific QoE requirements are explained in Chapter 3 of this thesis.

One further assumes that the length of every beam buffer is limited by q_{max}, so-called the maximum buffer length. Herein, it also needs to ensure that the QL at every beam does not surpass q_{max} beams as much as possible, otherwise, the processing of all data flows to the particular beam will be blocked. Regarding the network admission requirements, our design needs to maintain the BP below a predetermined threshold[4] for every time slot [78]. This requirement can be cast by the following constraint,

$$Pr\{q^b(t) \geq q_{\mathsf{max}}\} \leq \bar{P}_{\mathsf{Blk}} \quad \forall(t,b), \tag{2.7}$$

where $\bar{P}_{\mathsf{Blk}}$ is the target BP. Taking into account that $Pr\{q^b(t) \geq N\} = 1 - \sum_{n=1}^{N} P_{n,b}(t)$, our technical designs can be formulated into a statistical optimization problem as follows.

$$\begin{aligned}
\underset{\mathbf{W}}{min} \quad & f\left(\sum_{\forall b}\sum_{\forall k} MT_{\mathsf{TS}} W_k^b\right) && \text{(2.8a)}\\
\text{s.t.} \quad & \text{constraint (2.2)},\\
& \sum_{n=0}^{q_{\mathsf{max}}} P_{n,b}(t) \geq 1 - \bar{P}_{\mathsf{Blk}}, \forall(t,b), && \text{(2.8b)}\\
& \frac{1}{T}\int_0^T \left(\sum_{n=0}^{q_{\mathsf{QoE}}} P_{n,b}(t)\right) dt \geq 1 - \bar{P}_{\mathsf{QoE}}, \forall b, && \text{(2.8c)}
\end{aligned}$$

where $\mathbf{W}$ represents the matrix containing all W_k^b's. As observed, this presents a stochastic optimization problem wherein the constraints correspond to a random process. The primary challenge in resolving this problem stems from the statistical formulas articulated in constraints (2.8b) and (2.8c). In this context, while the problem data remains uncertain, the queuing model incorporating the Poisson process, as discussed in Section 2.2.2, serves as the foundation for our solution framework.

Remark 2. *It is worth noting that $f(X)$ is an increasing function so the SP has to pay more if it rents more capacity. Hence, problem (2.8) is equivalent to the following,*

$$\begin{aligned}
&\underset{\boldsymbol{W}}{min}\ MT_{\mathsf{TS}} \sum_{\forall b}\sum_{\forall k} W_k^b\\
&\textit{s.t. constraints (2.2), (2.8b), and (2.8c).}
\end{aligned} \tag{2.9}$$

[4]In practice, different services have different BP requirements. However, in this context, we associate the BP with the likelihood that the QL exceeds the maximum buffer size, which is assumed to be constant across all services

2.3 Queuing Stochastic Analysis and Problem Approximation

2.3.1 Time-Varying Queuing Stochastic Brief Discussion

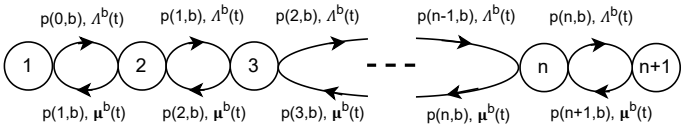

Figure 2.4: Queue state transition diagram of beam b.

The total demand in each beam, which is the sum of arrivals of all data flows, varies over time and can be modeled as a continuously varying arrival rate. Consequently, the number of packets in the buffers in each time slot is a stochastic process. To model this behavior, we represent the number of packets at each time slot as a CTMC, as shown in Fig. 2.4. This stochastic process can be described using a system of ordinary differential equations (ODEs) known as the Kolmogorov equations [71], and the QL follows a birth-death process. The transient solution of the Kolmogorov equation yields the stochastic QL values as:

$$\frac{\partial P_{0,b}(t)}{\partial t} = \begin{cases} -\lambda^b(t)P_{0,b}(t) + \mu^b(t)P_{1,b}(t), & \text{if } n = 0, \\ \lambda^b(t)P_{n-1,b}(t) + \mu^b(t)P_{n+1,b}(t) & \\ \qquad -(\lambda^b(t) + \mu^b(t))P_{n,b}(t), & \text{if } n > 0, \end{cases} \tag{2.10}$$

where $\frac{\partial P_{0,b}(t)}{\partial t}$ indicates the derivative of $P_{n,b}(t)$ at time t. However, since the Kolmogorov equation does not yield explicit solutions for the transition probabilities, various more suitable methods have been developed to approximate the solutions, as described in [71,74,79]. Denote $Q(t)$ as the QL at time t. Then, the transient probabilities can be approximated by a cumulative distribution function given by:

$$F(Q,t) = Pr(Q(t) \leq Q). \tag{2.11}$$

The expected value of the queue distribution at the buffer of beam b provides,

$$\int_{n}^{n+1} F(Q,t)dQ \approx P_{n,b}(t). \tag{2.12}$$

The beam utilization at any time slot t is calculated as,

$$\rho^b(t) = \frac{\lambda^b(t)}{\mu^b(t)}. \tag{2.13}$$

The continuous-model approximation is exact in steady-state [74]. Therefore, the approximated probability of the availability of n packets in the buffer system of beam b at any time slot t can be expressed as

$$\hat{P}_{n,b}(t) = \int_n^{n+1} F(Q)dQ = \rho^b(t)^n(1-\rho^b(t)). \tag{2.14}$$

2.3.2 Problem Approximation

This section exploits the continuous-model approximation in (2.14) to express the stochastic QL in terms of capacity and express the constraints as a function of capacity W_k^b. Expressing $\mu^b(t)$ in (2.5) in terms of W_k^b for $t \in ((k-1)M, kM)$ and $k \in \{1, .., K\}$, one can rewrite (2.14) as,

$$\hat{P}_{n,b}(t) = g_{n,b}(W_k^b, t) = \left(\frac{\sum_{f=1}^F \lambda_f^b(t) L_f}{T_{\mathsf{TS}} W_k^b}\right)^n \left(1 - \frac{\sum_{f=1}^F \lambda_f^b(t) L_f}{T_{\mathsf{TS}} W_k^b}\right), \quad \forall (k,b). \tag{2.15}$$

Since the beams can not serve beyond their maximum capacity, the system utilization constraint needs to satisfy $\rho^b(t) \leq 1$ [74]. Otherwise, $\rho^b(t) > 1$ indicates the system is over-congested and users are blocked from accessing the corresponding beam. Letting Ω_k denote the set $((k-1)M, kM]$, one can restate problem (2.9) as,

$$\min_{\mathbf{W}} \quad MT_{\mathsf{TS}} \sum_{b=1}^{B} \sum_{k=1}^{K} W_k^b \tag{2.16a}$$

$$\text{s.t.} \quad \text{constraint (2.2)},$$

$$\sum_{n=0}^{q_{\mathsf{max}}} g_{n,b}(W_k^b, t) \geq 1 - \bar{P}_{\mathsf{Blk}}, \forall k, \forall b \text{ and } t \in \Omega_k, \tag{2.16b}$$

$$\frac{1}{T} \sum_{k=1}^{K} \int_{(k-1)M}^{kM} \sum_{n=0}^{q_{\mathsf{QoE}}} g_{n,b}(W_k^b, t)dt \geq 1 - \bar{P}_{\mathsf{QoE}}, \forall b, \tag{2.16c}$$

$$0 \leq \rho^b(t) \leq 1, \ \forall t, \forall b. \tag{2.16d}$$

2.4 Dynamic Capacity Allocation Design

In this section, we aim to explain the step-by-step approach to find the optimal dynamic capacity allocated across all beams.

2.4.1 Problem Convexity Characterization

In order to solve problem (2.16), we first characterize its convexity. To begin with, we first define the lower bound capacity amount required per cycle in which $\mu^b(t)$ is fixed by considering the following proposition.

Proposition 1. *Constraints* (2.16b) *and* (2.16d) *in problem* (2.16) *can be merged into one constraint as*

$$W_k^b \geq \alpha_k^b = \max\left(\alpha_{k,1}^b, \alpha_{k,2}^b\right), \forall k, \forall b, \tag{2.17}$$

where $\alpha_{k,1}^b = \max_{t\in\Omega_k} L\lambda^b(t)/T_{\mathsf{TS}}$,
$\alpha_{k,2} = \max_{t\in\Omega_k} Lg_{q_{\max}}^{-1}(1-\bar{P}_{\mathsf{Blk}}, t)/T_{\mathsf{TS}}$, *and* $g_{q_{\max}}^{-1}(\bar{P}_{\mathsf{Blk}}, t)$ *is the inverse function of* $\sum_{n=0}^{q_{\max}} g_{n,b}(W_k^b, t)$.

Proof. The proof is given in Appendix 5.2 □

In the next move, based on the result of this proposition and the fact that (2.17) is a linear constraint, we state the convexity of problem (2.16) in the following theorem.

Theorem 1. *Problem* (2.16) *can be transformed into the following optimization problem which is convex,*

$$\min_{W^b} \quad \sum_{\forall b}\sum_{\forall k} MT_{\mathsf{TS}} W_k^b \tag{2.18a}$$

$$s.t. \quad \textit{constraint } (2.17),$$

$$\sum_{\forall k} z_k(W_k^b) \geq 1 - \bar{P}_{\mathsf{QoE}}, \tag{2.18b}$$

where $z_k(x) = MT_{\mathsf{TS}}/T - A_k^b/\left(Tx^{q_{\mathsf{QoE}}+1}\right)$.

Proof. The proof is given in Appendix 5.2 □

Thanks to Proposition 1 and Theorem 1, one can state that (2.16) is equivalent to convex problem (2.18). In the following section, a dynamic resource allocation algorithm is proposed by developing an optimization-based approach to obtain the optimal solution of this problem.

2.4.2 Duality-based Dynamic Capacity Allocation Algorithm

Duality Approach

We first define the Lagrangian function $\mathcal{L}$ associated with (2.18) as,

$$\mathcal{L}(\mathbf{W}, \boldsymbol{\beta}, \boldsymbol{\zeta}) = MT_{\mathsf{TS}} \sum_{\forall(b,k)} W_k^b + \sum_{\forall(k,c)} \boldsymbol{\zeta}^c \left(\boldsymbol{u}^c \mathbf{W}_k - W^{\mathsf{max}}\right) - \sum_{\forall b} \boldsymbol{\beta}^b \left(\sum_{\forall k} z_k(W_k^b) - 1 + \bar{P}_{\mathsf{QoE}}\right) \tag{2.19}$$

where β^b and ζ^c are the Lagrangian multipliers; $\mathbf{u}^c$ stands for the vector generated from the c-th row of $\mathbf{U}$; and $\mathbf{W}_k = [W_k^1, W_k^2, ..., W_k^B]^T$. Then, the dual function of W_k^b can be defined as the minimum of the Lagrangian function as,

$$\mathsf{g}(\beta) = \min_{\mathbf{W}} \mathcal{L}(\mathbf{W}, \boldsymbol{\beta}, \boldsymbol{\zeta}) \text{ s.t. } (2.17). \tag{2.20}$$

To find the best lower bound that can be obtained from the Lagrange dual function, the dual problem can be written as,

$$\max_{\beta^b, \zeta^c} \mathsf{g}(\beta, \zeta) \text{ s.t. } \beta^b \geq 0, \zeta^c \geq 0. \tag{2.21}$$

Since problem (2.18) is convex, the dual-gap between the primary and dual problem is zero [26]. In the following, one will describe a searching approach to define the optimal solution. In particular, the dual problem is always convex, $\mathsf{g}(\beta^b, \zeta^c)$ can be maximized by using the standard sub-gradient method where the dual variables β^b and ζ^c are first initialized to random values in the dual feasibility region of $\beta^b > 0$, $\zeta^c > 0$, $\mathsf{g}(\beta^b, \zeta^c) > -\infty$ [80]. The dual variables can be iteratively updated as follows:

$$\beta_{[\ell+1]}^b = \left[\beta_{[\ell]}^b - \delta_{[\ell]} \left(\sum_{k=1}^{K} z_k(W_k^b) - 1 + \bar{P}_{\mathsf{QoE}}\right)\right]^+, \tag{2.22}$$

$$\text{and} \quad \zeta_{k,[\ell+1]}^c = \left[\zeta_{k,[\ell]}^c + \delta_{[\ell]} \left(\mathbf{u}^c \mathbf{W}_k - W^{\mathsf{max}}\right)\right]^+, \tag{2.23}$$

where the suffix $[\ell]$ represents the iteration index, $\delta_{[\ell]}$ is the step size, and $[x]^+$ is defined as $\max(0, x)$. This sub-gradient method guarantees the convergence for any initial primary point of $\{W_k^b\}$'s if the step-size $\delta_{[\ell]}$ is chosen appropriately so that $\delta_{[\ell]} \overset{\ell \to \infty}{\longrightarrow} 0$ such as $\delta_{[\ell]} = 1/\sqrt{\ell}$ [26, 81].

Solving the optimization problem related to dual function

This section focuses on minimizing the Lagrangian function,

$$\min_{\mathbf{W}} \mathcal{L}(\mathbf{W}, \boldsymbol{\beta}, \boldsymbol{\zeta}) \text{ s.t. constraint (2.17).} \tag{2.24}$$

Proposition 2.

$$(W_k^b)^\star = \max(\alpha_k^b, \hat{W}_k^b), \tag{2.25}$$

where,

$$\hat{W}_k^b = \left\{ \frac{\beta^b A_k^b (q_{\mathsf{QoE}} + 1)}{\left[\left(MT_{TS} + \sum_{c=1}^{C} \zeta^c U_{c,b}\right) T\right]} \right\}^{1/(q_{\mathsf{QoE}}+2)}, \tag{2.26}$$

A_k^b *is as defined in* (5) *and* $U_{c,b}$ *is the element on row* c *and column* b *of matrix* $\boldsymbol{U}$.

Proof. The proof is given in Appendix 5.2. □

Proposed Duality-based Algorithm

Thanks to the duality approach, the optimal solution of problem (2.18) can be obtained by alternatively solving problem (2.24) - the right-hand-side of (2.20) - as presented in Proposition 2, and updating Lagrangian multipliers β^b and ζ^c as in (2.22) and (2.23) in each iteration until the convergence. The optimization-based approach is summarized in Algorithm 1 where the iteratively solving process can be stopped when the gaps $\Delta_1 = \sum_{b=1}^{B} |\beta_{[i+1]}^b - \beta_{[i]}^b|$ and $\Delta_2 = \sum_{c=1}^{C} |\zeta_{[i+1]}^c - \zeta_{[i]}^c|$ are sufficiently small.

2.4.3 Benchmark Algorithms

Greedy Algorithm

To mitigate the complexity of solving our problem given in the previous section, this section introduces a straightforward and efficient greedy algorithm. As evident, the primary challenge in addressing problem 2.16 arises from the coupling of all W_k^b throughout the entire time window T as illustrated in (2.16c) for each beam. In particular, directly handling this constraint needs to consider the average probability of QoE violation across the entire time window T. To simplify this process, we disregard the average value, prompting the system to meet the QoE requirement at every given moment. As such, constraint (2.16c) is replaced

Algorithm 1 DUALITY-BASED DYNAMIC CAPACITY ALLOCATION

Initialization:

- Choose initial dual vector values β^b and ζ^c.
- Select a tolerate ϵ, step size δ, and set $\Delta_1 = 1$, $\Delta_2 = 1$ $i = 0$.
- Define $\mathbf{U}$, W^{max} and provide values for q_{QoE}, $\bar{P}_{\mathsf{Blk}}$, $\bar{P}_{\mathsf{QoE}}$ and q_{max}.

while $\Delta_1 > \epsilon$ and $\Delta_2 > \epsilon$ **do**
  Given $\beta^b_{[i]}$ and $\zeta^c_{[i]}$, define $(W^b_k)^\star$'s as in (2.25) and (2.26).
  Based on $(W^b_k)^\star$'s, update $\beta^b_{[i+1]}$ as in (2.22).
  Based on $(W^b_k)^\star$'s, update $\zeta^c_{[i+1]}$ as in (2.23).
  Re-set $\Delta_1 := |\beta^b_{[i+1]} - \beta^b_{[i]}|$.
  Re-set $\Delta_2 := |\zeta^c_{[i+1]} - \zeta^c_{[i]}|$.
  Set $i := i + 1$.
end while
Return $\mathbf{W}^\star_k$.

Algorithm 2 GREEDY-BASED DYNAMIC CAPACITY ALLOCATION

Inputs:

- Provide initial values for $\lambda^b_{i,k}$, L_f.
- Provide values for q_{QoE}, $\bar{P}_{\mathsf{Blk}}$, $\bar{P}_{\mathsf{QoE}}$ and q_{max}.

for $b = 1$ to Number of beams **do**
  for $k = 1$ to Number of cycles **do**
    Calculate $\alpha_{k,1}, \alpha_{k,2}, \alpha_{k,3}$.
    Calculate $\max(\alpha_{k,1}, \alpha_{k,2}, \alpha_{k,3})$.
  end for
end for
Return $\mathbf{W}^\star$.

by a more stringent version, which is presented as follows:

$$\sum_{n=0}^{q_{\mathsf{QoE}}} g_{n,b}(W^b_k, t) \geq 1 - \bar{P}_{\mathsf{QoE}}, \forall k, \forall b \text{ and } t \in \Omega_k. \tag{2.27}$$

This new constraint is similar to (2.16b). By employing the same approach handling (2.16b) given in Proposition 1, we first define the maximum arrival rate over one cycle as,

$$\lambda^b_{i,k} = \underset{t \in \Omega_k}{max} \lambda^b_i(t). \tag{2.28}$$

Then, the new constraint in (2.27) can also be translated into,

$$W_k^b \geq \alpha_{k,3}^b = \max_{t \in \Omega_k} Lg_{q_{\mathsf{QoE}}}^{-1}\left(1 - \bar{P}_{\mathsf{QoE}}, t\right)/T_{\mathsf{TS}}. \tag{2.29}$$

Thanks to Proposition 1, we are able to estimate the required capacity of each beam over every cycle by taking the maximum capacity that satisfies the problem constraints. That is,

$$(W_k^b)^\star = \max\left(\alpha_{k,1}^b, \alpha_{k,2}^b, \alpha_{k,3}^b\right). \tag{2.30}$$

The greedy algorithm is summarized in Algorithm 2.

Iterative Staffing Algorithm (ISA)

This subsection introduces another benchmark solution for comparison purposes, which is developed by adapting the ISA given in [72]. The ISA is well-established for time-varying human resource management to satisfy the stochastic waiting time requirement of customers. In [72], the $M_t/M/N(t)$ queue model is employed where the serving capacity of one server (or employees) is fixed (M) while the number of servers (employees) can be varied over the time. Herein, $N(t)$ represents the number of allocated employees at time t, and the ISA is designed to determine $N(t)$ coping with the time-varying customer arrival rate efficiently.

As can be seen, the queuing model utilized in [72] is different from our $M_t/M_t/1$ scheme which is related to one server with variable serving capacity. Hence, in order to modify this work to address our problem, we assume that the capacity amount allocated to beam b in cycle k can be represented by a number of *"fixed capacity packages"*. Let W_0 (bps) be the capacity of one such package, and N_k^b denote the number of capacity packages assigned for beam b in cycle k. Then, we have,

$$W_k^b = N_k^b W_0. \tag{2.31}$$

In addition, the processing rate corresponding to one package can be estimated as

$$\mu_0 = W_0 T_{\mathsf{TS}}/L. \tag{2.32}$$

Now, we can employ the ISA to optimize $\{N_k^b\}$'s by regarding the constraints (2.8b) and (2.8c) instead of the stochastic waiting time as designed in [72]. Specifically, at the initialization, $\{N_k^b\}$'s are randomly selected and then adjusted over iterations. There are two

Algorithm 3 ISA-BASED CAPACITY ALLOCATION

Input:

- Initialize a vector of the number of packages $N_k^b(0)$.
- Set values of $\bar{P}_{\mathsf{Blk}}$, $\bar{P}_{\mathsf{QoE}}$, μ_0, Δ and Δ_0, $\epsilon_1 = 10^{-4}$, counter $i = 0$.

while $\Delta > \epsilon_1$ and $\Delta_0 > \epsilon_1$ **do**
  For every $t \in \Omega_k$, calculate $\rho^b(t) = \lambda^b(t)/(\mu_0 N_k^b(i))$ and $\hat{P}_{n,b}(t)$ according to (2.14).
  Calculate $V_{\mathsf{bl},k}^b(i)$ as in (2.35) and $V_{\mathsf{QoE},k}^b(i)$ as in (2.38).
  Calculate $\Upsilon_{\mathsf{bl},k}^b(i)$ as in (2.34) and $\Upsilon_{\mathsf{QoE},k}^b(i)$ as in (2.37).
  Calculate $N_{\mathsf{bl},k}^b(i+1)$ as in (2.33) and $N_{\mathsf{QoE},k}^b(i+1)$ according to (2.36).
  Set $\Delta = |V_{\mathsf{QoE},k}^b(i) - \bar{P}_{\mathsf{QoE}}|$.
  Set $\Delta_0 = |V_{\mathsf{bl},k}^b(i) - \bar{P}_{\mathsf{Blk}}|$.
  Set $i = i + 1$.
  Set $N_k^b(i) = \max\{N_{\mathsf{bl},k}^b(i+1), N_{\mathsf{QoE},k}^b(i+1), N_k^b(0)\}$.
end while
Return $\mathbf{W}_k^b = L\mu_0 \mathbf{N}_k^b / T_{\mathsf{TS}}$.

components to define N_k^b in every iteration i, the first is $N_{\mathsf{bl},k}^b(i)$ - being updated according to the BP requirement, and the latter is $N_{\mathsf{QoE},k}^b(i)$ - being adjusted due to QoE-related demand. Here, constraint (2.8c) is considered for every cycle to update $N_{\mathsf{QoE},k}^b(i)$. To ensure compliance with the BP requirement stated in (2.16b), $N_{\mathsf{bl},k}^b(i)$ is updated as follows:

$$N_{\mathsf{bl},k}^b(i+1) = \begin{cases} \lceil N_{\mathsf{bl},k}^b(i)\Upsilon_{\mathsf{bl},k}^b(i) \rceil & \text{if } \Upsilon_{\mathsf{bl},k}^b(i) \geq 1, \\ \lfloor N_{\mathsf{bl},k}^b(i)\Upsilon_{\mathsf{bl},k}^b(i) \rfloor & \text{otherwise}, \forall k, \end{cases} \tag{2.33}$$

where $\lceil . \rceil$ and $\lfloor . \rfloor$ indicate the ceil and floor operators and $\Upsilon_{\mathsf{bl},k}^b(i)$ is the blocking-probability influence factor corresponding to $N_k^b(i)$ and $\bar{P}_{\mathsf{Blk}}$. In particular, $\Upsilon_{\mathsf{bl},k}^b(i)$ can be given as

$$\Upsilon_{\mathsf{bl},k}^b(i) = 1 + \frac{V_{\mathsf{bl},k}^b(i) - \bar{P}_{\mathsf{Blk}}}{\bar{P}_{\mathsf{Blk}} i}, \forall k, \tag{2.34}$$

where $V_{\mathsf{bl},k}^b(i)$ indicates the maximum BP during cycle k corresponding to $N_k^b(i)$. Specifically, $V_{\mathsf{bl},k}^b$ is given as follows:

$$V_{\mathsf{bl},k}^b = \max_{t \in \Omega_k} \sum_{n=0}^{Q_{\max}} \hat{P}_{n,b}(t) \Big|_{W_k^b = W_0 N_k^b(i)}. \tag{2.35}$$

Similarly, the $N^b_{\mathsf{QoE},k}(i)$ in iteration i is updated as follows:

$$N^b_{\mathsf{QoE},k}(i+1) = \begin{cases} \lceil N^b_{\mathsf{QoE},k}(i)\Upsilon^b_{\mathsf{QoE},k}(i) \rceil & \text{if } \Upsilon^b_{\mathsf{QoE},k}(i) \geq 1, \\ \lfloor N^b_{\mathsf{QoE},k}(i)\Upsilon^b_{\mathsf{QoE},k}(i) \rfloor & \text{otherwise}, \forall k, \end{cases} \tag{2.36}$$

where $\Upsilon^b_{\mathsf{QoE},k}(i)$ is a QoE-related influence factor corresponding to $N^b_k(i)$ and $\bar{P}_{\mathsf{QoE}}$. Here, $\Upsilon^b_{\mathsf{QoE},k}(i)$ is expressed as,

$$\Upsilon^b_{\mathsf{QoE},k}(i) = 1 + \frac{V^b_{\mathsf{QoE},k}(i) - \bar{P}_{\mathsf{QoE}}}{\bar{P}_{\mathsf{QoE}} i}, \forall k, \tag{2.37}$$

where $V^b_{\mathsf{QoE},k}(i)$ indicates the maximum probability of violating the target QoE requirement during cycle k with $N^b_k(i)$ as

$$V^b_{\mathsf{QoE},k} = \max_{t \in \Omega_k} \sum_{n=0}^{q_{\mathsf{QoE}}} \hat{P}_{n,b}(t)\Big|_{W^b_k = W_0 N^b_k(i)}. \tag{2.38}$$

In addition, to meet the condition $\rho^b(t) \leq 1$ of (2.16c), it is essential to carefully set N^b_k in a way $\mu_0 N^b_k \geq \lambda^b(t)$ for every $t \in \Omega_k$. Then, N^b_k can be updated as

$$N^b_k(i) = \max\left\{N^b_{\mathsf{bl},k}(i+1), N^b_{\mathsf{QoE},k}(i+1), N^b_k(0)\right\} \tag{2.39}$$

Accordingly, the adapted ISA is summarized in Algorithm 3.

2.4.4 Complexity Analysis

The complexity of Algorithm 1 arises from calculating α^b_k and also processing a number of loops in each of that $\beta^b_{[\ell]}$, $\zeta^c_{[\ell]}$, and $(W^b_k)^\star$ are estimated as given in (2.22), (2.23), (2.26), respectively. As given in (2.17), the complexity of estimating α^b_k is the order of $\mathcal{O}\left(KBMq^2_{\mathsf{max}}\right)$. Regarding the effort of estimating $z_k(W^b_k)$ and $\sum_{k=1}^K z_k(W^b_k)$, the complexity due to equation (2.22) can be given as $\mathcal{O}\left(K^2BMq_{\mathsf{QoE}}\right)$. Similarly, the complexity due to equation (2.23) is the order of $\mathcal{O}(KBC)$. Next, the complexity due to equation (2.26) is associated with the summation of C elements and a power-of-q_{QoE} calculator. Hence, the computation effort for calculating $\left\{\hat{W}^b_k\right\}$'s corresponding to B beams and K cycles can be the order of $\mathcal{O}\left(KB(C + q_{\mathsf{QoE}})\right)$. One assumes that implementing Algorithm 1 required $\ell^{(1)}$ iterations to get convergence and obtain the solution, the overall complexity of the algorithm taking the

highest degree polynomial becomes

$$X^{\mathsf{Alg.1}} = \mathcal{O}\left(KB\left[Mq_{\mathsf{max}}^2 + \ell^{(1)}(KMq_{\mathsf{QoE}} + 2C + q_{\mathsf{QoE}})\right]\right).$$

This shows that our problem can be easily solved and converged in a polynomial amount of computation time. Considering the greedy algorithm, one can see that the outcome can be obtained by estimating $\alpha_{k,1}, \alpha_{k,2}, \alpha_{k,3}$. According to (2.17) and (2.29), the required computation effort for implementing Algorithm 2 can be described as

$$X^{\mathsf{Alg.2}} = \mathcal{O}\left(KBM(q_{\mathsf{max}}^2 + q_{\mathsf{QoE}}^2)\right). \tag{2.40}$$

Consequently, we study the complexity of the ISA method. As summarized in Algorithm 3, the process of ISA method encompasses multiple loops of estimating N_k^b through equations (2.33) and (2.36). In each loop, the heaviest task of determining N_k^b replies on calculating $V_{\mathsf{bl},k}^b$ and $V_{\mathsf{QoE},k}^b$ in (2.35) and (2.38), respectively. Therefore, the complexity of ISA can be given as

$$X^{\mathsf{Alg.3}} = \mathcal{O}\left(\ell^{(3)}KBM(q_{\mathsf{max}}^2 + q_{\mathsf{QoE}}^2)\right). \tag{2.41}$$

This has shown a relatively low computation effort. While both the greedy and ISA approaches are simpler than the duality method, we favored the latter because of its superior efficiency, as showcased in Section 2.5.2. Moreover, the duality method, unlike some algorithms which may require exponential time to converge, promises convergence in polynomial time. This not only ensures more predictable computational demands but also bolsters its viability as an optimal approach for real-world applications.

2.5 Performance Evaluation and Numerical Results

In this section, we simulate and analyze a time-varying queuing model to estimate the stochastic BP over time and to find the optimal capacity that can satisfy the defined QoE and BP requirements.

2.5.1 Simulation Setup and Parameters

In this subsection, we conduct a Monte Carlo simulation consisting of 5000 independent data trials. The simulation includes generating random arrival rates based on a time-varying

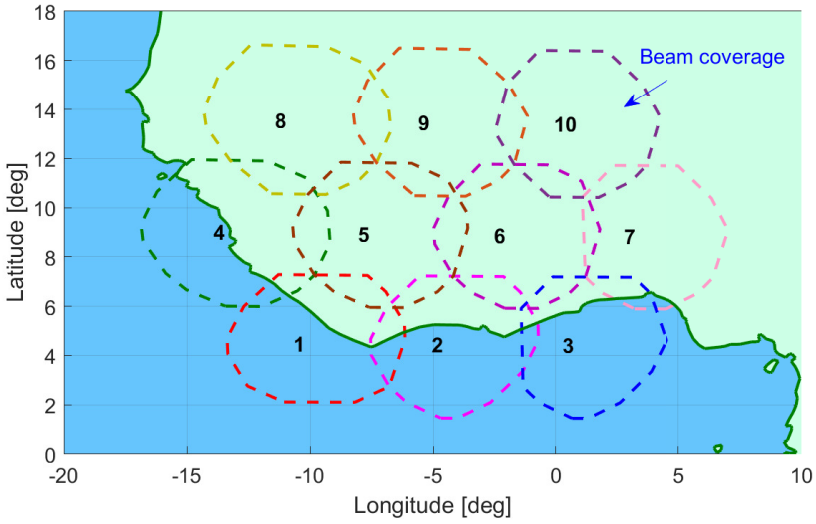

Figure 2.5: Considered GEO beam footprint pattern with $N = 10$.

Table 2.1: Simulation parameters.

Parameters	**Considered values**
Cycle duration (M)	10 minutes
Normalized packet length (L)	64 (KBytes) [82]
Maximum buffer size (q_{max})	30 packets 2 MB [83]
Total available capacity of the satellite (Gbps)	2.1 Gbps [84]
Number of beams (J) per cluster	3 [85]
Number of virtual beams (N)	10 [86]
Number of cycles (K)	6
Number of time slots	180000
Price per Mbits (γ)	0.1 Euros [87]
Random (r_f^b)	$[1-4]$
Random (a_f^b)	$[0-1]$
Random phase (ϕ_f^b)	$[1-360]$ degrees
Target BP ($\bar{P}_{\mathsf{Blk}}$)	0.01 [88]
Time slot duration (T_{TS})	20 ms [89]

Poisson process [75–77] for various time slots, as well as assigning time-varying service rate values for different cycles. In each iteration, the arrival rate function is chosen to represent time-varying demand that varies between zero and the assumed system's maximum capacity, using a sinusoidal representation as described in [90]. Three data flows are generated for every beam and the corresponding time-varying arrival-rate functions for beam b are given as

$$\lambda_i^b(t) = r_i^b(1 + \sin(a_i^b t + \phi_i^b)), \tag{2.42}$$

where suffix i stands for data flow i and r_i^b is an influencing factor corresponding to the average number of arriving packets at time t, a_i^b is a positive number influencing the periodicity of the arrival time of packets, and ϕ_i^b's are phase shift angles. Here, r_i^b is selected randomly in a range of $[1, 4]$ so that the average of the total demand $(\sum_{f=1}^{F} L\lambda_f^b(t)/T_{\mathsf{TS}})$ is not greater than the assumed beam capacity of 700 Mbps as presented in [84]; a_i^b is selected randomly a range of $(0, 1]$ as in [91], [92], while ϕ_i^b is chosen randomly within $[0, 360]$ to ensure all flows have different peak and off-peak periods. The remaining parameters provided in Table 2.1 are adopted for all simulations unless specified otherwise.

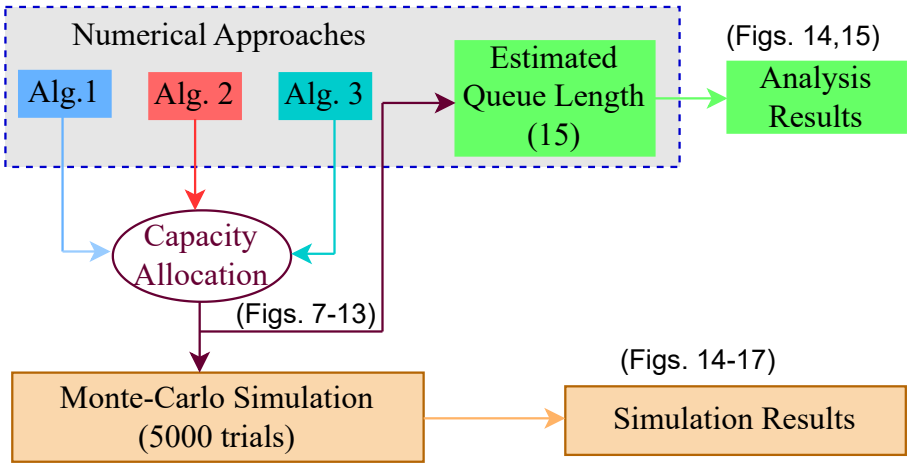

Figure 2.6: The diagram of obtaining numerical, analysis, and simulation results.

By utilizing the mean arrival rate function obtained from the Monte Carlo trials and the service rate values obtained from the optimal allocated capacity according to (2.5), we compute the QL, BP, and the probability of violating QoE requirements for each time slot t. The simulation results as compared to the analytical results are explained in the next sub-section for different values of the considered parameters. Regarding the renting cost function $f(W)$, we exploit a linear form as $f(W) = \gamma W$ [46, 93] where γ represents the price per capacity unit, i.e., Euros/Mbits. Additionally, Fig. 2.6 illustrates the diagram of obtaining numerical, analysis, and simulation results in this section. As can be seen, Algorithms 1-3 are first employed to determine the rented capacity solutions based on which the costs can be calculated. They are so-called numerical results which are demonstrated in Figs. 2.7-2.12. Furthermore, the capacity outcomes are utilized to obtain the analysis results by using (2.15), which are illustrated in Figs. 2.13 and 2.13a. Additionally, the Monte Carlo simulation results based on the numerical capacity solutions are illustrated in Figs. 2.13-2.15.

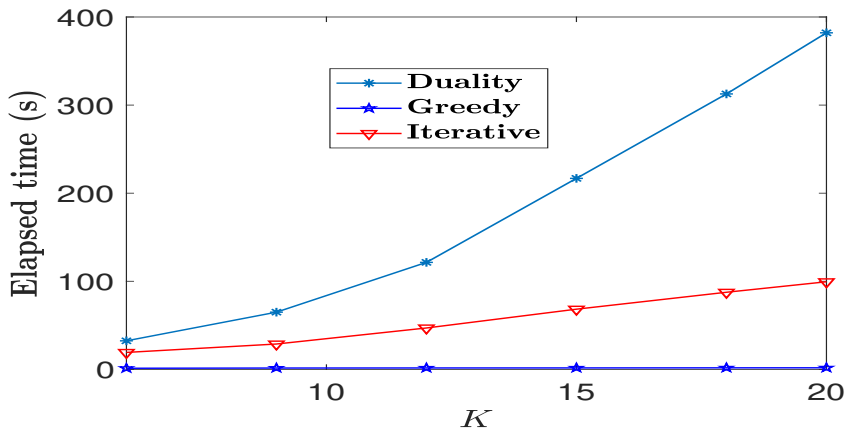

Figure 2.7: Running time versus the number of cycles (K).

2.5.2 Numerical Results and Discussion

This section first shows the running time and convergence of the proposed algorithm, then we investigate the effect of varying parameters, namely q_{QoE}, $\bar{P}_{\mathsf{Blk}}$, q_{max}, $\bar{P}_{\mathsf{QoE}}$, and K, on the optimal allocated capacity and total renting cost to meet the time-varying demand. Assuming both polarizations are used in all beams, we can put a minimum of 3 adjacent beams per cluster to avoid cross-beam interference [85]. Hence, our numerical results are based on 3-beam clustering framework arrangement with 10-beam footprints as described in Fig. 2.5. In particular, there are 10 clusters in this beam pattern setting which are $(1,4,5)$; $(1,2,5)$; $(2,5,6)$; $(2,3,6)$; $(3,6,7)$; $(4,5,8)$; $(5,8,9)$; $(5,6,9)$; $(6,9,10)$ and $(6,7,10)$. Accordingly, constraint (2.2) corresponding to cycle k is demonstrated as

$$\begin{pmatrix} 1 & 0 & 0 & 1 & 1 & 0 & 0 & 0 & 0 & 0 \\ 1 & 1 & 0 & 0 & 1 & 0 & 0 & 0 & 0 & 0 \\ 0 & 1 & 0 & 0 & 1 & 1 & 0 & 0 & 0 & 0 \\ 0 & 1 & 1 & 0 & 0 & 1 & 0 & 0 & 0 & 0 \\ 0 & 0 & 1 & 0 & 0 & 1 & 1 & 0 & 0 & 0 \\ 0 & 0 & 0 & 1 & 1 & 0 & 0 & 1 & 0 & 0 \\ 0 & 0 & 0 & 0 & 1 & 0 & 0 & 1 & 1 & 0 \\ 0 & 0 & 0 & 0 & 1 & 1 & 0 & 0 & 1 & 0 \\ 0 & 0 & 0 & 0 & 0 & 1 & 0 & 0 & 1 & 1 \\ 0 & 0 & 0 & 0 & 0 & 1 & 1 & 0 & 0 & 1 \end{pmatrix} \begin{pmatrix} W_k^1 \\ W_k^2 \\ W_k^3 \\ W_k^4 \\ W_k^5 \\ W_k^6 \\ W_k^7 \\ W_k^8 \\ W_k^9 \\ W_k^{10} \end{pmatrix} \leq W^{\mathsf{max}} \begin{pmatrix} 1 \\ 1 \\ 1 \\ 1 \\ 1 \\ 1 \\ 1 \\ 1 \\ 1 \\ 1 \end{pmatrix}. \tag{2.43}$$

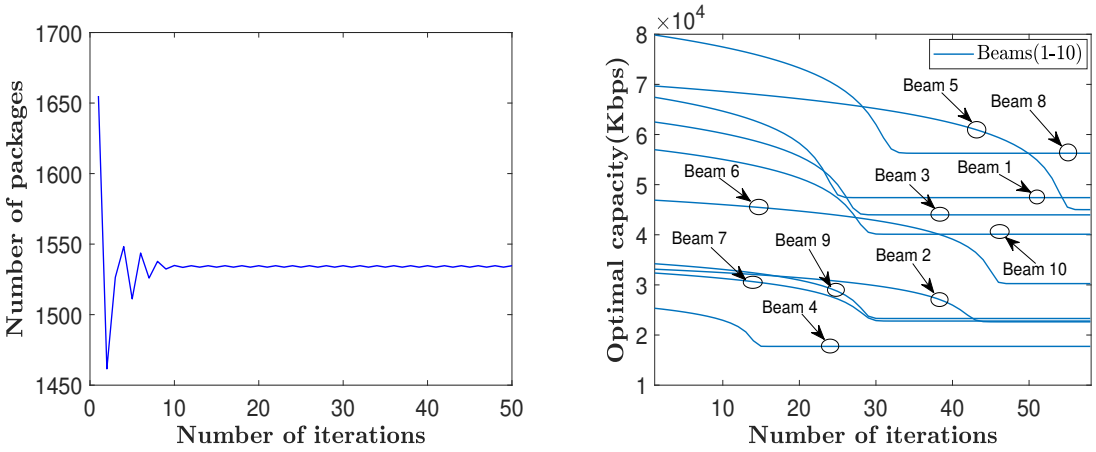

(a) ISA. (b) Lagrangian duality.

Figure 2.8: Convergence plot.

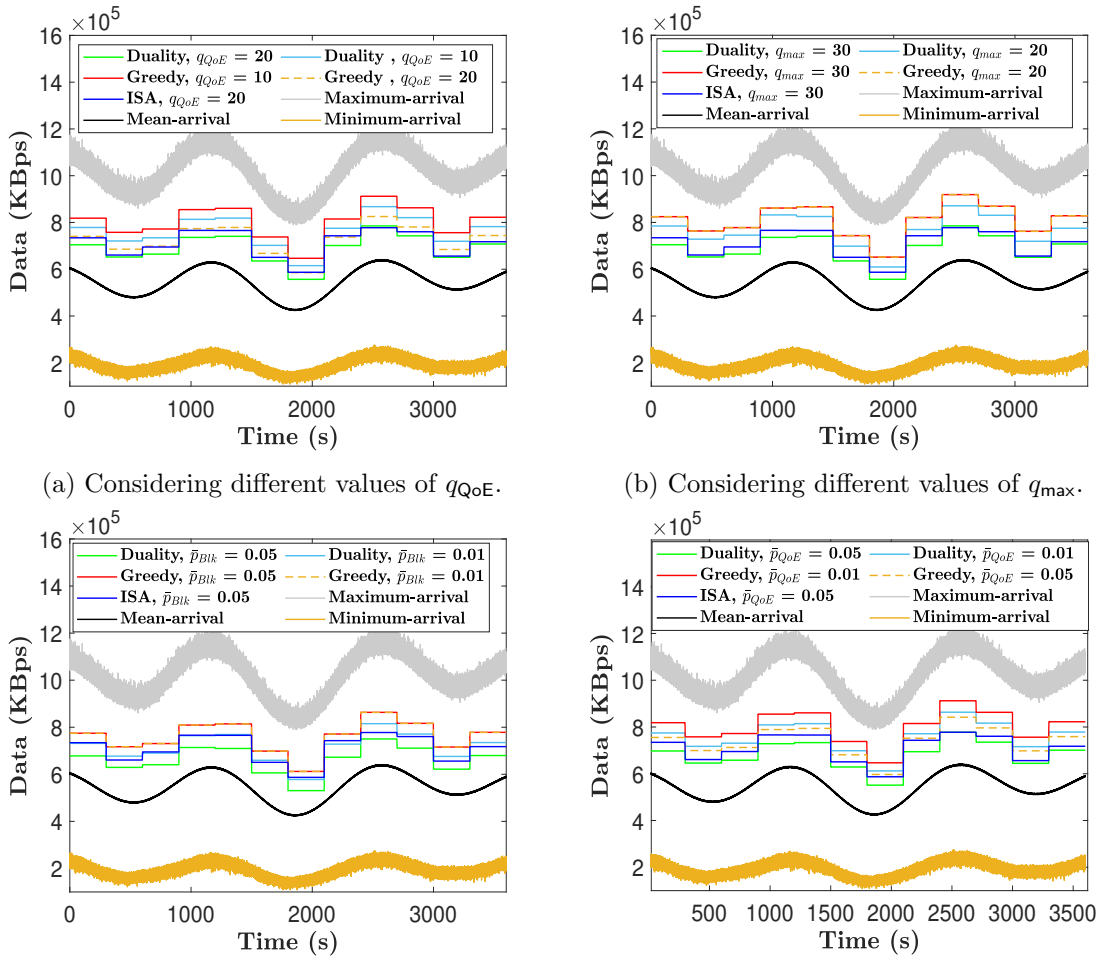

(a) Considering different values of q_{QoE}. (b) Considering different values of q_{max}.

(c) Considering different values of $\bar{P}_{\mathsf{Blk}}$. (d) Considering different values of $\bar{P}_{\mathsf{QoE}}$

Figure 2.9: Optimal allocated capacity to satisfy the time-varying arrivals (demand).

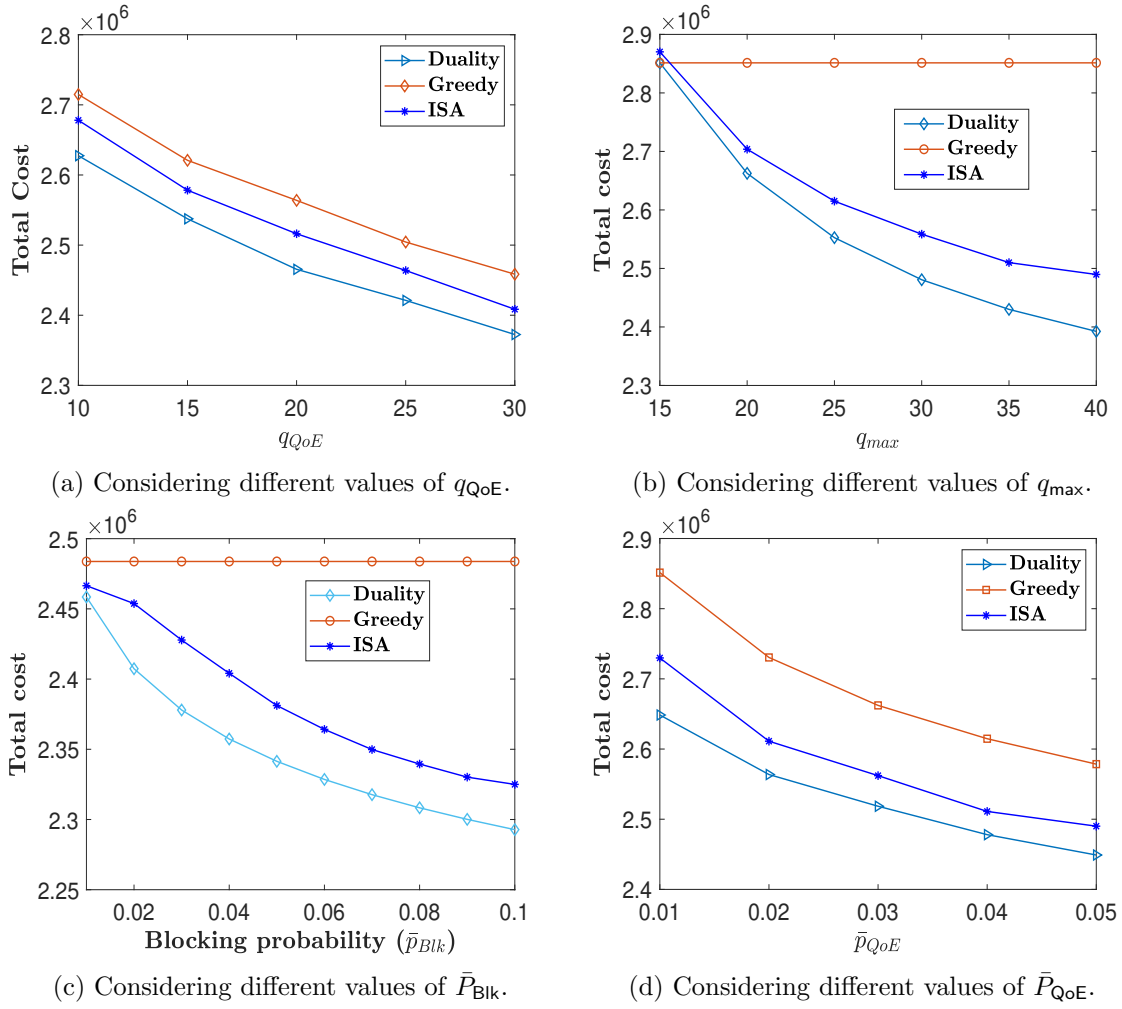

(a) Considering different values of q_{QoE}.

(b) Considering different values of q_{max}.

(c) Considering different values of $\bar{P}_{\mathsf{Blk}}$.

(d) Considering different values of $\bar{P}_{\mathsf{QoE}}$.

Figure 2.10: Total renting cost of the optimal allocated capacity to all beams.

Fig. 2.7 shows the running time of duality, greedy and ISA algorithms with varying values of K, using Matlab (tic-toc method) on an Intel(R) Core(TM) i7 processor. The plot for the duality algorithm indicates that it is close to the expected polynomial time complexity which is proportional to power 2 of the size of cycles, which confirms the analysis results given in Section 2.4.4. Next, we present the convergence plot of our proposed algorithm alongside the benchmark ISA in Fig.2.8. The figure in 2.8b illustrates the changes in capacities assigned to the beams when Algorithm 1 is implemented. As shown, the assigned capacity for each beam decreases before stabilizing at its minimum value across iterations. Moreover, different beams necessitate various numbers of iterations to reach convergent capacity values. Similarly, the fluctuations in the total number of packages allocated to all beams in Fig. 2.8a are the result of employing Algorithm 3 across iterations. The consistent increment or decrement by 1

package in the plot arises from the rounding effects in the expression (2.33) of Algorithm 3.

Figs. 2.9a and 2.10a show the total allocated capacity per cycle ($\sum_{b=0}^{B} W_k^b$) and the total capacity rental cost ($\sum_{b=0}^{B}\sum_{k=0}^{K} \gamma M T_{\mathsf{TS}} W_k^b$) obtained by using the Lagrangian duality, ISA and greedy algorithms at varying q_{QoE} values, respectively. The parameters $q_{\mathsf{max}} = 32$, $\bar{P}_{\mathsf{Blk}} = 0.01$, $\bar{P}_{\mathsf{QoE}} = 0.05$, $K = 12$, and $T_{\mathsf{TS}} = 20\ ms$ have been taken into account. Here, one assumes that the capacity of one package is set to 5 Mbps for implementing ISA algorithm, which is equivalent to the scenario of the transmission over a 1 MHz sub-channel with 32-QAM modulation at acceptable signal-to-noise ratio [94]. The study results indicate that a system catering to users with a higher tolerance for waiting requires less capacity and thus incurs lower costs. Moreover, higher values of q_{QoE} and q_{max} can lead to lower required capacity, resulting in smaller costs.

Figs. 2.9b and 2.10b show the sum of optimal allocated capacity per cycle and total rental cost of all beams, respectively, when varying q_{max} while keeping other parameters ($q_{\mathsf{QoE}} = 15$, $K = 12$, $\bar{P}_{\mathsf{Blk}} = 0.01$, and $\bar{P}_{\mathsf{QoE}} = 0.05$) constant. The results obtained through the Lagrangian duality and ISA method indicate that allowing more packets stored during congestion requires less allocated capacity. In contrast, the greedy algorithm assumes the maximum capacity required to meet the target q_{QoE} requirement, neglecting the buffer size and its influence on . The figures also reveal that a larger buffer size and greater queuing delay tolerance result in lower allocated capacity and rental costs.

Fig. 2.9c demonstrates the allocated capacity per cycle at various $\bar{P}_{\mathsf{Blk}}$ values using the Lagrangian duality, ISA, and greedy algorithms at $q_{\mathsf{max}} = 32$, $q_{\mathsf{QoE}} = 20$, $\bar{P}_{\mathsf{QoE}} = 0.05$, and $K = 12$. The Lagrangian duality and ISA approaches show that systems with lower BP requirements have greater allocated capacities than those with higher blocking probabilities. However, the greedy algorithm provides the same optimal capacity for all $\bar{P}_{\mathsf{Blk}}$ values, as it only considers the maximum value associated with queuing delay violations and not with BP. This makes our model more efficient in accounting for BP. Fig. 2.10c shows the relationship between BP and total rental costs at different q_{QoE} values. As can be seen, the lower BP requirements return higher allocated capacities and costs. For example, based on the obtained results, an increase in $\bar{P}_{\mathsf{Blk}}$ from 0.01 to 0.05 results in a cost reduction of approximately 5%, while an increase from 0.01 to 0.1 leads to a reduction of 7.23%.

Next, Figs. 2.9d and 2.10d depict the relationship between $\bar{P}_{\mathsf{QoE}}$ and total allocated capacity as well as rental costs obtained by implementing the three algorithms. As expected,

the outcomes of all three algorithms imply that a smaller probability of violating the QoE requirement necessitates the SP to allocate a higher capacity and, conversely, less capacity for a higher probability of violation. For instance, the obtained result indicates, an increase in $\bar{P}_{\mathsf{QoE}}$ from 0.01 to 0.05 results in a reduction of the renting cost by 6.11%.

Figs. 2.11a and 2.11b present the total allocated capacities per cycle and the associated renting costs for the three algorithms for various values of K. From the figures, it's evident that when K rises, there's a decrease in the optimal . This trend suggests that a more adaptive system can fulfill demand using less capacity, leading to reduced costs. For instance, results show that when K increases from 6 to 18, the renting cost drops by 11.38%, and a surge from 12 to 18 results in a decline of 6.1%. Parameters for this analysis, including $q_{\mathsf{max}} = 32$, $q_{\mathsf{QoE}} = 20$, $\bar{P}_{\mathsf{Blk}} = 0.01$, and $\bar{P}_{\mathsf{QoE}} = 0.05$, were consistently considered.

The results, as depicted in all the above figures, highlight the superiority of the duality method over both ISA and greedy algorithms in terms of flexibility and adaptiveness. For instance based on the obtained result and for the case where $q_{\mathsf{max}} = 32$, $q_{\mathsf{QoE}} = 20$, $\bar{P}_{\mathsf{Blk}} = 0.01$, $\bar{P}_{\mathsf{QoE}} = 0.05$ and $K = 6$, the proposed model can meet the requirement at a 9.85% and 3.1% lower cost compared to the greedy and ISA algorithms. However, as K increases, the greedy algorithm becomes as efficient as the proposed method, as larger values of K represent nearly immediate capacity changes, which are ideal conditions for greedy algorithms to perform well.

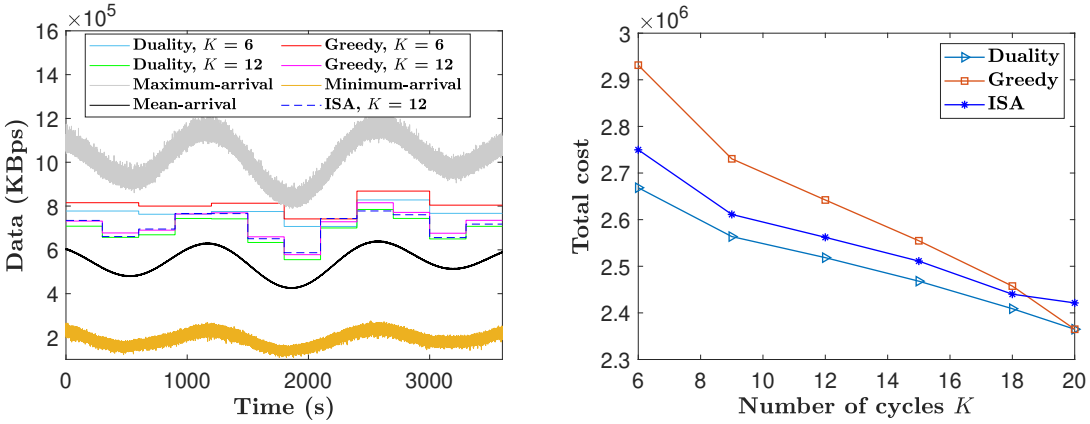

(a) Allocated Capacity. (b) Cost.

Figure 2.11: Sum of the optimal allocated capacity and cost of all beams at different values of K

We need to examine if the capacity is shared among beams based on corresponding demand. We also need to assess whether the proposed model meets the requirements discussed

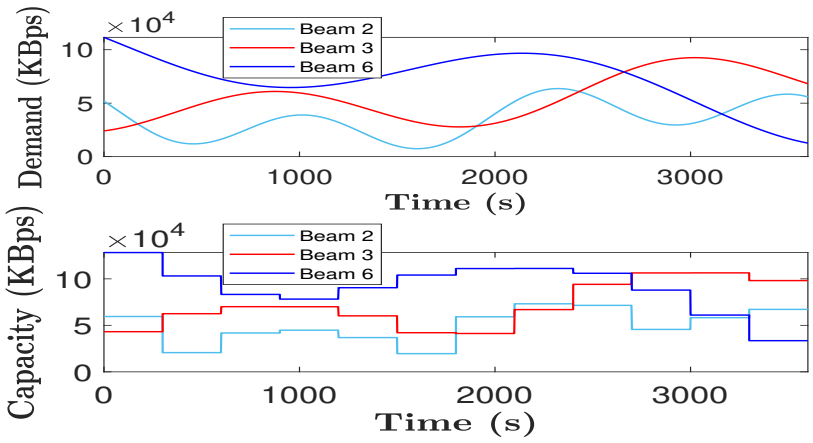

Figure 2.12: Optimal capacity allocation to beams in the same cluster for different arrival rates.

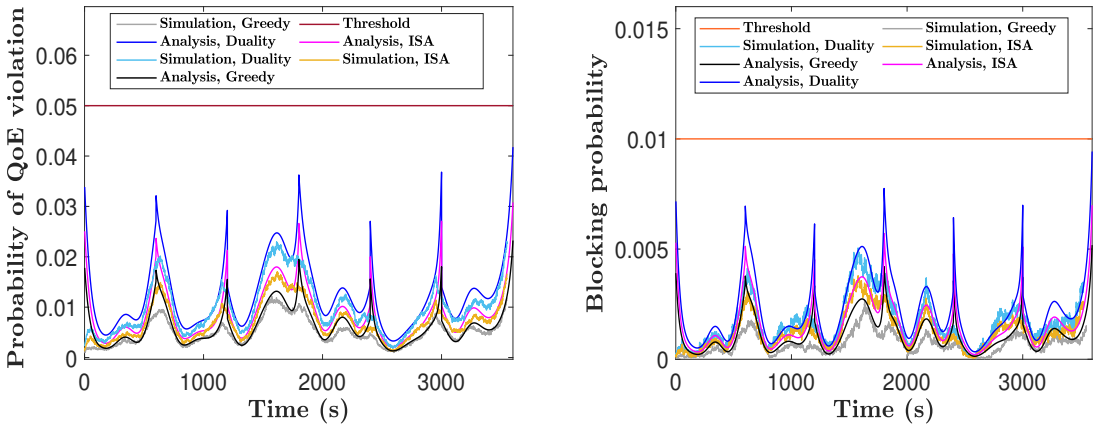

(a) Average probability of QoE violation for all beams.

(b) Average blocking probability for all beams.

Figure 2.13: Blocking probability achieved by analysis and simulation.

in Section 2.2.3. Fig. 2.12 displays the demand per beam as a function of the mean arrival rate ($L\lambda^b(t)/T_{\mathsf{TS}}$) and the optimal allocated capacity to different beams in a random cluster consisting of beams 2, 3, and 6. In every cycle, a higher capacity is assigned to the beam with the highest arrival rate, which corresponds to the highest demand, as demonstrated in the figure. This allocation meets the requirements in equation (2.2). For this demonstration, the parameters used are $q_{\mathsf{max}} = 32$, $q_{\mathsf{QoE}} = 20$, $\bar{P}_{\mathsf{Blk}} = 0.01$, $\bar{P}_{\mathsf{QoE}} = 0.05$, and $K = 12$.

The Figs. 2.13a and 2.13b depict the mean QoE requirement violation probability and the mean BP of all beams, respectively. The target BP of $\bar{P}_{\mathsf{Blk}} = 0.01$ was set with the parameters $q_{\mathsf{max}} = 32$, $q_{\mathsf{QoE}} = 20$, $\bar{P}_{\mathsf{QoE}} = 0.05$, and $K = 6$. The results show that all techniques satisfy the BP requirement. Figs. 2.13a and 2.13b, and Table 2.2 clearly illustrate

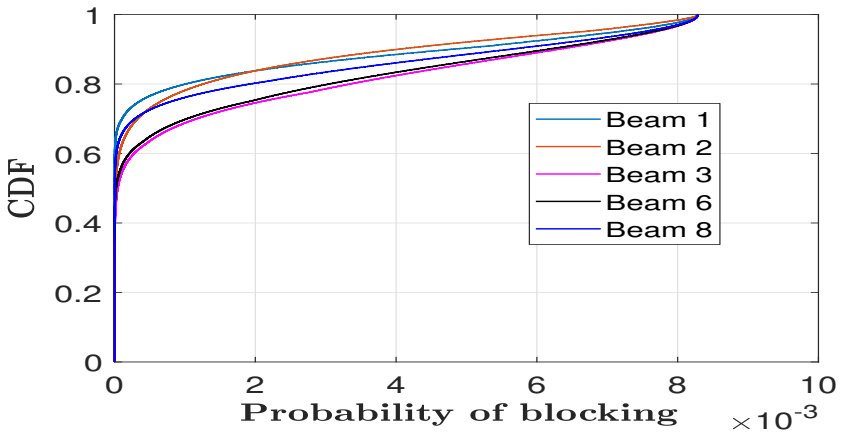

Figure 2.14: Cumulative Distribution Function (CDF) of blocking probabilities over time-window of beams $1, 2, 3, 6, 8$.

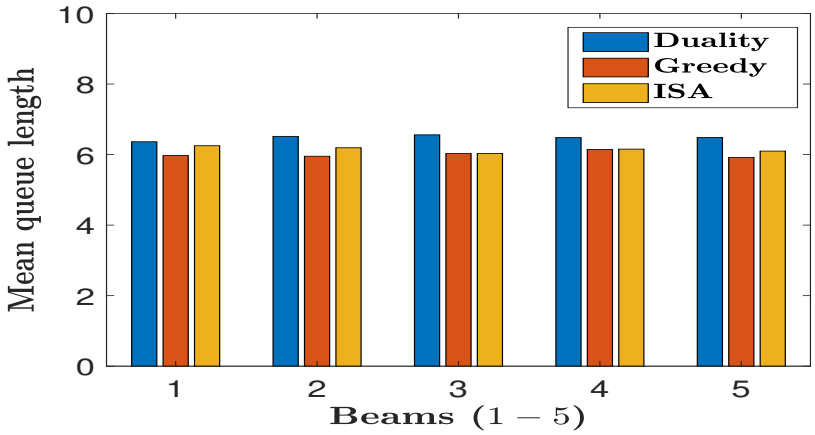

Figure 2.15: Mean value of QL over time-window T and 5000 trials due to beams $1-5$.

Table 2.2: $\bar{P}_{\mathsf{QoE}}$ values at $Q \geq q_{\mathsf{QoE}} = 20$ threshold using optimal capacity.

	q_{QoE}	**20**	**24**	**28**	**32**
Duality	Analysis	0.01	0.0066	0.0025	0.0016
	Simulation	0.0093	0.0061	0.0021	0.0014
Greedy	Analysis	0.0089	0.0052	0.0019	0.0011
	Simulation	0.0083	0.0048	0.0017	0.0010
ISA	Analysis	0.009	0.0062	0.0020	0.0013
	Simulation	0.0086	0.0059	0.0018	0.0012

the close alignment between our analytical and simulation methods. Furthermore, the minor differences in average BP and QL across various beams, as depicted in Figs. 2.14 and 2.15, affirm the accuracy and validity of our proposed method. This shows an effective integration of the inherent randomness and stochastic nature of user traffic demands for capacity management. Additionally, Table 2.2 shows that the queuing delay requirement is duly met

across all instances of Q surpassing the threshold q_{QoE}. Interestingly, the greedy and ISA algorithms result in lower blocking and QoE violation probabilities than the proposed duality method. Similarly, the greedy and ISA algorithms result in lower queuing length than the proposed duality method as shown in Fig. 2.15. This is because of that these benchmarks return the higher assigned capacity for beams.

2.5.3 Discussion on Feasibility of Practical Implementation

The simulation results underscore the computational efficiency of the proposed method, demonstrating its capability to adeptly manage the dynamic and fluctuating traffic demands inherent to SatCom systems. Specifically, as illustrated in Fig. 2.7, the method takes mere minutes (under 100 seconds when $K \leq 12$) to determine the optimal amount of rented BW over a one-hour time window. It's pertinent to highlight that this execution time can be further trimmed when the proposed algorithm runs on a more powerful industrial-grade computer. Such a run-time is practically viable, allowing the SPs to ascertain the necessary capacity prior to entering rental agreements with the operators. Another pivotal factor for the successful implementation of our proposed algorithm in the practical systems is a deep understanding and accurate estimation of the time-varying arrival rate function, specifically, $\left\{\lambda_f^b(t)\right\}$'s. However, within the scope of this study, one does not delve into traffic model estimation. Several existing studies, including those by [95–97], have dedicated efforts to unpack this intricate domain. Their insights suggest that a machine-learning-based model, which adjusts based on real-time data and historical patterns, could be the most efficient way to determine the stochastic information of the network traffic.

2.6 Conclusion

In conclusion, this chapter has proposed a novel and efficient DCA model for multi-beam GEO satellite systems. The method aims to minimize the renting cost while ensuring the target BP and QoE violation requirements. Traffic arrivals are modeled using the $M_t/M_t/1$ queueing model, and the stochastic QL was estimated using the CTMC. The optimization problem has been solved using the Lagrangian duality method and the obtained results demonstrate its effectiveness and superiority over the benchmark ISA and greedy algorithms.

Chapter 3

DQN for QoE-aware dynamic capacity allocation

This chapter is based on work published in IEEE Transactions on Vehicular Technology, Early Access, 2025, DOI: 10.1109/TVT.2025.3599772.

3.1 Introduction

SatCom networks have emerged as a promising technology, offering ubiquitous wireless connectivity in regions that lack terrestrial radio access service. They are expected to play an important role in the improvement of resilience for different applications and contribute significantly to future communication networks and services [98]. SatCom operators worldwide are racing to provide the fastest, most reliable, and extensive 5G coverage, catering to heterogeneous services. Their main aspect is to satisfy their users with various QoE requirements under limited network resources [11].

In wireless communication systems, QoE-aware dynamic DCA strategies have been considered advanced technologies that significantly impact network operators' revenue and rental costs incurred by SPs [52]. A key component in this process is the MAC layer, which manages packet transmissions and buffer queue status [68]. The MAC layer formats data for physical transmission and coordinates closely with the physical and radio link control (RLC) layers [99], facilitating effective scheduling, resource allocation, and traffic prioritization [100, 101]. By flexibly prioritizing capacity based on SLA and user QoE, SatCom operators can implement proactive and effective DCA policies. Such policy design is crucial,

as allocating the minimum capacity needed to ensure satisfactory QoE effectively reduces capital and operational expenditures [102, 103]. The primary challenges are due to the following.

- Network operators often struggle with defining metrics to accurately model the QoE, a challenge exacerbated by evolving stochastic quality expectations [12, 15, 104].
- Traffic demands fluctuate unpredictably over time, making it difficult to pre-allocate capacity without risking over-provisioning or service degradation.
- Different services exhibit distinct packet inter-arrival characteristics, complicating the modeling of burstiness and increasing the complexity of traffic handling [105].
- Dynamically coordinating limited capacity among multiple services is challenging due to competing demands, which complicate the prioritization of services during congestion, necessitating more intelligent and adaptive CA policies.

To handle these challenges, SatCom operators must model the time-varying characteristics of packet arrivals and inter-arrival times for various service types. Assuming simplistic or homogeneous traffic models, such as applying a Poisson distribution to all traffic, fails to capture the burstiness and diversity of real-world traffic [7, 8]. To address this, we tackle the more realistic and complex nature of SatCom traffic by incorporating diverse inter-arrival distributions and service-specific behaviors. Yet, due to the inherent uncertainty in user demand, real-time performance indicators are still necessary for effective decision-making. Due to limited capacity, satellites cannot admit every incoming packet instantly. Instead, packets are buffered, and traffic fluctuations lead to time-varying QL within the system. In this context, QL naturally emerges as a key metric. The QL serves as a critical indicator of network congestion, providing insight into allocated capacity, queueing delay, packet drop probability, and overall QoE. This makes it a valuable indicator to optimize network performance [106, 107]. Traffic demand is inherently time-varying and uncertain, making it challenging to ensure that a preallocated capacity consistently satisfies the requirements of the target QL. To address this, we propose a stochastic evaluation framework for QoE that quantifies the probability of meeting the target queuing delay thresholds. This approach provides a more realistic and comprehensive assessment of the interaction between unpredictable traffic demand, preallocated capacity, and QoE performance, effectively addressing the challenges posed by dynamic network conditions.

Telecom operators engage in periodic planning and optimization of available capacity to ensure efficient utilization and meet SLAs. These optimization activities occur at varying intervals, ranging from minutes, hours, and days to monthly, guided by operator policies and network stability [108], [109]. Despite enhancing capacity utilization efficiency, these methods often exhibit a reactive nature, leading to potential resource under-utilization or over-utilization between optimization intervals. Consequently, there is a growing need for adaptive strategies that can dynamically respond to changing network conditions and optimize planning strategies effectively [110].

In the quest to improve adaptive and flexible CA in SatCom networks, numerous optimization approaches have been explored. However, traditional optimization techniques often break down or become intractable in highly dynamic, uncertain, and partially observable environments—exactly the kind of environment where satellite networks operate. A significant advancement in dealing with time-varying traffic models is to exploit ML techniques, particularly RL algorithms. Notably, DRL algorithms, such as Multi-agent DQN, DDQN, and D3QN offer promising solutions for addressing the challenges of flexible CA in these networks [29–31,35,36]. Using these advanced techniques, we can quickly obtain near-optimal CA solutions, even amidst significant fluctuations in network traffic demands. This is achieved by preemptively learning the intricate relationship between traffic patterns of different services and optimal CA, ultimately enhancing the QoE for users across various services.

Q-learning has been widely used for resource allocation, but it becomes impractical for large-scale problems due to the complexity of managing a Q-table in high-dimensional state and action spaces [36]. To enable decentralized decision-making, where individual agents can optimize CA for different services independently, and for additional reasons explained in Section 3.5, this paper proposes leveraging a multi-agent DDQN to address QoE-aware flexible CA planning in multi-beam SatCom networks. Using advanced ML techniques, such as DDQN, the proposed approach aims to proactively optimize CA decisions, thus improving QoE for diverse service requirements and improving overall network efficiency.

3.1.1 Related works

The limited availability of satellite spectrum capacity has become a significant obstacle in fully meeting customer demands. This issue can be alleviated by employing capacity-enhancing techniques, such as advanced 5G CA methods, or by minimizing unutilized and wasted ca-

pacity during off-peak hours. As discussed in Section 2.1.1, most existing studies primarily focus on augmenting available capacity to meet aggregate traffic demand. However, they often overlook the importance of minimizing unused capacity and explicitly accounting for QoE requirements. Another approach to capacity planning in [31,111,112] focuses on meeting specific demand and coverage requirements by dimensioning the available spectrum band capacity. The works can notably balance the required and maximum capacities to meet target demands, thereby enhancing the capacity utilization efficiency. However, these works focused on aggregate demands and did not explicitly address service-specific QoE or the unpredictably time-varying demands of different services in their research.

QoE estimation and evaluation is another research topic in the literature. Most works use the subjective Mean Opinion Score (MOS) as a metric for estimating QoE [113], [114]. The authors in [115] and [116] work on extending QoE analysis beyond traditional MOS by introducing the concept of $\theta-$acceptability, defined as the probability of an opinion score exceeding a given threshold θ_{Tr}. The works further evaluate QoE by taking the percentage of good or better and the percentage of poor or worse opinion scores as metrics. However, their work still relies on subjective opinions in the modeling, and it does not account for time-varying traffic demand or resource allocation models. The authors in [117], [118] work on the objective estimation of QoE without considering resource allocation.

Resource allocation to meet QoE demands has been extensively studied in the literature. In [16], the authors investigate QoE-aware pricing, power allocation, and admission control to ensure a minimum data rate to maintain the QoE of video call services. Similarly, [119] examines the joint QoE-based subcarrier and power allocation for multi-user, multi-service 5G networks. QoE-driven resource allocation frameworks for video streaming on 5G networks are proposed in [120, 121]. Additionally, the works in [122, 123] introduce a self-tuning algorithm for optimizing QoE across multiple services in LTE networks by adjusting service priority parameters based on network performance statistics. However, these works neglect the consideration of time-varying traffic demand, flexible CA, and stochastic variation in QoE requirements. Furthermore, these works estimate QoE solely based on the basic MOS approach. In dynamic multi-service environments, quality can fluctuate rapidly, and the MOS approach might not accurately reflect these variations, as it is based on post-experience feedback.

Conventional optimization methods have limitations in harnessing historical data, accu-

rately predicting outcomes, and managing large datasets for adaptable and flexible capacity management. Although traffic prediction followed by optimization techniques can be applied, the time complexity of optimizing post-prediction is significantly higher than utilizing online RL methods.

Recently, the application of RL has been getting attention for demand-aware resource allocation. Authors in [124] exploit the Q-learning approach to develop a CA mechanism for heterogeneous three-layer SatCom networks. Similarly, the study in [125] introduces a dynamic channel reservation approach grounded in a DQN tailored for multi-service LEO SatCom systems. While the work accounts for service type-specific traffic demand with prioritization, it does not address the crucial factors of QoE and the diverse arrival distribution patterns of packets across different service types. Another study on ML-based QoE estimation in multiple-service 5G Networks is presented in [104]. However, the authors relied on the traditional MOS for QoE estimation, overlooking the optimal capacity required to achieve the estimated QoE. To the best of our knowledge, the existing literature has not yet explored QoE-aware flexible CA planning that accommodates multiple coexisting services, each with distinct QoE requirements and varying arrival rate distributions. The method proposed in our work aims to fill this gap in the literature.

3.1.2 Contributions

In this study, we focus on QoE-aware flexible CA planning, leveraging time-varying QL dynamics and DDQN to derive an optimal CA planning policy. Our primary contributions are:

- Diverse service scenarios: We consider multiple co-existing services, each characterized by distinct inter-arrival distributions. This nuanced approach captures the varied communication patterns inherent in real-world scenarios, providing a more comprehensive understanding of system behavior.

- Customized QoE requirements: We introduce a novel dimension by considering the diverse QoE requirements associated with different services. Recognizing the varying sensitivities of services to allocated capacity enables us to tailor our CA planning strategy and to optimize user experience based on specific preferences.

- Service prioritization: Developed a novel flexible CA planning mechanism using DDQN,

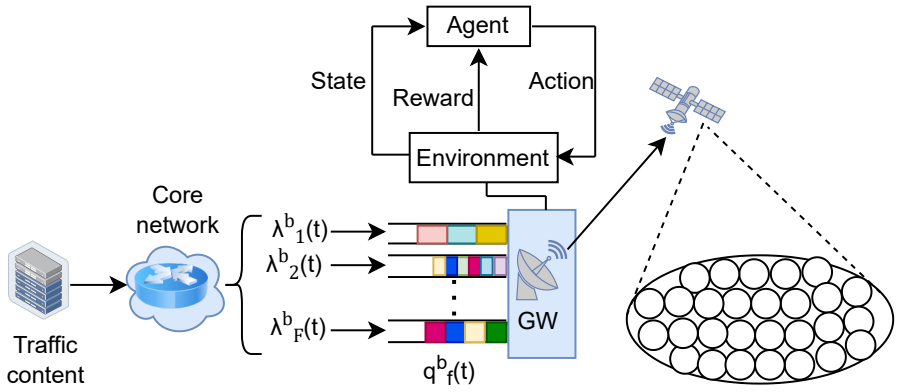

Figure 3.1: CA for a queued flow of packets using RL.

integrating QoE-awareness and priority-based service provisioning to efficiently manage capacity across diverse services, mitigating performance degradation during congestion. During high-congestion periods, priority levels can be dynamically adjusted to ensure essential services receive adequate resources.

- Prediction followed by optimization: The traffic demand expected in future time slots (TSs) is not known in advance, making it difficult to apply optimization techniques for CA online.

In summary, our proposed approach leverages multi-agent DDQN for adaptable capacity dimensioning, to aid satellite SPs in optimizing capacity for delivering multiple services while prioritizing QoE requirements.

3.2 System Model and Problem Formulation

We consider a GEO satellite capable of providing multiple radio access services over B radiation beams to users randomly distributed across these beams' coverage areas. In this scheme, the downlink traffic demand (transmission requests) from various users within the coverage of beam b comes from the core network and is aggregated at the top of Layer 2, within the Service Data Adaptation Protocol (SDAP) [100] and represented as multiple packet flows. We assume that there are F different data flows, each with different packet lengths, arriving at the GW buffer, specific to a particular satellite beam. These data flows are assumed to originate from user requests within the coverage area of that beam. The GW is aware of the users residing in each beam and accordingly routes packets from external networks to the

appropriate buffers. In this system, the dynamic CA mechanism is developed centrally at the network controller located on the ground, e.g., integrated at the GW side as shown in Fig. 3.1. This centralization enables informed decision-making in real time based on a holistic view of network conditions, ensuring efficient resource allocation and adaptability to dynamic traffic flows. Using this mechanism, the SatCom operator can dynamically and efficiently allocate varying amounts of capacity to different beams based on the needs of the flows within them, satisfying user QoE requirements over time and minimizing operator costs.

3.3 Time-Varying Capacity Allocation

Let W^{max} (bps) denote the maximum satellite capacity that the operator can allocate to serve F traffic flows in all beams. Each flow in each beam is assigned a portion of the capacity at any time t, denoted by $W_f^b(t)$, which can range from 0 to W^{max}, i.e., $0 \leq W_f^b(t) \leq W^{\mathsf{max}}$. In addition, it is imperative to allocate capacity to each type of service (flow), ensuring that the total capacity assigned to all flows across all beams does not exceed the maximum available capacity of the operator, which yields the following constraint.

$$\sum_{b=1}^{b=B} \sum_{f=1}^{f=F} W_f^b(t) \leq W^{\mathsf{max}}. \tag{3.1}$$

Following the model described in Section 2.2, the design framework in this chapter also assumes that $W_f^b(t)$ remains constant $\forall(b, f)$ during each cycle of M time slots. Therefore, we denote $W_f^b(kM)$ as $W_{f,k}^b$.

Extending the work in Chapter 2, this chapter addresses the challenges of managing heterogeneous traffic demand varying in time, originating from various services, each of which exhibits diverse patterns of arrival rate distribution and distinct QoE requirements. To address this issue, the demands from end users in different services are classified by service type and modeled as service-specific flows of packets queued to access each beam.

The data flows are categorized according to their respective statistical parameters, including arrival rates, service rates, and packet lengths. Consider F data flows corresponding to F services that tend to access each of B beams, as shown in Fig. 3.1. We further assume that the flow f $(f = 1, ..., F)$ transports data packets of length L_f bits. Additionally, flow f corresponding to beam b has a time-varying arrival rate of $\lambda_f^b(t)$ packets. The service rate

given in Equation 2.5, for a flow f of beam b at any time t can be re-expressed as follows:

$$\mu_f^b(t) = W_f^b(t) T_{\mathsf{TS}} / L_f. \tag{3.2}$$

Consequently, the QL of packets due to flow f of beam b at any time t is given as

$$q_f^b(t+1) = \min\Big(\max\left(q_f^b(t) + \lambda_f^b(t) - \mu_f^b(t), 0\right), q_{\mathsf{max}}\Big), \tag{3.3}$$

where $\max\left(q_f^b(t) + \lambda_f^b(t) - \mu_f^b(t), 0\right)$ is to ensure that the QL is always non-negative. Similarly, the minimization process assumes that the QL will not exceed the maximum. Here, q_{max} indicates the maximum buffer length. Having $q_f^b(t)$, the mean QL of flow f in beam b over a cycle k can be simply calculated as

$$\bar{q}_{f,k}^b = \frac{\sum_{t=(k-1)M}^{t=kM} q_f^b(t)}{M}. \tag{3.4}$$

3.4 QoE Requirements

Similar to what is discussed in Section 2.2.3, we define QoE as the probability that data packets of a specific service type will not encounter a QL exceeding a threshold q_{QoE}, upon their first arrival in the GW buffer, along with a predetermined probability of violating it. The probability that the expected QL exceeds the required target should not surpass a designated threshold known as the probability of QoE violation. Hence, Equation 2.6 concerning this requirement can be re-expressed as

$$\mathbf{Prob}\left\{q_f^b(t) \geq q_{\mathsf{QoE}}^f\right\} \leq \bar{P}_{\mathsf{QoE}}, \quad \forall(t, b, f) \tag{3.5}$$

where q_{QoE}^f and $\bar{P}_{\mathsf{QoE}}$ stand for the target QL requirement of flow f (i.e. service f), and the threshold probability of QoE violation. Here, we assume that the different flows corresponding to different services have different QoE requirements (q_{QoE}^f). Similarly, the probability of the QL reaching or exceeding the maximum QL given in Equation 2.7 can be re-expressed as

$$\mathbf{Prob}\left\{q_f^b(t) \geq q_{\mathsf{max}}\right\} \leq \bar{P}_{\mathsf{Blk}}, \quad \forall(t, b, f) \tag{3.6}$$

where $\bar{P}_{\mathsf{Blk}}$ is the target BP of all flows.

3.4.1 Problem Formulation

To enhance the revenue of satellite operators by accommodating more users, we need to allocate the minimal capacity that meets the QoE and BP requirements. Hence, the problem can be formulated as follows

$$\min_{\{W^b_{f,k}\}'s} \quad \sum_{\forall b}\sum_{\forall f}\sum_{\forall k} W^b_{f,k} \tag{3.7a}$$

$$\text{s.t.} \quad \mathbf{Prob}\{q^b_f(t) \geq q^f_{\mathsf{QoE}}\} \leq \bar{P}_{\mathsf{QoE}}, \forall(k,b,f), \tag{3.7b}$$

$$\mathbf{Prob}\{q^b_f(t) \geq q_{\mathsf{max}}\} \leq \bar{P}_{\mathsf{Blk}}, \forall(k,b,f), \tag{3.7c}$$

$$\text{Constraint (3.1)}, \tag{3.7d}$$

where constraint (3.7b) stipulates that the probability of the QL exceeding q^f_{QoE} throughout the period must not surpass $\bar{P}_{\mathsf{QoE}}$ for all flows across all beams and cycles. Likewise, (3.7c) ensures that the BP of packets in each flow within beam b at every cycle and time t remains below the target. Constraint (3.7d) ensures that the total allocated capacity to all flows in all beams at every cycle k cannot exceed the available satellite spectrum capacity. The primary challenge in solving the problem arises from the stochastic nature of the formulas in constraints 1 and 2, rendering it difficult to provide explicit solutions. Therefore, to solve the problem, it is necessary to approximate the constraints with equivalent expressions.

A certain number n of newly arrived packets at time t is blocked if the total packets comprising accumulated packets from the previous TS and newly arriving packets, minus the processed packets (service rate), exceed the maximum QL. Hence, the number of flow f packets blocked from accessing beam b at time t, denoted as $n^b_{f,\mathsf{Blk}}(t)$, is given by

$$n^b_{f,\mathsf{Blk}}(t) = \max\Big(0, q^b_f(t-1) + \lambda^b_f(t) - \mu^b_f(t) - q_{\mathsf{max}}\Big), \tag{3.8}$$

where $q^b_f(t-1)$ is the QL in the previous TS for packets flow f tending to access beam b. Similarly, the number of flow f of beam b packets with QoE requirements violated at time t, denoted as $n^b_{f,\mathsf{QoE}}(t)$, is given by

$$n^b_{f,\mathsf{QoE}}(t) = \max\Big(0, q^b_f(t-1) + \lambda^b_f(t) - \mu^b_f(t) - q^f_{\mathsf{QoE}}\Big). \tag{3.9}$$

For short periods, such as a single TS, $n^b_{f,\mathsf{QoE}}(t)$ and $n^b_{\mathsf{Blk}}(t)$ may not represent meaningful

averages to calculate the probability of blocking and the probability of QoE violation. However, over a sufficiently large number of TSs, the problem constraints can be approximated by their probabilities of occurrence as

$$\varphi^b_{f,k} = \mathbf{Num}\{q^b_f(t) \geq q^f_{\mathsf{QoE}}\}/M \leq \bar{P}_{\mathsf{QoE}}, \forall f, b, k, \tag{3.10}$$

and

$$\Theta^b_f(k) = \mathbf{Num}\{q^b_f(t) = q_{\mathsf{max}}\}/M \leq \bar{P}_{\mathsf{Blk}}, \forall f, b, k, \tag{3.11}$$

where $\mathbf{Num}\{.\}$ indicates the number of occurrences the expression is true.

3.5 DRL for Optimal CA Planning

This section explores how DRL, specifically DQN, DDQN, and D3QN, can be applied to develop a flexible CA approach for establishing optimal policies in proactive capacity planning across multiple QoE-centric satellite services. In DRL, agents interact with the network environment by taking actions based on the current state, aiming to maximize cumulative rewards. Through repeated interactions and feedback, the agent learns an optimal policy via trial and error. We explore two different multi-agent models: (1) one agent per flow, resulting in a total of BF agents, and (2) one agent per beam, a total of B agents. The choice of the number of agents involves a trade-off: Assigning BF agents (one agent per flow) provide fine-grained control and smaller action spaces per agent but at the cost of significant computational complexity. In contrast, using B agents (one agent per beam) strikes a balance between granularity and complexity, offering moderate action spaces while potentially facing challenges in fair resource allocation among flows within each beam. While a single centralized agent could theoretically manage the entire system, this approach is not considered in our work due to the high training complexity associated with the large action space, as discussed in Section 3.5.1.

3.5.1 Elements of RL

Environment: The environment is the considered B-beam satellite system, as depicted in Section 3.2, which imposes specific constraints on CA. The dynamics of the environment encompass the evolution of the queue state in response to allocated capacity and external

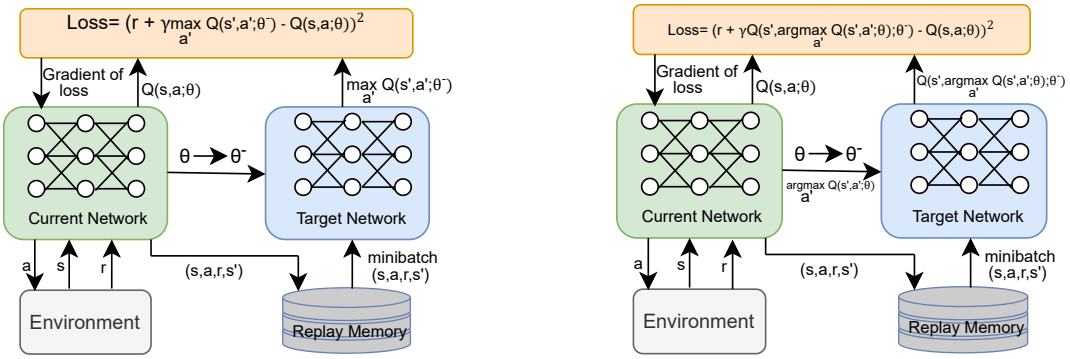

(a) DQN. (b) DDQN.

Figure 3.2: Training process in DQN and DDQN.

factors, including packet arrival rates and traffic patterns. These environmental dynamics are critical for the RL model to adapt and optimize CA, thereby ensuring the target QoE requirements.

Agent: In our context, an agent (whether an agent of a single flow or an agent of all flows accessing a particular beam) refers to a CA manager and decision maker, co-located at the GW. Its role is engaging with the environment to develop an optimal CA policy that minimizes capacity consumption while satisfying users' requirements on the QoE and BP.

State: The state is defined as the specific instance of congestion in the satellite environment, which is determined by measuring the QL at the GW. In particular, the QL of flow f of beam b at TS t ($q_f^b(t)$) can be calculated based on (3.3). However, the CA system is designed to work per cycle. Therefore, we model the state of an agent managing the flow f accessing beam b in cycle k, denoted as $s_{f,k}^b$ as the mean QL of all time intervals within a cycle k, that is, $s_{f,k}^b = \{\bar{q}_{f,k}^b\}$. Similarly, the state of an agent that manages the CA of F flows accessing beam b at cycle k is expressed as

$$s_k^b = \left\{\bar{q}_{1,k}^b, \bar{q}_{2,k}^b, \bar{q}_{3,k}^b, ..., \bar{q}_{F,k}^b\right\} \in \mathcal{S}, \ \forall(b,k), \tag{3.12}$$

where $\mathcal{S}$ denotes the set of all possible states of the agent.

Action: Both the one agent per flow and one agent per beam models utilize the epsilon-greedy strategy, a commonly employed action selection technique in RL. Under this approach,

agents predominantly select the best action with the highest Q-value, optimizing the CA decision based on accumulated knowledge, with a probability of $1-\epsilon$, and introduce an element of randomness by occasionally allocating a random capacity from the action space, with a probability of ϵ as

$$a = \begin{cases} \text{random action}, & \text{with probability } \epsilon, \\ \underset{a}{arg\,max}\,\{Q(s,a)\}, & \text{with probability } 1-\epsilon. \end{cases} \tag{3.13}$$

where $Q(s,a)$ is the Q-value corresponding to the action a at state s. This approach applies regardless of whether the model involves one agent per flow or one agent per beam. This dual strategy effectively strikes a balance between exploiting the agent's accumulated experience to maximize immediate rewards and exploring the environment to enhance the learning process over time.

Reward: After taking action, agents receive immediate rewards from the environment, which evaluates how well the allocated capacity meets demand and QoE requirements across all service types. These rewards are calculated based on episodes involving diverse traffic demand scenarios across all service types for the agents to interact with. The goal is to identify a policy that maximizes the expected future rewards based on feedback from these simulated episodes. In the one agent per flow model, during an episode, when the combined capacity needed by the BF flows exceeds the maximum beam capacity, the available capacity is allocated based on service priority. This priority is quantified by a weight vector $\mathbf{p} = (p_1, p_2, ..., p_F)$, indicating the reward penalties imposed on the RL agents. Consequently, during congestion, we assume that the service with the highest tolerance (highest q^f_{QoE}) to wait in a queue is assigned the highest penalty weight. The total reward is then given as a sum of the two sub-rewards. The first sub-reward is expressed in terms of the allocated capacity relative to the available capacity as follows:

$$r^b_{f,k,1} = \begin{cases} 0, & \text{if } \sum_{\forall(b,f)} W^b_f(t) \leq W^{\mathsf{max}}, \\ -100 * \frac{p_f}{\sum_{f=1}^{f=F} p_f}, & \text{otherwise.} \end{cases} \tag{3.14}$$

This reward component penalizes agents if the total allocated capacity exceeds the maximum available capacity W^{max}. The reward of -100 is used to discourage the agents from allocating

capacity values that exceed the maximum available capacity for the flows. The penalty per flow is proportional to the priority of the flows. The other sub-reward can be given as a weighted sum of the mean QL and the inverse of allocated capacity depending on requirement satisfaction as

$$r^b_{f,k,2} = \begin{cases} \zeta \bar{q}^b_{f,k} + \frac{\delta}{W^b_{f,k}}, & \text{if } \frac{\varphi^b_{f,k}}{M} \leq \bar{P}_{\mathsf{QoE}} \wedge \frac{\Theta^b_{f,k}}{M} \leq \bar{P}_{\mathsf{Blk}}, \\ -\bar{q}^b_{f,k}, & \text{otherwise.} \end{cases} \tag{3.15}$$

This secondary reward component incentivizes the agent to allocate the minimal capacity necessary to achieve and maintain low average QLs, $\bar{q}^b_{f,k}$. Here, ζ and δ are weighting factors that balance the effects of QL and allocated capacity on the reward. The total reward per flow is then given as

$$R^b_{f,k} = r^b_{f,k,1} + r^b_{f,k,2}. \tag{3.16}$$

Similar to the one agent per flow case, the reward is calculated as a sum of two sub-rewards.

$$r^b_{k,1} = \begin{cases} 0, & \text{if } \sum_{\forall(b,f)} W^b_f(t) \leq W^{\mathsf{max}}, \\ -100, & \text{otherwise.} \end{cases} \tag{3.17}$$

This reward component penalizes agents from making allocation decisions that violate the global capacity constraint. Here, each agent takes a combined action for all flows resulting in different QoE requirement violations and blocking probabilities for each service type. Hence, the second sub-reward is the sum of the rewards from each flow as follows

$$r^b_{k,2} = \sum_{f \in \mathcal{F}} (\zeta \bar{q}^b_{f,k} + \frac{\delta}{W^b_{f,k}}) - \sum_{f \notin \mathcal{F}} \bar{q}^b_{f,k}, \tag{3.18}$$

where $\mathcal{F} = \left\{ f \mid \frac{\varphi^b_{f,k}}{M} \leq \bar{P}_{\mathsf{QoE}} \wedge \frac{\Theta^b_{f,k}}{M} \leq \bar{P}_{\mathsf{Blk}} \right\}$. The total reward is then calculated by summing the sub-rewards, given as

$$R^b_k = r^b_{k,1} + r^b_{k,2}. \tag{3.19}$$

In both the one agent per flow and one agent per beam cases, coordination among agents primarily arises from the shared penalty mechanism and the global capacity constraint, reflecting characteristics of reward shaping and environmental interaction.

3.5.2 Deep Q-Network

The DQN utilizes Deep Neural Networks (DNN) to approximate action-value functions for dealing with high-dimensional state space problems, such as flexible CA with time-varying demand, by utilizing the representational power of deep learning. In DQN, each agent creates its own model with two DNNs: the online and the target networks. In each cycle, the agents use the online network to approximate the Q-function $\mathcal{Q}(s, a; \omega)$ and choose an action, where ω is the weights of the agent's online network. The target network, with weights $\hat{\omega}$, is used to stabilize the learning process by copying ω after a set number of cycles.

During the training phase, the agent employs the experience replay strategy to enhance convergence speed and solution quality by incorporating a wide range of experiences from different regions of the state space, various actions, and corresponding rewards. By using this method, its transition (s, a, r, s') is stored in the experience replay memory. At each iteration, a random batch of experiences is sampled from this memory to train the learning model. In particular, the application of DQN to solve the problem (2.8) can be represented as follows: In each learning step (cycle), the agent takes an action of bandwidth allocation after observing its current state. Then it receives a reward from the environment and moves to the next state. After that, its respective experience tuple of (s, a, r, s') is stored in its experience replay memory. A mini-batch of experiences is then sampled to train the online network. Based on that, the parameters of the online network ω are updated to minimize the loss function. The loss function for the one agent per flow configuration is defined as

$$\mathcal{L} = \left(\mathcal{Q}' - \mathcal{Q}(s^b_{f,k}, a^b_{f,k}; \omega)\right)^2, \tag{3.20}$$

where $\mathcal{Q}'$ is the target Q-value which is computed based on the Bellman optimality principle by adding the reward to the maximum Q-value at the next state as follows:

$$\mathcal{Q}' = R^b_{f,k} + \gamma \max_{a'^b_{f,k}} \mathcal{Q}(s'^b_{f,k}, a'^b_{f,k}; \hat{\omega}), \tag{3.21}$$

where γ is the discount factor and $\hat{\omega}$ represent the combination of updated weights and biases in the target network. The Q-value of the online network is updated using the following equation:

$$\mathcal{Q}(s^b_{f,k}, a^b_{f,k}; \omega) = \mathcal{Q}(s^b_{f,k}, a^b_{f,k}; \omega) + \alpha \left(\mathcal{Q}' - \mathcal{Q}(s^b_{f,k}, a^b_{f,k}; \omega)\right), \tag{3.22}$$

where α is the learning rate, which controls the step size for the update. This equation adjusts the predicted Q-value towards the target Q-value, scaled by the learning rate. Through this iterative process, the parameters of the online network are updated to minimize the loss function, and the online Q-values gradually converge to the optimal Q-values, improving the agent's decision-making ability.

Similarly, for the one agent per beam model, the parameters of the online model ω_b are updated to minimize the loss function as follows

$$\mathcal{L}_b = \Big(\mathcal{Q}'_b - \mathcal{Q}_b(s^b_k, a^b_k; \omega_b)\Big)^2, \tag{3.23}$$

where $\mathcal{Q}'_b$ is the target Q-value which is computed as follows:

$$\mathcal{Q}'_b = R^b_k + \gamma \max_{a'^b_k} \mathcal{Q}_b(s'^b_k, a'^b_k; \hat{\omega}_b), \tag{3.24}$$

where ω_b is the weight of agent b's online network and $\hat{\omega}_b$ represents the combination of updated weights and biases in the target network of the agent. By minimizing the loss function, the DQN iteratively improves its policy, enabling it to effectively learn optimal actions in complex, high-dimensional environments. After a given number of learning steps, the target network parameters $\hat{\omega}$ and $\hat{\omega}_b$ are updated by copying the values of ω and ω_b. Training continues until convergence. The detailed implementation of the two models is summarized in Algorithm 4.

Remark 3. *Although DQN models have proven their efficiency and effectiveness for resource allocation problems, they sometimes encounter overestimation problems, where the agent consistently selects sub-optimal actions in a given state merely because these actions have the highest Q-value estimates [35]. This overestimation occurs because the Q-values predicted by the DQN may not accurately reflect the true expected rewards, leading the agent to make poor decisions. This overestimation problem can be better addressed by using a DDQN.*

3.5.3 Double Deep Q-Network

DDQN is an improved version of DQN that addresses the issue of Q-value overestimation encountered in DQN by decoupling action selection and evaluation as shown in Fig. 3.2. Unlike in DQN, where the target network is used for both action selection and evaluation,

Algorithm 4 DQN-BASED CA ALGORITHM

Initialization:

- Initialize replay memory $\mathcal{D}$, $\mathcal{D}_b$.
- Initialize the online network with random weights ω, ω_b.
- Initialize the target network with weights $\hat{\omega}$, $\hat{\omega}_b$.

for each episode ($i = 0$ to max episode) **do**
  Initialize the state $s^b_{f,k}$, s^b_k .
  for each cycle ($k = 0$ to K) **do**
    Choose an action from the action space using the epsilon-greedy method as in (3.13).
    Calculate the total reward according to (3.16), (3.19) and observe the next state $s'^b_{f,k}$, s'^b_k.
    Store experiences $(s^b_{f,k}, a^b_{f,k}, R^b_{f,k}, s'^b_{f,k})$ in $\mathcal{D}$
    and $(s^b_k, a^b_k, R^b_k, s'^b_k)$ in $\mathcal{D}_b$.
    Take sample minibatch experiences $(s^b_{f,k}, a^b_{f,k}, R^b_{f,k}, s'^b_{f,k})$ from $\mathcal{D}$ and $(s^b_k, a^b_k, R^b_k, s'^b_k)$ from $\mathcal{D}_b$.
    Calculate the target Q_value according to (3.21) and (3.24).
    Calculate the loss using gradient descent as in (3.20) and (3.23).
    Update online network parameters ω and ω_b to minimize the loss function.
    Update target network parameters after every $\hat{k}$ ($\hat{k} > 0$) cycles: $\hat{\omega} \leftarrow \omega$ and $\hat{\omega}_b \leftarrow \omega_b$.
  end for
end for

in DDQN, the online network selects the best action for the next state. In this subsection, we focus exclusively on the one-agent-per-beam DDQN model to reduce the architectural complexity associated with managing a separate agent for each flow. This approach simplifies the overall framework while still leveraging the advanced capabilities of DDQN compared to DQN. Hence, the best action selection is given as

$$a = \arg\max_{a'^b_k} Q(s'^b_k, a'^b_k; \theta), \tag{3.25}$$

and the selected action is evaluated by the target network. The target Q-value is then estimated as

$$Q' = R^b_k + \gamma Q(s'^b_k, a; \theta^-). \tag{3.26}$$

The gradient descent step can be used to calculate the loss as follows

$$\mathcal{L}' = \Big(Q' - Q(s^b_k, a^b_k; \theta)\Big)^2 \tag{3.27}$$

The detailed implementation steps of the DDQN-based CA algorithm, which is developed to address problem (2.8) are summarized in Algorithm 5.

Algorithm 5 DDQN/D3QN-based CA Algorithm

Initialization:

- Initialize replay memory $\mathcal{D}'$.
- Initialize the online network with random weights θ.
- Initialize the target network with weights θ^{-}.

for each episode ($i = 0$ to max episode) **do**
  Initialize the state (s_k^b) for all beams and flows.
  for each cycle ($k = 0$ to K) **do**
    Choose an action from the action space using the epsilon-greedy method as in (3.13).
    Calculate the total reward according to(3.16), (3.19) and observe the next state s'^b_k.
    Store experiences $(s_k^b, a_k^b, R_k^b, s'^b_k)$ in $\mathcal{D}'$.
    Sample random minibatch of experiences $(s_k^b, a_k^b, R_k^b, s'^b_k)$ from $\mathcal{D}'$.
    Select the best action according to (3.25).
    Calculate the target Q-value according to (3.26).
    Perform a gradient descent step to calculate the loss according to (3.27), where the Q-value in the D3QN model is calculated according to (3.28).
    Update online network parameters θ to minimize the loss function.
    Update the target network's parameters after every $\hat{k}$ ($\hat{k} > 0$) cycles: $\theta^{-} \leftarrow \theta$.
  end for
end for

3.5.4 Dueling Double Deep Q-Network

In scenarios where the value of being in a particular state is more significant than the specific actions taken, DDQN may not be efficient due to its inability to estimate state values and action advantages separately [36], [126]. By decoupling the state value and action advantage estimations the D3QN model helps to reduce Q-value overestimation further and enhance the stability of learning. The Q-value estimation comparison of DDQN and D3QN is shown in Figure 3.3. Here, D3QN separates the state value $V(s_k^b)$, i.e. the value to be in a particular QL state regardless of the action taken and the action advantage function $A(s_k^b, a_k^b)$, i.e. the advantage of taking a specific action (such as CA) at that specific state for more precise and stable value estimation. We estimate the Q-values by adding the outputs of the state value and advantage values as follows [36], [126]

$$Q(s_k^b, a_k^b; \theta, \theta^S, \theta^A) = V(s_k^b) + A(s_k^b, a_k^b) - \frac{1}{|A_n|} \sum_{a_k^b \in A_n} A(s_k^b, a_k^b), \tag{3.28}$$

where θ^S, θ^A are the parameters related to the state value function and action advantage function, $|A_n|$ is the number of available actions in the action space and $\frac{1}{|A_n|} \sum_{a_k^b \in A_n} A(s_k^b, a_k^b)$ represents the mean advantage across all possible actions, which is subtracted to normalize the advantage function. The detailed implementation of the CA algorithm is also given in

(5), as the only difference with DDQN is in the Q-value estimation given in step 11 of the algorithm.

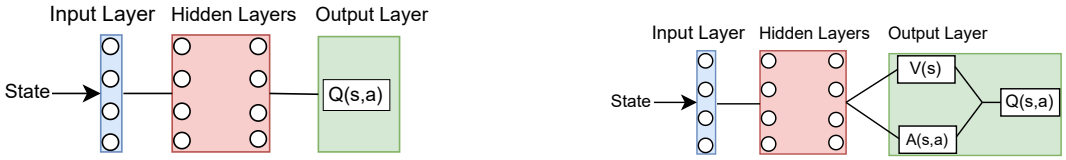

(a) DDQN. (b) D3QN.

Figure 3.3: Q-value estimation process in DDQN and D3QN as in [126].

3.5.5 Computational Complexity Analysis

While the overall complexity of the DRL architecture can be influenced by the design of its input, hidden, and output layers, the primary factors are the sizes of the state and action spaces. For the one agent per flow model, where the QL for packets of flow f ranges from 0 to $q_{\max}$, and actions are selected from N discrete options, the complexity scales linearly with the product of the number of beams, flows, and $q_{\max}$. In contrast, for the one agent per beam model, each agent takes actions for multiple flows simultaneously, resulting in a state size of $(q_{\max}+1)^F$ and an action space size of N^F. The complexities of the two scenarios are summarized in Table 3.1.

Scenario	**State Complexity**	**Action Complexity**
1 Agent per Beam	$B \cdot (q_{\max}+1)^F$	$B \cdot N^F$
1 Agent per Flow	$B \cdot F \cdot (q_{\max}+1)$	$B \cdot F \cdot N$

Table 3.1: Complexity analysis of the proposed method.

3.5.6 Benchmark Algorithm

This section modifies the algorithm developed in Section 2.4.2 to obtain a benchmark solution for comparison purposes by assuming Poisson arrivals for all flows. This solution approach utilizes the Lagrangian duality optimization method for CA. It consolidates packet arrivals from all service types into a single queue, which is then served based on a *first-come-first-served* scenario. However, it is worth noting that the CA results obtained by this optimization approach are determined based on perfect knowledge of the arrival rates.

To adapt this benchmark solution to our scheme, we use the predicted traffic demand of an LSTM recurrent neural network as input, as outlined in [32]. To gain a comprehensive understanding of future traffic demand beyond the immediate horizon and to capture longer-term trends more effectively, we employed a multi-horizon LSTM network to predict the input traffic demand of all the TSs of the next cycle for the optimization approach. This approach optimizes forecasting accuracy by concurrently predicting traffic demand for multiple future TSs, enhancing the effectiveness of CA strategies.

3.6 Performance Evaluation and Numerical Results

In this section, we outline the dataset preparation process, discuss the considered hyper-parameter values, present the results obtained using the proposed techniques, conduct a performance comparison, and assess the efficiency of the implemented algorithms.

3.6.1 Input Traffic and Traffic Distribution Models

To create diverse services, various distributions of packet arrival rates can be exploited according to the specific services. Common arrival rate distributions encompass the Poisson distribution [127], known for modeling random arrivals, and heavy-tailed distributions [128], [129] which capture the variability and unpredictability often encountered in modern communication networks. We analyze three distinct traffic flows, each corresponding to a different set of characteristics. For the considered 3 service types, Poisson, Pareto (heavy-tailed), and Weibull (heavy-tailed) distributions for estimating the inter-arrival time of packets in the flows. The inter-arrival time for the Poisson distribution denoted τ_{Poi} is calculated from the CDF of the inter-arrival time given as

$$\mathbf{Prob}\{\tau_{\mathsf{Poi}} \leq t\} = 1 - e^{-\lambda \tau_{\mathsf{Poi}}}, \tag{3.29}$$

where τ_{Poi} is determined by taking the ratio of the negative natural logarithm of the complement of a random value uniformly sampled between 0 and 1 to the arrival rate of the Poisson-process based flow 1, which is given as

$$\tau_{\mathsf{Poi}} = -\log(1 - R_1)/\lambda_1(t). \tag{3.30}$$

The CDF of the inter-arrival time of Pareto distribution (τ_{Pa}) is given as [130]

$$\mathbf{Prob}\{\tau_{\mathsf{Pa}} \leq t\} = 1 - (\beta_{pa}/\tau_{\mathsf{Pa}})^{\eta}\,, \tag{3.31}$$

hence, the inter-arrival time of flow 2's packets assumed to follow Pareto distribution is given by

$$\tau_{\mathsf{Pa}} = [\beta_{pa}/(1-R_2)]^{(1/\eta)}/\lambda_2(t). \tag{3.32}$$

Similarly, the CDF of the inter-arrival time of the Weibull distribution (τ_{Wei}) is expressed as

$$\mathbf{Prob}\{\tau_{\mathsf{Wei}} \leq t\} = 1 - e^{-\beta_{Wei}\tau_{\mathsf{Wei}}^{\eta_1}}, \tag{3.33}$$

then, the inter-arrival time of flow 3 packets assumed to follow Weibull distribution is provided by [131],

$$\tau_{\mathsf{Wei}} = \beta_{Wei}\left[-\log(1-R_3)^{\frac{1}{\eta_1}}\right]/\lambda_3(t), \tag{3.34}$$

where β_{pa} and β_{Wei} are the scale parameters, η and η_1 are the shape parameters and R_1, R_2, R_3 are random numbers between 0 and 1. Assuming that the traffic pattern evolves over 24 hours following the trend of the dataset in [132], we generated a random number of packets per second for 10 beams, each supporting 3 distinct service types. The Probability Mass Function (PMF) of the packet arrivals for the services is shown in Fig. 3.4, and the flow of packets for the considered services varies over time as illustrated in Fig. 3.5.

For the benchmark algorithm, Lagrangian duality, the input traffic was forecasted from historical traffic demand using an LSTM RNN model. The forecasting process is explained in Section 4.3.1.

3.6.2 Numerical Results and Comparative Analysis

In this section, we analyze and compare the numerical outcomes of various approaches: DQN with one agent per flow (referred to as DQN model 1), DQN with one agent per beam (referred to as DQN model 2), DDQN with one agent per beam, D3QN with one agent per beam and the benchmark optimization approach utilizing Lagrangian duality explained in Section 2.4.2. For the DQN, DDQN, and D3QN models, the agent selects actions from an action space comprising 12 equally spaced values between 0 and the maximum capacity demand of the corresponding flows, generated using the NumPy linspace function. For DQN

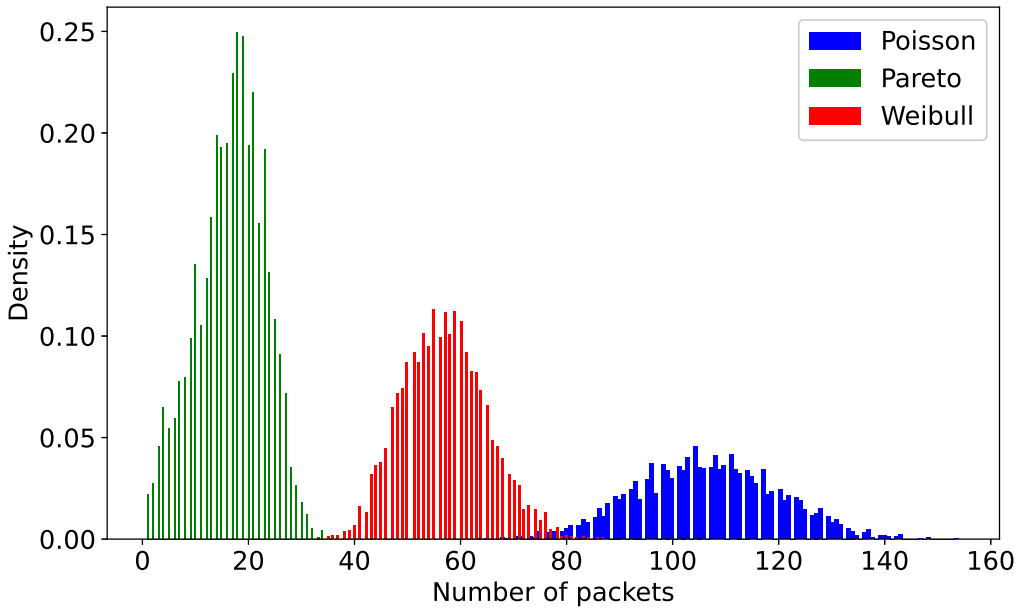

Figure 3.4: Probability mass function of the considered flows. Each value on the horizontal axis reflects an arrival rate in a TS, and the corresponding vertical coordinate shows the probability of observing that rate in that TS. The area under the function of each distribution type is 1 to indicate the sum of all probabilities is 1.

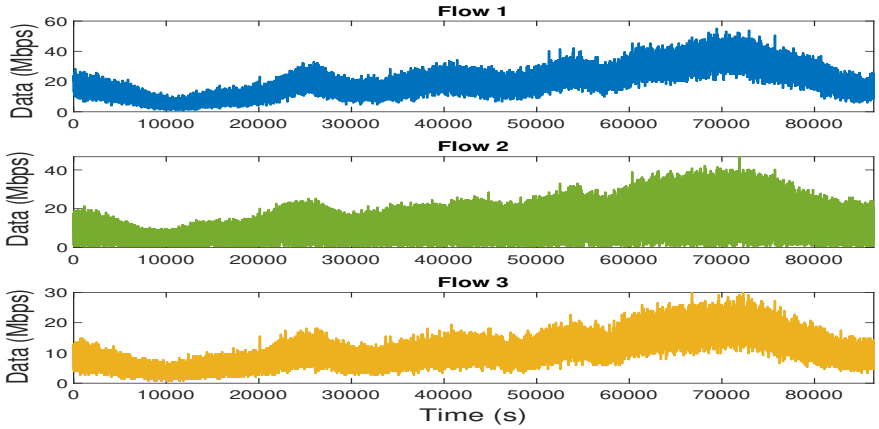

Figure 3.5: Example of time-varying traffic demand for the analyzed flows over a 24-hour period.

model 1, the epsilon decay rate (σ) value is 0.9995. If not explicitly specified, the remaining parameter values default to those listed in Table 3.2.

Fig. 3.7 shows the CDF of the demand-to-allocated capacity ratio. Flow 1 has a higher proportion of samples with lower ratios, indicating less congestion. This reflects its lower priority penalty weight compared to Flows 2 and 3, demonstrating that our CA model effectively prioritizes more critical and delay-sensitive services.

Fig. 3.6 indicates the convergence of the simulated RL algorithms concerning QL, total

Table 3.2: Considered parameter values.

Parameters	**Values**
Activation function	Relu, Linear
Cycle duration (M)	1 Hour [133]
Discount factor	0.1
Duration of 1 episode	1 day
Epsilon decay (σ)	0.9998
Loss function	MSE
Experience-replay pool size	50000 [125]
Experience-replay mini-batch size	128
Learning rate	0.01
Maximum QL (q_{max})	2 Mbytes (30 packets) [83]
Maximum capacity (W^{max})	1 Gbps
Normalized packet length	65(KBytes) [82]
Optimizer	Adam [35]
Priority weights	$[0.1, 0.3, 0.6]$
Target update ratio	0.01
Target QoE violation probability ($\bar{P}_{\mathsf{QoE}}$)	0.1 [115], [116]
Target QL (q_{QoE})	$[15, 20, 25]$ packets
The minimal exploration probability	0.001
Target BP ($\bar{P}_{\mathsf{Blk}}$)	0.05 [88]
TS duration (T_{TS})	1 Second

reward, probability of QoE violation, and total allocated capacity. Fig. 3.6a illustrates the convergence of the mean QL over episodes for the three considered flows when using the DDQN method. The figure indicates that the mean QL converges for all flows. Differences in QL values among flows are attributable to the varying target QL requirements and priority weights. Specifically, flow 1 has the lowest target QL and the highest priority weight. This incurs the lowest reward penalty during congestion, leading to the lowest mean QL for this flow. Similarly, Figs. 3.6b, 3.6c, and 3.6d indicate the reward, probability of QoE violation, and total allocated capacity convergence, respectively. The plots reveal that both D3QN and DDQN achieve similar performance and outperform both the DQN models 1 and 2. This can be attributed to the ability of D3QN and DDQN to mitigate the overestimation bias commonly encountered in DQN models. The plot also indicates that the DQN model 1 outperforms the DQN model 2 due to the use of individual agents for each flow within every beam. This approach allows each agent to specialize in a specific flow and learn to select the best action from the action space. In contrast, the DQN model 2 assigns one agent per beam, which must manage a larger action space of 12^3 possible actions, making it harder to coordinate multiple flows and resulting in lower performance.

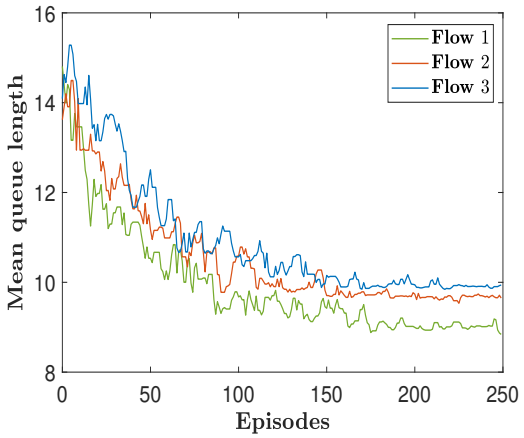

(a) Mean QL convergence.

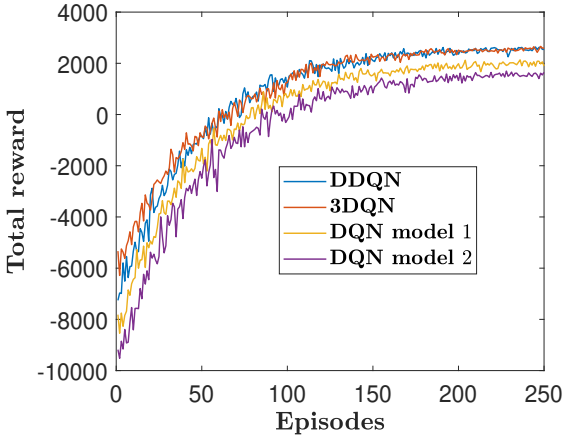

(b) Total reward convergence

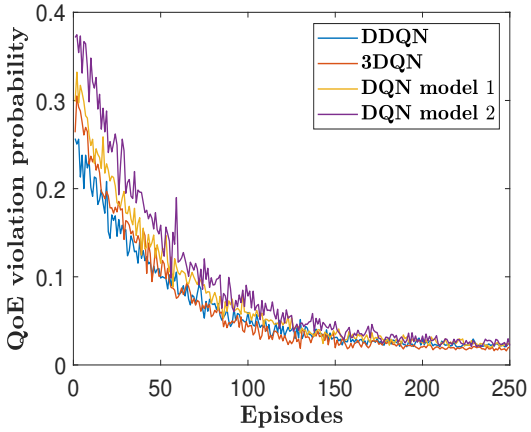

(c) Mean QoE violation probability convergence.

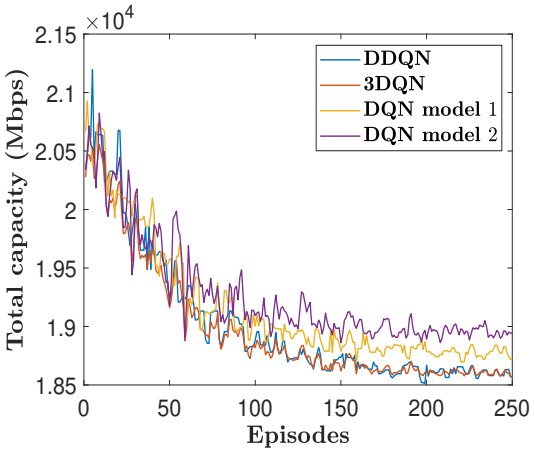

(d) Total allocated capacity convergence

Figure 3.6: Convergence plots of the implemented DQN algorithms.

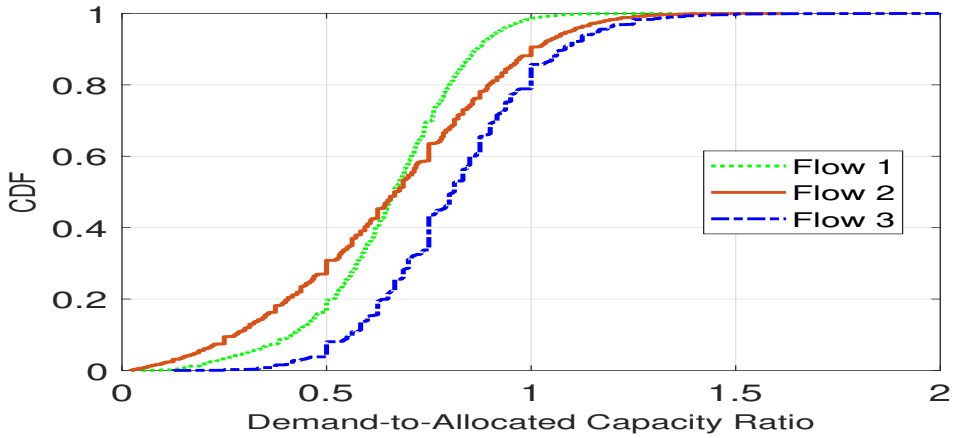

Figure 3.7: Demand to capacity ratio of all the flows.

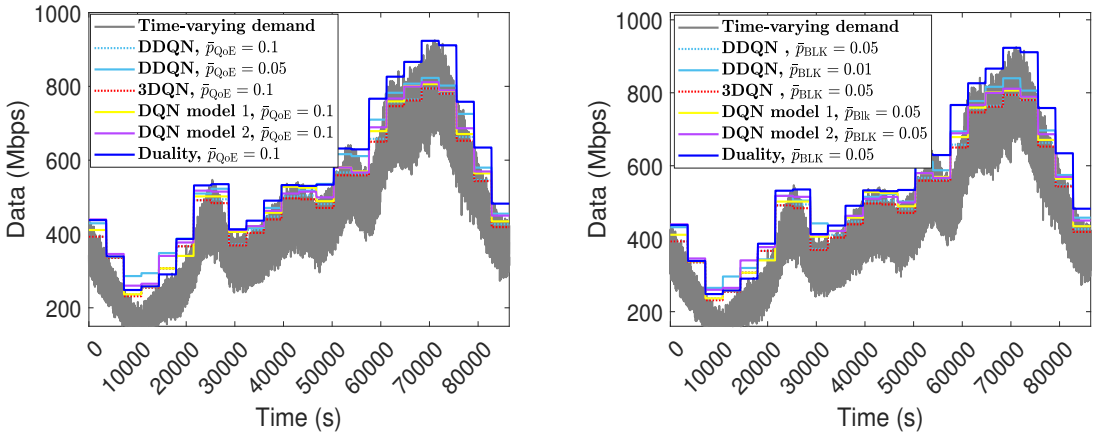

(a) Capacity at different values of $\bar{P}_{\text{QoE}}$.

(b) Capacity at different values of $\bar{P}_{\text{Blk}}$

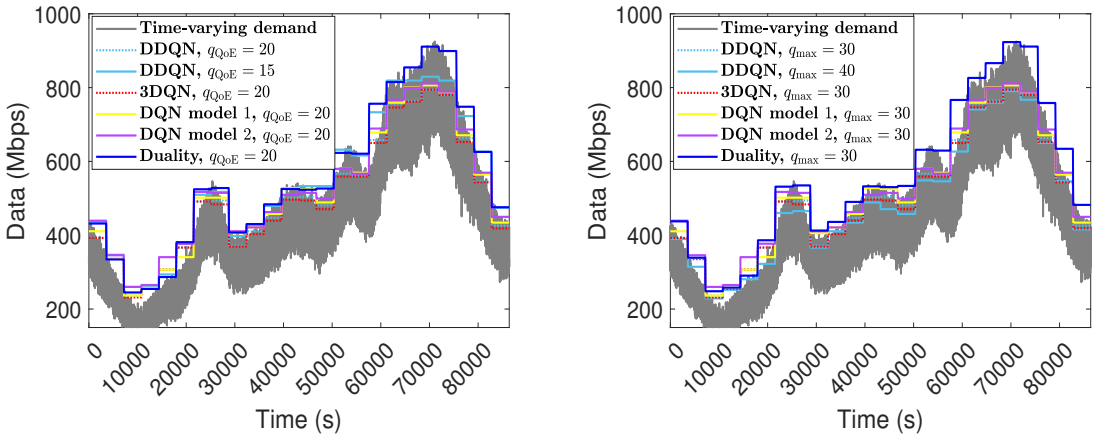

(c) Capacity at different values of q^f_{QoE}.

(d) Capacity at different values of q_{max}

Figure 3.8: Total allocated capacity per cycle and total traffic demand over time.

The plots in Fig. 3.8 indicate the total capacity allocated per cycle, along with the total traffic demand for all the simulated models. To analyze scalability and system performance under varying conditions, the total allocated capacity using the proposed DDQN model is evaluated for different values of $\bar{P}_{\text{QoE}}$, $\bar{P}_{\text{Blk}}$, q_{QoE}, and q_{max}, assuming all flows have the same target QL requirement. The total allocated capacity using the DDQN model in Figs. 3.8a and 3.8b is given at different values of the target QoE violation ($\bar{P}_{\text{QoE}}$) and target BP ($\bar{P}_{\text{Blk}}$). The plots demonstrate that the system requires allocating a higher capacity for stricter targets, such as a lower QoE violation probability (0.05) compared to a higher value (0.1) and a lower BP (0.01) compared to a higher value (0.05), consistent with the findings discussed in Section 2.5.2. In addition, the DDQN model results in Figs. 3.8c and 3.8d show the total allocated capacity per cycle at different values of target QL (q_{QoE}) and q_{max}. The plots indicate that a CA system intended for services with a higher tolerance for waiting in a

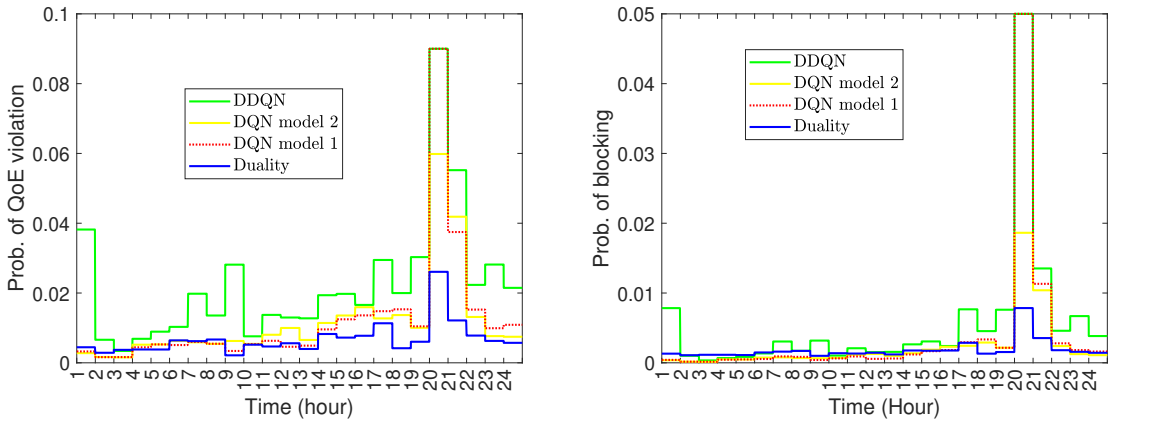

(a) Mean probability of blocking per cycle. (b) Mean probability of QoE violation per cycle.

Figure 3.9: Probability of blocking and probability of QoE violation.

queue ($q_{\mathsf{QoE}} = 20$) requires less capacity than a lower tolerance ($q_{\mathsf{QoE}} = 15$) and vice versa. Similarly, a higher value of buffer size ($q_{\mathsf{max}} = 40$) can satisfy the BP requirements with a lower allocated capacity as compared to lower values ($q_{\mathsf{max}} = 30$). This aligns with the observations in Section 2.5.2, a larger buffer size can store more packets that would likely be dropped with a smaller buffer size. However, admitted packets in a system with a large buffer size do not necessarily meet QoE requirements and may lead to buffer bloating.

From the figures we can observe that the D3QN and the proposed multi-agent DDQN demonstrate a superior performance in allocating less capacity that meets the target QoE requirement compared to the other models. Typically, the Lagrangian duality optimization approach is expected to outperform other methods. However, that approach assumes all arrivals follow a Poisson distribution which fails to accurately capture the traffic flexibility of the diverse traffic patterns of the considered flows. Furthermore, the Lagrangian duality method applied the $M_t/M_t/1$ queueing method which limits the traffic utilization ($\lambda_f^b(t)/\mu_f^b(t)$) value to remain below 1 for all time intervals. This implies that the allocated capacity always exceeds the demand, regardless of the queue state. Such an assumption can lead to an inefficient QL approximation and lower efficiency in CA, as it leaves unutilized capacity to handle any spikes in demand that may exceed the optimal capacity. Consequently, when evaluating the trade-offs between efficiency, adaptability, and scalability, deep learning approaches emerge as promising solutions for QoE-aware dynamic CA in 5G networks.

Figs. 3.9a and 3.9b indicate the mean blocking and QoE requirement violation probability per cycle, respectively. The plots demonstrate that all models achieve a value lower than

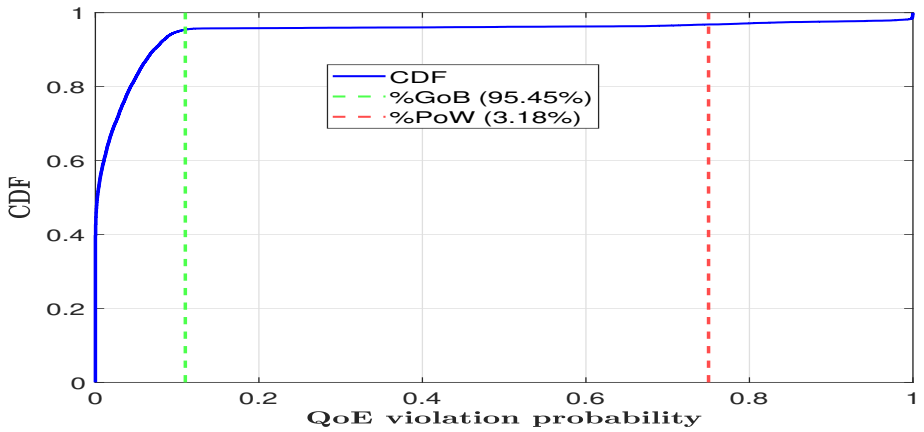

Figure 3.10: CDF Plot of QoE Violation Probability: This plot shows the percentage of good or better (%GoB) and poor or worse (%PoW) experiences based on the specified target QoE requirement violation probability of 0.1 for good or better, and the worst 25% for poor or worse.

the target value of 0.05 for BP and 0.1 for QoE requirement, indicating their effectiveness. Moreover, these figures, along with Fig. 3.8, demonstrate that the D3QN and DDQN methods, which exhibit nearly identical performance, outperform the other methods considered in terms of meeting the target requirements with relatively lower allocated capacity.

We can also assess the efficiency of our model by comparing the obtained QoE violation probability results with experimental metrics. These metrics are based on MoS measurements, categorized as a percentage of good or better (%GoB) and poor or worse (%PoW), as described in [115] and [116]. As we do not consider users in our work, we consider the probability of QoE violation per cycle for different samples after the model is trained. As shown in Figure 3.10, our model achieves a performance equivalent to the acceptability level of a service with excellent quality, indicated by a MOS above 4.5.

Table 3.3 shows the total runtime of the simulated algorithms on a High Performance Computer (HPC) system using Python 3.8.6 and GCCcore 10.2.0 with 28 CPU cores. From the table, we can observe that the trained DDQN, D3QN and DQN models have faster inference time compared to the optimization approach, indicating their effectiveness in handling time-varying demands with different arrival rate distributions. The total time and average time per episode needed for DQN model 1 are higher than the other DRL models. This is because model 1 assumes one agent per flow and requires a total of 30 agents, necessitating a more complex DQN model architecture compared to DQN model 2, D3QN and DDQN, which assume one agent per beam (10 agents in total). DDQN emerges as a balanced choice, offering a reasonable average time per episode and total convergence time while achieving comparable

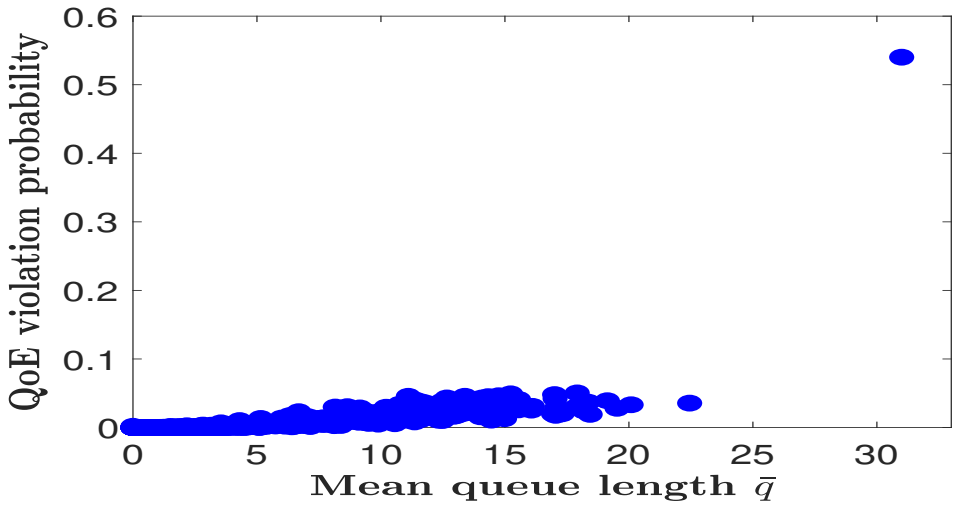

Figure 3.11: Figs/Mean QL versus Probability of QoE violation.

performance to D3QN. While D3QN slightly outperforms DDQN, its higher time complexity makes DDQN a more computationally efficient choice. The increased computational complexity of DDQN compared to DQN model 1 and DQN model 2, is due to the separate action selection and evaluation steps. Similarly, D3QN introduces higher complexity than DDQN by decoupling the state value and action advantage when calculating Q-values, requiring additional computation to combine them. The scatter plot in Fig. 3.11 illustrates the relationship between the mean QL and the probability of QoE violation probability, taking the capacity values obtained using DDQN. The results reveal a clear trend: as the mean QL increases, the likelihood of QoE violations also rises. This correlation underscores we can accurately estimate the demand-capacity relationship, allowing for more effective CA strategies.

In summary, DDQN, D3QN, and DQNs demonstrate comparatively better efficiency in handling various arrival distribution types, optimizing total allocated capacity, and exhibiting inherent adaptability, making them invaluable for meeting the unpredictable demands of dynamic environments as compared to the benchmark method. The main reason for this efficiency is the assumption of different arrival distribution types for all flows in the proposed method, in contrast to the optimization approach that assumes a Poisson process for all flows. Selecting the optimal strategy among the models requires balancing computational resources, system complexity, and the need for tailored decision-making. In our specific simulation, we propose the DDQN model as it shows almost the same performance but lower complexity as compared to D3QN, and better performance than DQN models 1 and 2.

Table 3.3: Convergence time of the simulated algorithms.

Algorithm	**Average time per episode (s)**	**Total convergence time (s)**	**Episodes to converge**
DQN model 1	440.94	110235.755	250
DQN model 2	244.96	61242.086	250
DDQN	273.29	68324.367	250
D3QN	329.85	82463.45	250
Duality	1228.36	122836	100

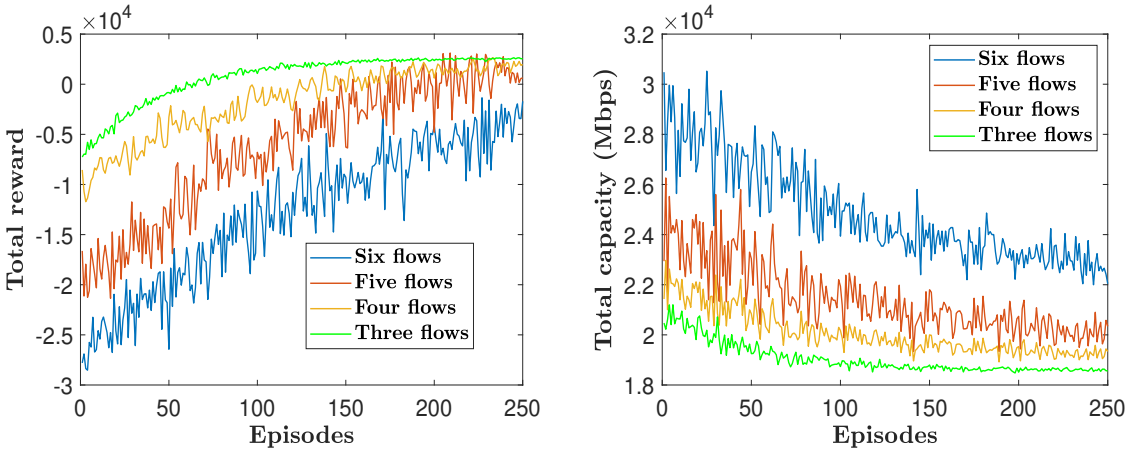

(a) Reward convergence.

(b) Capacity convergence.

Figure 3.12: Convergence for different number of flows.

3.6.3 Impact of Increased Number of Flows on Convergence

Managing CA for thousands of service types with QoE-specific requirements poses significant challenges, particularly when considering the computational burden of a large state and action space. To address this, similar service types can be grouped based on QoE requirements, traffic patterns, or priority levels, resulting in fewer traffic flows. The three traffic flow distributions considered in this study, Poisson, Pareto and Weibull represent many existing service types [127–129]. However, a substantial number of service groups may follow other distribution types.

In this subsection, we extend our analysis to include additional traffic arrival patterns: Normal, Exponential, and Gamma distributions. These distributions collectively capture a wide range of packet arrival distributions observed in real-world service types. To evaluate the impact of the number of flows, we simulate and compare scenarios with three, four, five, and six flows using a DDQN-based model. Action masking is applied in scenarios with four, five, and six flows to reduce the action space by removing action combinations that

exceed the maximum capacity. The convergence results are presented in Figure 3.12. The simulations indicate that models with fewer flows (three) converge faster than those with more flows. This behavior can be attributed to the increased complexity of managing a larger state and action space with additional flows, and the heightened traffic variability resulting from greater variations in arrival distributions. Despite this, the convergence trends are promising, showing an increasing trajectory in the reward and a decreasing trajectory in the capacity convergence. These trends suggest that, although increased flows demand more computational resources and training episodes to reach convergence, the model is capable of achieving optimal performance with further training or the application of complexity-reducing techniques. The results underscore the importance of balancing computational feasibility with the accuracy of CA models in scenarios involving a larger number of traffic flows.

3.7 Conclusion

This chapter proposed a QoE-aware flexible CA mechanism, leveraging multi-agent DDQN, that offers significant advancements in optimizing capacity utilization while prioritizing QoE across multiple services. The mechanism exhibits resilience in dynamically adapting to fluctuating traffic demand, ensuring consistent performance and user satisfaction. The simulation results demonstrate that the proposed method enhances the overall capacity utilization efficiency and QoE across various satellite services.

Chapter 4

Proactive Traffic Matching and Load Balancing

4.1 Introduction

The drive for increased capacity in GEO SatCom systems has led to a growing interest in the utilization of Extremely High Frequency (EHF) bands such as Ka, Q, and V bands, where larger bandwidths are available. Leading operators such as SES, Eutelsat, Telesat, and Viasat are exploring these bands to provide high capacity broadband services [41–43, 134]. While these bands offer expanded bandwidth, they introduce significant challenges: unpredictable rain attenuation severely affects feeder link (FL) performance, and dynamic, uneven traffic demand across multi-beam, multi-gateway (GW) networks creates congestion and service degradation [135], [136], [137]. These uncertainties often lead to critical challenges for managing resource allocation, traffic steering, and persistent GW load imbalances to serve distributed users efficiently [138]. It is further complicated by the heterogeneous time-varying traffic demand from various users. Moreover, satisfying QoE and BP requirements further requires adaptive solutions that can predict network conditions and intelligently balance traffic in real time [139].

In response to changing network conditions, it is essential to adopt dynamic B2G matching strategies informed by accurate, real-time predictions not only of traffic demand but also of the evolving effective capacity of each GW under current channel conditions. When certain GWs experience overload due to elevated demand or adverse weather, traffic must be proactively redistributed to underutilized GWs to prevent congestion and maintain service

continuity [140]. Furthermore, even during periods of low demand, keeping all GWs engaged ensures the system can promptly accommodate sudden load surges without delays associated with reactivation. Such a capacity-aware, predictive management approach enables full utilization of the existing infrastructure, enhances network resilience, and sustains consistent, high-quality service under dynamic operating conditions. However, existing GW traffic management solutions often rely on reactive mechanisms, leading to delayed responses to congestion or rain attenuation [141]. These approaches lack real-time adaptability, resulting in service outages and inefficient resource utilization. To address this, this paper leverages a stacked multi-output, multi-horizon Long Short-Term Memory (LSTM) model to predict per-beam traffic demand and per-GW rain attenuation. These forecasts are then used as inputs to an adaptive genetic algorithm that performs proactive, capacity-aware B2G matching and load balancing (LB), aiming to maximize GW utilization and meet QoE and BP targets.

4.1.1 Related Works

Advanced artificial intelligence (AI) models, particularly deep neural networks (DNN), have been widely applied to predict rain attenuation in satellite FLs. For example, [142, 143] employed deep learning techniques to forecast rain-induced fading in the EHF bands, offering valuable tools to mitigate weather-related impairments. Similarly, DNN-based models have been used to forecast traffic demand for enhanced resource management [144, 145]. However, these two aspects, rain attenuation prediction and traffic forecasting, are typically treated in isolation, without accounting for their joint impact on GW resource planning. Moreover, the prior works rely on single-step forecasts, which provide only a short-term view and are insufficient for proactive decision-making that requires foresight over multiple future intervals. There remains a critical gap in integrating both aspects into a unified framework capable of dynamically adapting to simultaneous weather fluctuations and traffic variations, enabling more effective and resilient GW resource management.

Various techniques have been explored to enhance resource allocation under rain-fading channels. Notably, machine learning-based adaptive modulation and coding, power control, and rate adaptation are discussed in [146, 147]. However, such techniques are primarily employed to mitigate minor rain attenuation and are not specifically designed to address system-level traffic demand variations. Moreover, they are typically applied in the context of a single FL (single GW). In addition to the above methods, satellite GW diversity (SGD)

is an effective solution to reduce system outages by rerouting all the traffic from the fading GWs to the unfading ones [141], [148], [149]. However, SGD has drawbacks regarding GW redundancy and resource utilization (under-utilization). GW switching is another important research well studied in the literature [150], [151]. However, these works are based on reactive GW switching when rain events occur. Immediate switching in response to such events can introduce latency and potentially lead to service interruptions. Furthermore, the aforementioned works fail to account for traffic demand variations in their GW-switching decisions. They also overlook the importance of LB among GWs, the QoE, and the BP requirements.

Efficient LB among satellite GWs is a topic discussed in the literature. The most common techniques typically employ LB routing [152], LB traffic management [153], and QoS/QoE aware LB [139]. However, the papers mentioned above assume that traffic demand and environmental attenuation are well-known in advance. While not directly related to satellite GW LB, various methods such as ant colony optimization [28] have been explored for user association and LB. Additionally, LB approaches based on remaining capacity [154] and weighted strategies [155] have been employed in the context of 5G cloud services.

4.1.2 Contributions

Despite notable progress in satellite GW resource management, a clear research gap remains in integrating traffic demand forecasting, FL rain attenuation prediction, B2G traffic matching, LB, and simultaneous fulfillment of QoE and BP requirements. This work addresses this gap by developing an AI-driven proactive framework for beam traffic assignment and GW LB, explicitly designed to maintain QoE and BP constraints. In contrast to previous reactive GW-switching methods, our approach proactively optimizes traffic distribution based on jointly forecasted rain attenuation and traffic demand, enabling dynamic and capacity-aware resource management. To the best of our knowledge, no existing study has explored this comprehensive, multi-faceted approach. Our primary contributions are as follows.

- We employ stacked multi-horizon multi-output LSTM models to forecast traffic demand per beam and rain attenuation per GW. It offers accurate estimates of future traffic and attenuation for multiple beams and GWs in various time intervals. This approach provides a robust input for a comprehensive traffic management model that dynamically adjusts to variations in demand and capacity.

- Using predicted traffic demand and rain attenuation, we proactively determine B2G matching and optimize the capacity needed to meet stochastic QoE and BP requirements.
- Developing a proactive and adaptive LB framework across GWs to prevent any single GW from overloading while ensuring that the available capacity in other GWs is properly utilized.
- We formulate a stochastic non-convex mixed-integer program, which is challenging to directly solve due to the high search space. We then approximate it into a two-stage problem and used a lower-complexity adaptive genetic algorithm for a near-optimal solution.

4.2 System model and problem formulation

Consider a forward end-to-end SatCom system, where a GEO satellite (GEOSat) with a bent-pipe (non-regenerative) payload connects to G GWs via FLs, generates B beams to provide radio access service to multiple ground users, as depicted in Fig. 4.1. Here, the FL communication between GWs and GEOSat is operated via the Q/V or Ka-bands, while the user-link transmission is processed over the Ku bands. Each beam in this system (beam $b \in \{1, ..., B\}$) covers a specific ground cell, where users are located and generate diverse downlink service requests. We consider a total system operation period of T time slots (TS). In each TS t, the traffic demand from all users in beam b is retrieved from the core network and aggregated into a flow of L-bit packets arriving at a rate $\lambda^b(t)$ modeled as a Poisson process.

In this work, we assume that the channels connecting the GWs and GEOSat fluctuate over time due to weather conditions. Denote the time-varying attenuation on the FL of GW g at TS t as $A_g(t)$ (dB). Assuming flat fading with respect to the FL carrier bandwidth and no interference due to frequency orthogonalization or antenna directivity, the corresponding channel gain can be calculated as

$$a_g(t) = 10^{A_g(t)/10}. \tag{4.1}$$

Then, the maximum available FL capacity of GW g can be written as

$$C_g^{\mathsf{fd,max}}(t) = W^{\mathsf{fd}} \log\left(1 + P^{\mathsf{fd}} a_g(t)/\sigma^2\right), \tag{4.2}$$

where $C_g^{\mathsf{fd,max}}$ is the maximum FL capacity of GW g, W^{fd} and P^{fd} represent the FL bandwidth (Hz), GW transmit power (watts), and σ^2 is the noise power (Watts).

4.2.1 B2G Matching and Data Traffic Steering at GWs

Regarding B2G matching and data traffic steering at GWs, we first introduce a binary variable $\vartheta_{g,b}(t)$ that

$$\vartheta_{g,b}(t) = \begin{cases} 1, & \text{if data of beam } b \text{ is steered} \\ & \text{over FL of GW } g \text{ in TS } t, \\ 0, & \text{otherwise.} \end{cases} \tag{4.3}$$

In this work, the traffic demand of beam b is assumed to be handled by a single[1] GW which yields:

$$\sum_{g \in \mathcal{G}} \vartheta_{g,b}(t) = 1, \quad \forall b, t, \tag{4.4}$$

where $\vartheta_{g,b}(t)$ is a binary B2G matching variable and $\mathcal{G}$ stands for the set of all GWs. We further denote $f_{g,b}(t)$ (bps) as the FL capacity of GW g allocated to serve the traffic flow of beam b in TS t. To prevent packet drops, the traffic throughput transmitted through any GW's FL should not exceed its maximum capacity, which yields:

$$\sum_{b \in \mathcal{B}} \vartheta_{g,b}(t) f_{g,b}(t) \leq C_g^{\mathsf{fd,max}}(t), \quad \forall g, \tag{4.5}$$

where $\mathcal{B}$ represents the set of all beams. We note that $f_{g,b}(t)$ is always non-negative.

$$f_{g,b}(t) \geq 0, \quad \forall g, \forall b. \tag{4.6}$$

[1] While current systems handling multiple services may support beam traffic assigned to multiple GWs, the assumption of matching beam traffic to a single GW remains appropriate under aggregate traffic modeling.

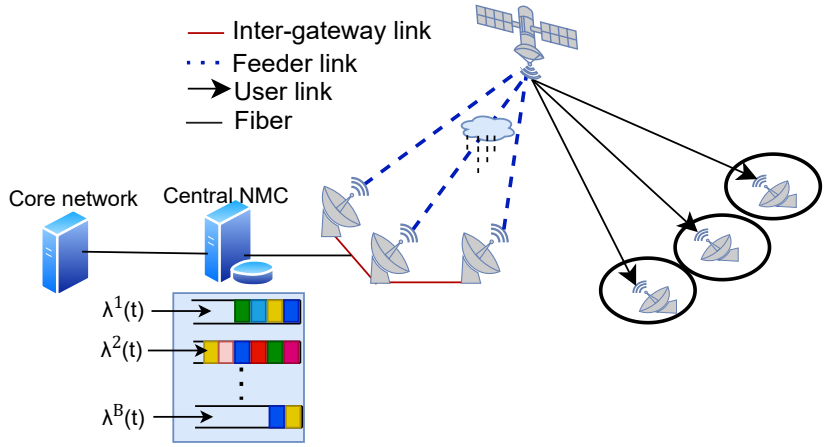

Figure 4.1: System model illustrating traffic management.

If we denote $\ell_g(t) \in [0,1]$ as a load factor for each GW g, which measures the proportion of its capacity used relative to its maximum available capacity, it is given by

$$\ell_g(t) = \sum_{b \in \mathcal{B}} \vartheta_{g,b}(t) f_{g,b}(t) / C_g^{\mathsf{fd,max}}(t). \tag{4.7}$$

For practical operation, we assume that B2G traffic management and matching are centrally coordinated by a network management center (NMC). Furthermore, $\vartheta_{g,b}(t)$ and $f_{g,b}(t)$ remain fixed over a cycle of M TSs, after which they can be updated. As a result, the system operates over $K = \frac{T}{M}$ cycles, during which B2G matching and CA decisions are made[2]. Hence, $\forall t \in [(k-1)M+1, kM]$, we have the following constraint,

$$f_{g,b}(t) = f_{g,b}^k, \quad \ell_g(t) = \ell_g^k, \quad \vartheta_{g,b}(t) = \vartheta_{g,b}^k, \quad \text{and} \quad C_g^{\mathsf{fd,max}}(t) = C_g^{\mathsf{fd,max}}(k), \tag{4.8}$$

where $\vartheta_{g,b}^k$ and $f_{g,b}^k$ represent the B2G matching and FL capacity of GW g allocated to serve beam b in cycle k, respectively.

4.2.2 Queue Length and QoE Requirement

Assume that there are B buffers assigned for B traffic flows corresponding to each beam at the NMC. The queue length (QL) corresponding to the traffic of beam b at any time t

[2]Per-TS decisions incur high signaling and computation overhead; thus, the NMC performs centralized B2G matching and allocation per cycle, whose duration M is defined based on operator system capabilities.

is determined by the arrival rate $\lambda^b(t)$ and service rate $\mu^b(t)$. The service rate represents the transmission capacity (packets per second) the NMC allocates to the GW responsible for handling packets associated with beam b during the specified cycle. Here, $\mu^b(t)$ given in Equation 2.5 can be expressed as

$$\mu^b(t) = \sum_{g \in \mathcal{G}} \vartheta_{g,b}(t) f_{g,b}(t)/L, \tag{4.9}$$

Let $f_b(t) = \sum_{g \in \mathcal{G}} \vartheta_{g,b} f_{g,b}(t)$. Then we have,

$$\mu^b(t) = f_b(t)/L. \tag{4.10}$$

Let $q^b(t)$ denote the QL of data packets stored in the NMC buffer corresponding to beam b at time t. The design in this work focuses on fulfilling QL requirements of the buffer corresponding to beam b to satisfy the QoE and BP requirements given in Equations 2.6 and 2.7 over the window time of $[0, T]$. The requirements are re-expressed as

$$\frac{1}{T} \int_0^T Pr\{q^b(t) \geq q^{\mathsf{QoE}}\} dt \leq \bar{P}_{\mathsf{QoE}}, \forall b, \tag{4.11}$$

and

$$Pr\{q^b(t) \geq q^{\mathsf{max}}\} \leq \bar{P}_{\mathsf{Blk}} \quad \forall (t, b). \tag{4.12}$$

4.2.3 Problem Formulation

This paper considers a stochastic optimization problem for an optimal B2G matching, aiming to achieve a balanced load distribution among the GWs. To ensure that no single GW becomes a bottleneck, thereby promoting a more balanced and efficient load distribution, we need to minimize the expected maximum load, which can be stated as

$$\min_{\{f_{g,b}(t)\}, \{\vartheta_{g,b}(t)\}} \max_g \mathbb{E}_T \left[\ell_g(t)\right], \tag{4.13a}$$

subject to:

$$(4.4), (4.5), (4.6), (4.8), (4.11), (4.12), \tag{4.13b}$$

where $\mathbb{E}_T \left[\ell_g(t)\right] = \frac{1}{T} \sum_{t=1}^{T} \ell_g(t)$ and (4.5) indicates that the FL capacity connecting any GW g and the satellite should be higher than the combined traffic throughput transmitted

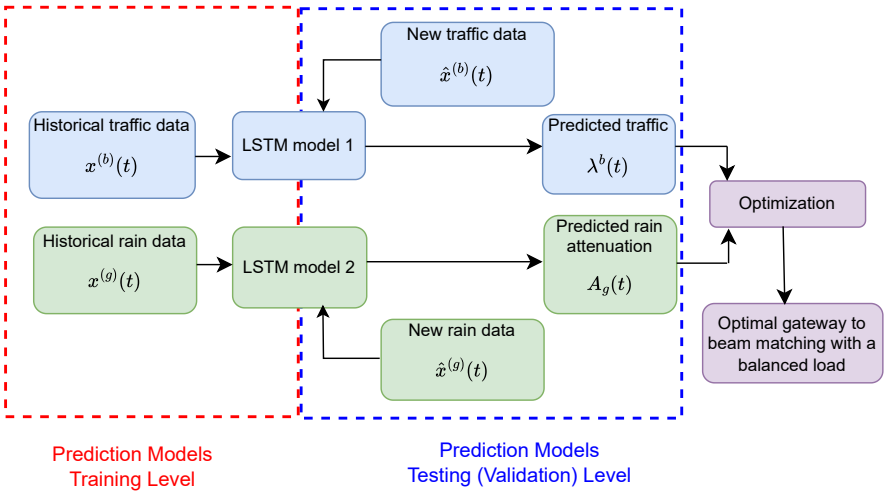

Figure 4.2: Proposed method.

through it; (4.6) indicates the FL capacity of GW g allocated to serve the traffic of beam b is non-negative; while (4.11) and (4.12) indicate the QoE and BP requirements. Herein, (4.4), (4.11), and (4.12) are non-convex; then, the problem is a non-convex mixed-integer program. Therefore, a globally optimal solution for this problem cannot be achieved using the standard convex optimization tools [26].

To solve this complicated problem, we first predict per-beam traffic demand and FL rain attenuation for the upcoming cycle. Based on these predictions, we apply an optimization approach to determine the optimal B2G matching and LB. An overview of the solution methodology is summarized in Fig. 4.2.

4.3 Data-driven Traffic Demand and Rain Attenuation Prediction

The methods for predicting traffic demand and rain attenuation are detailed in Sections 4.3.1 and 4.3.2 respectively.

4.3.1 Traffic Demand Prediction

Designing optimal B2G matching, LB, and CA with minimal service outage is challenging without knowledge of the time-varying traffic demands. To address this, it is necessary to predict incoming traffic for the next cycle. Fortunately, historical traffic data collected by operators and satellite SPs [156] makes such prediction feasible. Among various forecasting

techniques, the LSTM model has proven particularly effective due to its ability to capture long-term dependencies and patterns in sequential time series data, outperforming alternatives like RNN and GRU in prediction accuracy [157]. LSTM models have been successfully applied to traffic forecasting in both terrestrial and satellite networks [144], making them well-suited for optimizing modern communication systems. The following sections detail how the LSTM model is employed in this study to predict traffic demand.

Data Set Preparation and Pre-processing

Obtaining a readily available traffic data set with a resolution per beam in multiple beams is challenging. Initially, we modeled the hourly traffic demand over a single day for the first 3 beams by fitting the traffic trend available in [132], and for 2 additional beams based on the traffic patterns reported in [156]. Given the limited availability of long-term historical traffic data across all beams, and to avoid uniform peak and off-peak patterns across beams and cycles, we applied scaling and time-shifting to the remaining 15 beams' to achieve a multi-beam dataset.

Since operator-collected datasets are typically aggregated at hourly, daily, weekly, or monthly levels, they are not directly suitable for short-interval traffic prediction (e.g., seconds or minutes). To address this, we used hourly traffic data to generate packet-level traffic flows following IEEE standards [158], modeled using a Poisson arrival process. For each beam, we generated minute-level traffic demand data spanning three months. To ensure uniform scaling across samples, we applied Min-Max normalization to the dataset. Fig. 4.3 illustrates the temporal variation in input traffic demand for three randomly selected beams.

Once the dataset is prepared, it is converted into a form that can be used for training and prediction by preparing a sequence of inputs and outputs. As shown in Fig. 4.4, let S denote the sequence length (i.e., the number of observed values used as input), H the prediction horizon (i.e., the number of future steps to forecast), and Z the number of training sequences per beam per cycle. Let $\{x_t^{(b)}\}_{t=1}^{\hat{T}}$ denote the traffic demand time series for beam b, where $\hat{T}$ is the total number of time steps. The goal is to predict the next H future values of each beam based on the past S observed values. For each beam, the training dataset is constructed using a sliding window of size $S+H$, resulting in $Z = \hat{T} - S - H + 1$ training samples. Here,

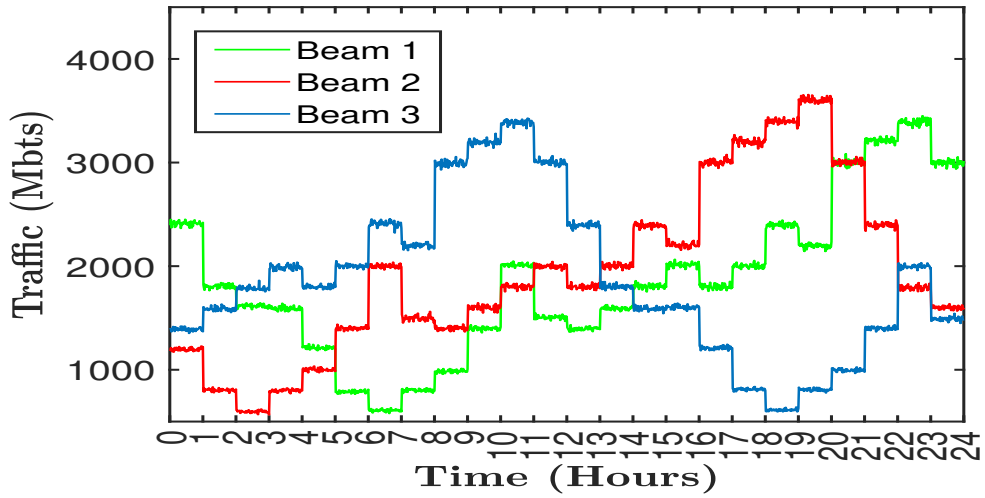

Figure 4.3: Input traffic demand for randomly selected beams.

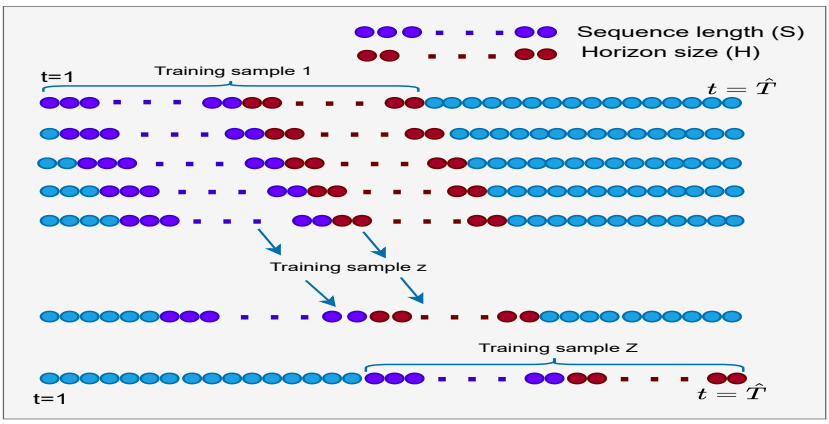

Figure 4.4: Illustration of LSTM training sample sequence preparation.

each training sample consists of an input sequence given as

$$\mathbf{X}^{(i,b)} = [x_i^{(b)}, x_{i+1}^{(b)}, \ldots, x_{i+S-1}^{(b)}] \in \mathbb{R}^S, \tag{4.14}$$

and a target output sequence given as

$$\mathbf{Y}^{(i,b)} = [x_{i+S}^{(b)}, x_{i+S+1}^{(b)}, \ldots, x_{i+S+H-1}^{(b)}] \in \mathbb{R}^H, \tag{4.15}$$

which results in a training dataset given by

$$\mathcal{D}^{(b)} = \left\{ \left(\mathbf{X}^{(i,b)}, \mathbf{Y}^{(i,b)} \right) \mid i = 1, \ldots, Z \right\}. \tag{4.16}$$

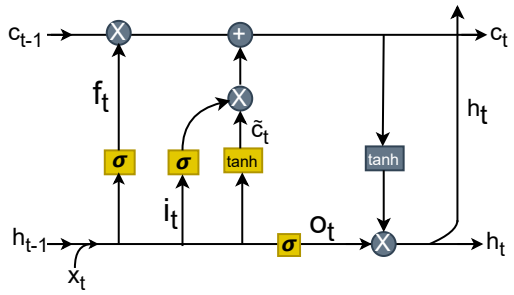

Figure 4.5: LSTM cell illustration.

LSTM Model Architecture

Among the well-known LSTM time series prediction techniques, such as vanilla, bidirectional, stacked, and convolutional, stacked LSTMs offer an effective balance between model capacity and training complexity, particularly for unidirectional, multi-step forecasting tasks [159]. By processing data through multiple layers of memory cells, stacked LSTMs can capture more intricate temporal patterns. Additionally, predicting each short-interval time slot independently would require running the model repeatedly, increasing computational load. To address this, we adopt a multi-horizon prediction approach, forecasting all time slots within the next cycle in a single run, as demonstrated in [160]. Accordingly, each beam is modeled with a dedicated two-layer stacked LSTM, designed to forecast traffic demand across all upcoming time slots efficiently.

The LSTM cell, along with its components—the input gate, forget gate, output gate, hidden state, and cell state of the LSTM model is crucial for regulating information flow and maintaining long-term dependencies during the prediction process. The cell state ($\mathbf{c}_t$) serves as the long-term memory, updated by the input ($\mathbf{i}_t$), forget ($\mathbf{f}_t$), and output ($\mathbf{o}_t$) gates. The hidden state ($\mathbf{h}_t$) represents the short-term memory used for predictions at each time step, influenced by the cell state and output gate. An illustration of the LSTM components is provided in Fig. 4.5. Since we have B models, the gates and the states for any beam b are

updated as

$$\mathbf{i}_t^b = \sigma(\mathbf{W}_{ix}^b \mathbf{x}_t^b + \mathbf{W}_{ih}^b \mathbf{h}_{t-1}^b + \mathbf{b}_i^b) \tag{4.17a}$$

$$\mathbf{f}_t^b = \sigma(\mathbf{W}_{fx}^b \mathbf{x}_t^b + \mathbf{W}_{fh}^b \mathbf{h}_{t-1}^b + \mathbf{b}_f^b) \tag{4.17b}$$

$$\mathbf{o}_t^b = \sigma(\mathbf{W}_{ox}^b \mathbf{x}_t^b + \mathbf{W}_{oh}^b \mathbf{h}_{t-1}^b + \mathbf{b}_o^b) \tag{4.17c}$$

$$\tilde{\mathbf{c}}_t^b = \tanh(\mathbf{W}_{cx}^b \mathbf{x}_t^b + \mathbf{W}_{ch}^b \mathbf{h}_{t-1}^b + \mathbf{b}_c^b) \tag{4.17d}$$

$$\mathbf{c}_t^b = \mathbf{f}_t^b \odot \mathbf{c}_{t-1}^b + \mathbf{i}_t^b \odot \tilde{\mathbf{c}}_t^b \tag{4.17e}$$

$$\mathbf{h}_t^b = \mathbf{o}_t^b \odot \tanh(\mathbf{c}_t^b), \tag{4.17f}$$

where $\mathbf{W}^b$'s represent the weights, $\mathbf{b}^b$'s are the biases, $\tilde{\mathbf{c}}_t^b$'s are the candidate cell state and $\mathbf{c}_t^b$'s are the final cell states. Once the LSTM processes the sequence and produces $\mathbf{h}_t^{(b)}$, we use the dense layer to map it to the desired prediction. Since our LSTM model is multi-horizon it outputs all future steps at once as follows:

$$\hat{\mathbf{y}}_{t+1:t+H}^{(b)} = \mathbf{W}_y^{(b)} \mathbf{h}_t^{(b)} + \mathbf{b}_y^{(b)}. \tag{4.18}$$

Training Process

Our training process spans 100 epochs, during which the LSTM processes the entire training dataset and adjusts its weights through forward and backward propagation through time. To optimize memory usage and computational efficiency, appropriate batch sizes of 256 is considered. Additionally, to prevent the model from becoming too reliant on specific neurons and to avoid overfitting, a dropout rate of 0.2 is applied. The dropout technique involves randomly deactivating a fraction of input units, effectively regularizing the model and minimizing the risk of overfitting. Our model is trained utilizing traffic demand data spanning over 89 days.

Model Evaluation

Following the training phase, we must ensure the model generalizes to unseen data. Hence, after training our model, we evaluated the performance using data from the subsequent (90^{th}) day. This evaluation was conducted over 96 cycles, each with a duration of 15 minutes. The prediction loss per beam, considered as a performance metric, is calculated using mean

squared error (MSE) as follows:

$$\mathcal{L}^{(b)} = \frac{1}{ZH} \sum_{i=1}^{Z} \sum_{h=1}^{H} \left(\hat{x}^{(b)}_{i+S+h-1} - x^{(b)}_{i+S+h-1} \right)^2, \tag{4.19}$$

where $\hat{x}^{(b)}_{i+S+h-1}$ is the models prediction of the next value and $x^{(b)}_{i+S+h-1}$ is the ground true next value.

4.3.2 Rain Attenuation Prediction

Accurate prediction of rain attenuation events is essential because weather conditions, particularly rain, significantly impact signal quality and FL capacity. In the following sections, we explain the dataset preparation, the model architecture, the training method, and the validation process.

Data Set Preparation and Preprocessing

To facilitate accurate LSTM predictions, we first need to gather and prepare the necessary data. Accordingly, we considered 3 years (1.1.2022–1.1.2025) of historical rain rate (R) data for the SES GEO GWs in Luxembourg, Munich (Germany), and Stockley (UK), obtained from [161] on a daily granularity. Using the collected rain rate data, we apply ITU model standards to convert these rain rates (precipitation levels) into attenuation values [162–164] at the receiver end. Given the meteorological rain rate $R(t)$, the corresponding rain attenuation of the FL connecting GW g to the satellite is calculated based on the ITU-R P.838-3 standard for rain attenuation modeling as follows:

$$A_g(t) = \mathcal{K} R_g^{\alpha}(t) * d, \tag{4.20}$$

where $\mathcal{K}$ and α are frequency and polarization-dependent constants given in a tabular format as in [165], d is the path length over which the signal travels with rain, and $R_g(t)$ is the rain rate at time t. The FL attenuation values per cycle are synthesized using a log-normal distribution[3]. The corresponding time-varying FL capacity is given as in Equation 4.2 with

[3] Although the log-normal distribution provides a good approximation of the daily rain distribution at the cycle level, satellite operators need to collect rain events at a granularity matching the cycle duration or smaller time intervals for practical rain attenuation prediction.

the Signal to Noise Ratio (SNR) obtained as

$$SNR_g(t) = P^{\mathsf{fd}} a_g(t)/\sigma^2. \tag{4.21}$$

To assess the independence of rain attenuation across the three GW locations, we computed Pearson correlation coefficients [166] on rain rate data over the study period. The results showed weak correlations, indicating that rain events at different GWs are largely independent; Fig. 4.6 presents the correlation matrix supporting this observation.

Following a similar notation as in the traffic prediction case, let $\{x_t^{(g)}\}_{t=1}^{T'}$ denote time series rain attenuation for the FL of GW g, where T' is the total number of time steps. The goal is to predict the next time step based on the preceding S' time steps. The training dataset is constructed for each GW using a sliding window of size $S'+1$, resulting in $Z' = T' - S'$ training samples. Here, the input sequence of each training sample is given as

$$\mathbf{X}^{(i,g)} = [x_i^{(g)}, x_{i+1}^{(g)}, \ldots, x_{i+S'-1}^{(g)}] \in \mathbb{R}^{S'}, \tag{4.22}$$

and the target output sequence is defined as

$$\mathbf{Y}^{(i,g)} = [x_{i+S'}^{(g)}] \in \mathbb{R}^1, \tag{4.23}$$

to provide a training dataset of:

$$\mathcal{D}^{(g)} = \left\{ \left(\mathbf{X}^{(i,g)}, \mathbf{Y}^{(i,g)} \right) \mid i = 1, \ldots, Z' \right\}. \tag{4.24}$$

LSTM Model Architecture

Similar to the traffic demand prediction, the rain attenuation prediction applies the stacked multi-input, multi-output LSTM architecture with dropout. Here, the LSTM model predicts attenuation for multiple FLs, each corresponding to a ground GW susceptible to rain fading. The independence in rain attenuation between GWs is preserved by training separate models, allowing for parallel and decoupled learning without requiring inter-GW dependencies. Similar to traffic prediction, each GW is modeled using a dedicated stacked LSTM. The LSTM

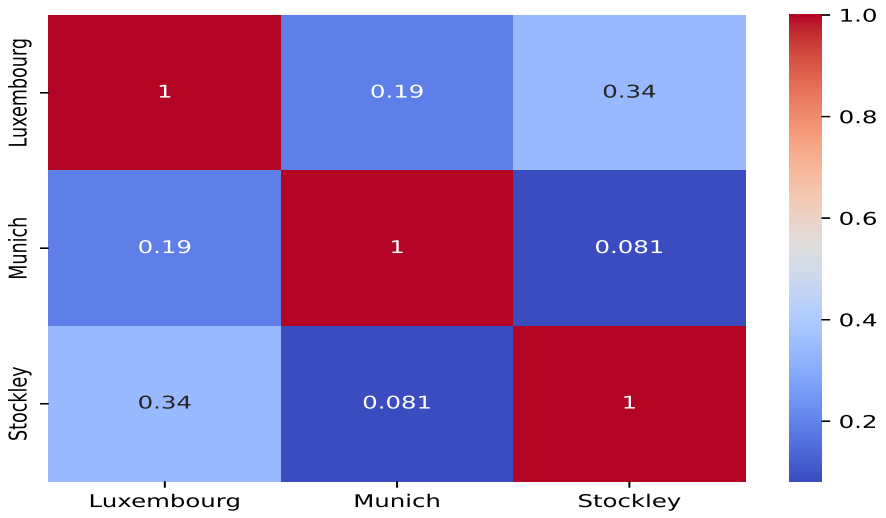

Figure 4.6: Correlation matrix of rain data.

components are updated as

$$\mathbf{i}_t^g = \sigma(\mathbf{W}_{ix}^g \mathbf{x}_t^g + \mathbf{W}_{ih}^g \mathbf{h}_{t-1}^g + \mathbf{b}_i^g) \tag{4.25a}$$

$$\mathbf{f}_t^g = \sigma(\mathbf{W}_{fx}^g \mathbf{x}_t^g + \mathbf{W}_{fh}^g \mathbf{h}_{t-1}^g + \mathbf{b}_f^g) \tag{4.25b}$$

$$\mathbf{o}_t^g = \sigma(\mathbf{W}_{ox}^g \mathbf{x}_t^g + \mathbf{W}_{oh}^g \mathbf{h}_{t-1}^g + \mathbf{b}_o^g) \tag{4.25c}$$

$$\tilde{\mathbf{c}}_t^g = \tanh(\mathbf{W}_{cx}^g \mathbf{x}_t^g + \mathbf{W}_{ch}^g \mathbf{h}_{t-1}^g + \mathbf{b}_c^g) \tag{4.25d}$$

$$\mathbf{c}_t^g = \mathbf{f}_t^g \odot \mathbf{c}_{t-1}^g + \mathbf{i}_t^g \odot \tilde{\mathbf{c}}_t^g \tag{4.25e}$$

$$\mathbf{h}_t^g = \mathbf{o}_t^g \odot \tanh(\mathbf{c}_t^g), \tag{4.25f}$$

where $\mathbf{W}^g$'s represent the weights, $\mathbf{b}^g$'s are the biases, $\tilde{\mathbf{c}}_t^g$'s are the candidate cell state and $\mathbf{c}_t^g$'s are the final cell states. The final predicted output is then given as

$$\hat{\mathbf{y}}_{t+1}^{(g)} = \mathbf{W}_y^{(g)} \mathbf{h}_t^{(g)} + \mathbf{b}_y^{(g)}. \tag{4.26}$$

Training Process

Similar to the traffic prediction, the training process spans 100 epochs, during which the neural network processes the entire training dataset and adjusts its weights. To optimize memory usage and computational efficiency, a batch size of 128 is considered. Additionally, to prevent the model from becoming too reliant on specific neurons and to avoid overfitting, a dropout rate of 0.2 is applied.

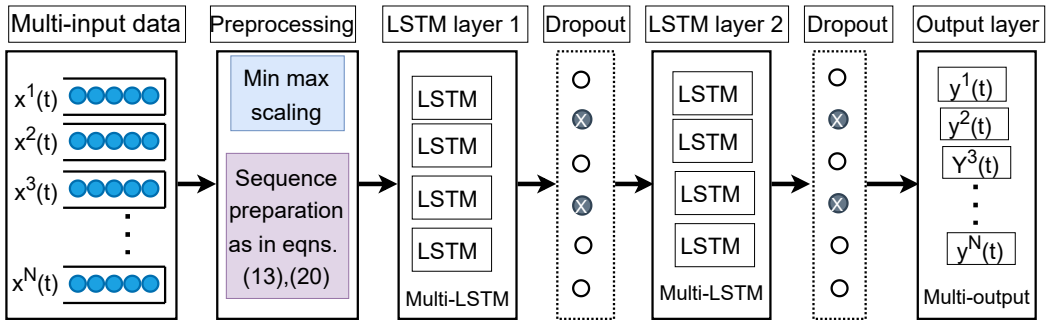

Figure 4.7: LSTM Architecture.

Model Evaluation

The performance of the rain attenuation prediction is assessed using new, previously unseen data of the next day following the model's training with the collected data. Each GW's model is tested individually on its respective dataset, and the prediction error is quantified using MSE as the evaluation metric as follows:

$$\mathcal{L}^{(g)} = \frac{1}{Z'} \sum_{i=1}^{Z'} \left(\hat{x}^{(g)}_{i+S'} - x^{(g)}_{i+S'} \right)^2, \tag{4.27}$$

where $\hat{x}^{(g)}_{i+S'}$ is the models prediction of the next value and $x^{(g)}_{i+S'}$ is the ground true next value.

Both LSTM architectures for traffic and rain attenuation can be described by Fig. 4.7. Although the underlying LSTM structure remains similar for both models, the input-output granularity, and the number of time steps to predict as given in (4.18) and (4.26) are different. The difference in input-output granularity between the two LSTM models arises from the nature of the data. Specifically, for traffic demand prediction, it is possible to capture the fine-grained temporal patterns inherent in the Poisson process, allowing for accurate traffic estimation. In contrast, rain attenuation prediction relies on the ITU model's capability, which is more suited for coarser time granularity [167].

4.4 Proposed B2G Matching and Load Balancing Approaches

4.4.1 Problem Approximation

Given that the packet arrivals follow a Poisson process, and following the steps presented in Section 2.3, Equations (4.11) and (4.12) can be re-expressed as

$$\frac{1}{M}\int_{(k-1)M}^{kM}\sum_{n=0}^{q^{\mathsf{QoE}}} g_{n,b}(f_b^k,t)\,dt \geq 1-\bar{P}_{\mathsf{QoE}}, \tag{4.28}$$

and

$$\sum_{n=0}^{q^{\max}} g_{n,b}(f_b^k,t) \geq 1-\bar{p}_{Blk}, \forall k, t\in\Omega_k. \tag{4.29}$$

Equation (4.28) can be transferred to:

$$z_k(f_b^k) \geq 1-\bar{P}_{\mathsf{QoE}}, \tag{4.30}$$

where $z_k(x) = 1-\frac{\phi_k^b}{\left(Mx^{q^{\mathsf{QoE}}+1}\right)}$ and $\phi_k^b = (L\sum_{t\in\Omega_k}\lambda^b(t))^{q^{\mathsf{QoE}}+1}$. As presented in proposition 1, Equations (4.6), (2.13) and (4.29) can be merged into a single convex constraint as

$$f_b^k \geq \zeta_k^b = \max\left(0,\zeta_{k,1}^b,\zeta_{k,2}^b\right), \forall k, \forall b. \tag{4.31}$$

which is equivalent to:

$$\sum_{\forall g}\vartheta_{g,b}^k f_{g,b}^k \geq \zeta_k^b, \tag{4.32}$$

where $\zeta_{k,1}^b = \max_{t\in\Omega_k} L\lambda^b(t)$, $\zeta_{k,2}^b = \max_{t\in\Omega_k} Lx_{q^{\max}}^{-1}(1-\bar{P}_{\mathsf{Blk}},t)$, and $x_{q^{\max}}^{-1}(\bar{P}_{\mathsf{Blk}},t)$ is the inverse function of $\sum_{n=0}^{q^{\max}} g_{n,b}(f_b^k,t)$.

In addition, we introduce an auxiliary variable $\upsilon_k = \max \ell_g^k$ and add a constraint $\upsilon_k \geq \ell_g^k$ to ensure that the *min-max* load always exceeds other GWs' loads. Hence, problem (4.13) can be modified as

$$\min_{f_{g,b}^k,\vartheta_{g,b}^k} \upsilon_k \tag{4.33a}$$

$$\text{subject to:} \quad (4.4),(4.5),(4.30),(4.32),$$

$$\upsilon_k \geq \ell_g^k, \quad \forall g,k. \tag{4.33b}$$

Remark 4. *Problem (4.33) remains a non-convex mixed-integer linear program (MILP) due to the binary B2G matching variable. Since the problem is non-convex, directly finding the optimal solution is challenging. Below we divide (4.33) into a two-stage optimization problem to efficiently solve it.*

- ***Stage One:*** *Optimizing the capacity (f_b^k) required to meet the QoE and BP requirements of traffic flows in each beam. The optimal capacity identified in this stage represents the necessary allocation that must be assigned to the beams from any GWs to facilitate the packet flows.*
- ***Stage Two:*** *Optimizing the B2G matching ($\vartheta_{g,b}^k$) to ensure efficient GW load balancing, thus meeting the capacity demands of the beams identified in Stage One.*

4.4.2 Stage One - Capacity Optimization

To optimize the capacity utilization, we find the minimum capacity f_b^k required from GW g to satisfy the BP and QoE requirements without taking the rain fading into account. The problem is given as

$$\min_{f_b^k} \quad f_b^k \text{ subject to } (4.30), (4.32). \tag{4.34}$$

This is a linear convex optimization problem and can therefore be solved optimally using standard optimization techniques. The optimal solution is presented in the following proposition.

Following proposition 2, the optimal solution of (4.34) is given as

$$\hat{f}_b^k = \max(0, \zeta_k^b, \mathcal{X}^\star), \tag{4.35}$$

where $\mathcal{X}^\star$ is given as

$$\mathcal{X}^\star = \left[\phi_k^b/(M\bar{P}_{\mathsf{QoE}})\right]^{\frac{1}{q^{\mathsf{QoE}}+1}}. \tag{4.36}$$

Algorithm 6 WEIGHTED LOAD BALANCING ALGORITHM

for $k = 1$ to K **do**
  Solve the convex problem in (4.34) as in (4.35) and (4.36) to get $\hat{f}_b^k$.
  Sort $\hat{f}_b^k$ in descending Order.
  Sort $C_g^{\mathsf{fd,max}}$ in descending Order.
  for $b = 1$ to B **do**
    Check if $C_g^{\mathsf{fd,max}} \geq \hat{f}_b^k$.
    Assign beam b to GW g.
    Calculate the remaining GW capacity.
  end for
end for
Return $\vartheta_{g,b}^k$.

4.4.3 Stage Two - B2G Matching

Once $\hat{f}_b^k$'s are defined in *Stage One*, $\vartheta_{g,b}^k$ can be optimized by considering the following problem,

$$\min_{\{\vartheta_{g,b}^k\}} \quad \upsilon_k \tag{4.37a}$$

$$\text{subject to:} \quad \sum_{g\in\mathcal{G}} \vartheta_{g,b}(t) = 1, \quad \forall b, k \tag{4.37b}$$

$$\upsilon_k \geq \sum_{b\in\mathcal{B}} \vartheta_{g,b}^k \hat{f}_{g,b}^k / C_g^{\mathsf{fd,max}}(k), \quad \forall g, k, \tag{4.37c}$$

$$\upsilon_k \leq 1. \tag{4.37d}$$

Here, constraint (4.5) is changed to its equivalent constraint (4.37d). Problem (4.37) is a linear integer program that can be effectively solved using established optimization techniques, such as B&B [168]. However, the B&B algorithm generally exhibits exponential complexity. In the following, we discuss **four low complexity methods** for B2G matching design.

Weighted Load Balancing Method (WLB)

Traffic matching based on the available capacity of GWs is a well-established method [154], [155]. The WLB B2G matching relies on GW capacity, which varies due to SNR fluctuations across all GWs. Allocation is performed on iterations over all beams based on the remaining capacity of the GWs. However, this approach can result in significant load imbalances, particularly when certain GWs consistently have higher remaining capacities over iterations compared to others, causing traffic to be matched predominantly to the GWs with higher capacity. The WLB method is summarized in Algorithm 6.

Ant Colony Optimization (ACO)

ACO is a metaheuristic algorithm in which a colony of artificial ants cooperates to find the best solutions to complex optimization problems [28], [169], such as B2G matching. Ants use pheromone trails to communicate, make probabilistic decisions based on pheromone levels, and collectively improve solutions through cooperation.

To adapt the algorithm to our problem, we assume each ant explores the possible solutions of assigning one beam to a GW sequentially until all beams are assigned to a suitable GW. Hence, an ant represents a full solution of B2G matching. These ants calculate the desirability for each beam to be assigned to a specific GW based on the pheromone levels and heuristic desirability, which mainly depends on the beam traffic and GW capacity. To match the approach to solve our problem, the pheromone level $\tau_{b,g}$ associated with assigning beam b to GW g is designed in a way that minimizes the maximum load and balances the load among GWs as follows:

$$\tau_{b,g} = 1/\max \ell_g^k. \tag{4.38}$$

In addition, the probability of assigning beam b to GW g is given as

$$Pr_{b,g} = \frac{[\tau_{b,g}]^{\omega_p} \cdot [\eta_{b,g}]^{\beta_h}}{\sum_{g \in \mathrm{G}} [\tau_{b,g}]^{\omega_p} \cdot [\eta_{b,g}]^{\beta_h}}, \tag{4.39}$$

where $\eta_{b,g}$ is the heuristic desirability of assigning beam b to GW g, ω_p and β_h are parameters that control the relative importance of pheromone level and heuristic information, respectively. Furthermore, the heuristic desirability of beam b to be assigned to GW g can be represented as

$$\eta_{b,g} = \max\left(0, \frac{C_g^{\mathsf{fd,max}} - \sum_{t \in \Omega_k} \lambda^b(t)}{C_g^{\mathsf{fd,max}}}\right). \tag{4.40}$$

To balance exploration and exploitation over I iterations, the ω_p and β_h parameters are updated at every iteration i as follows:

$$\omega_{p,i} = \omega_{p,\text{start}} + (\omega_{p,\text{final}} - \omega_{p,\text{start}}) i / I_{Aco}^2, \tag{4.41}$$

and

$$\beta_{h,i} = \beta_{h,\text{start}} \cdot e^{-\beta_{h,i}}. \tag{4.42}$$

These equations ensure that ω increases progressively to exploit the learned pheromone trails,

Algorithm 7 ACO Algorithm

Input:

- Initialize iterations I_{Aco}, number of ants J, parameters $\omega_p, \beta_h, \psi_{phe}$.
- Initialize the minimum of the maximum load $\upsilon_k^* = \infty$ and the best solution $\mathbf{X}^*$.

for $k = 1$ to K **do**
  Solve the convex problem in (4.34) as in (4.35) and (4.36) to get $\hat{f}_b^k$.
  Compute heuristic desirability as in (4.40).
  Initialize pheromone matrix $\tau_{b,g} = 1, \forall b \in B, g \in \mathcal{G}$.
  for $i = 1$ to I_{Aco} **do**
    Update the pheromone influence and heuristic influence as in (4.41) and (4.42).
    for $j = 1$ to J **do**
      Each ant constructs a B2G matching solution $\mathbf{X}^{(j)}$:
      Compute beam b to GW g matching probability as in (4.39).
      Assign all the beams to corresponding GWs.
      Compute the minimum of the max load $\min \upsilon_k$.
      if $\upsilon_k^{(j)} < \upsilon_k^*$ **then**
        Update best solution: $\mathbf{X}^* \leftarrow \mathbf{X}^{(j)}$, $\upsilon_k^* \leftarrow \upsilon_k^{(j)}$.
      end if
      Pheromone evaporation: $\tau_{b,g} \leftarrow (1 - \psi_{phe})\tau_{b,g}$.
      for each solution $\mathbf{X}^{(j)}$ **do**
        Update pheromone levels as in (4.43).
      end for
    end for
  end for
end for
Return $\vartheta_{g,b}^k \leftarrow \mathbf{X}^*$.

while β decreases exponentially to reduce the impact of heuristics. This dynamic adjustment helps balance exploration and exploitation, enhancing the overall performance of the ACO algorithm. The pheromone level is updated over iterations as follows:

$$\tau_{b,g} = (1 - \psi_{phe})\tau_{b,g} + \Delta\tau_{b,g}, \tag{4.43}$$

where $\Delta\tau_{b,g}$ is the total residual amount of pheromone deposited during the global updating phase. The whole process of the ACO method is summarized in Algorithm 7.

Genetic Algorithm (GA)

GAs are an evolutionary optimization techniques inspired by natural selection. It iteratively refines a population of candidate solutions (chromosomes) through selection, crossover, and mutation, guided by a fitness function to converge toward an optimal solution. GAs are widely recognized for their robust optimization capabilities and adaptability in dynamic environments [170], [27]. The GAs generally have the following components or operators that work together to optimize the solution.

Chromosomes Representation Each chromosome represents a potential solution for the B2G matching. It is defined as an array of length B, where each element denotes the GW g to which the traffic of beam b is assigned. Since a beam's traffic needs to be assigned to only one GW, the elements of each chromosome array hold an integer value between zero and G. Hence, the chromosome is represented by

$$\mathcal{C} = [c_1, c_2, \ldots, c_B], \quad c_b \in \{1, 2, \ldots, G\}, \quad \forall b, \tag{4.44}$$

where $\mathcal{C}$ denotes the chromosome, and the gene c_b represents the GW assigned to beam b.

Initial Population A population refers to a collection of individual chromosomes that represent a possible B2G matching solution to our problem. The population is often randomly initialized, and its size is a crucial parameter that influences the algorithm's performance by balancing exploration and computational complexity. For a population P of size Y, we represent the initial population as a matrix of Y rows and B columns.

Fitness Calculation Each chromosome in the population is evaluated by the fitness value to test how well it fits to solve the B2G matching problem. To achieve the objective, we define a fitness function based on the distribution of traffic loads across GWs. Hence, the fitness function of the chromosome $\mathcal{C}$ can be defined as

$$F(\mathcal{C}) = 1/\max_g \ell_g. \tag{4.45}$$

The fitness function, $\frac{1}{\max_g \ell_g}$, penalizes solutions with high load factors. This approach directly addresses the capacity constraint by discouraging overloaded GWs and minimizing the variation in load distribution among GWs, thereby promoting a more balanced allocation of resources.

Selection The selection process is crucial for improving the population's fitness over generations by favoring chromosomes with higher fitness values. This is essential for effectively assigning beams to GWs. There are several types of selection methods, with Roulette Wheel Selection being the most common [171]. If the fitness of the chromosome $\mathcal{C}_y$ is given as $F(\mathcal{C}_y)$, then the probability of selecting the parent y using the Roulette Wheel Selection is expressed

as

$$Pr(\mathcal{C}_y) = \frac{F(\mathcal{C}_y)}{\sum\limits_{y \in Y} F(\mathcal{C}_y)}. \tag{4.46}$$

Crossover Crossover is a fundamental operator that facilitates the exchange of genetic material between parent chromosomes (solutions) to create offspring with potentially better fitness. For efficient performance of the GA, it is crucial to set the crossover rate parameter properly.

Mutation Mutation is a small, random tweak in the chromosome used to maintain and introduce diversity in the genetic population, potentially leading to new and better solutions. To ensure efficient performance of the GA, it is essential to correctly set the mutation rate parameter.

The basic GA method can be summarized in Algorithm 8, excluding the r_c and r_m update in step 7.

Proposed Adaptive Genetic Algorithms

The basic GA operates over a fixed value of parameters such as mutation rate, and crossover rate throughout the process. This makes the exploration and exploitation process of the algorithm remain unchanged over time which may lead to early convergence of local optimal solutions [171]. Hence, the basic GA may be inefficient for a problem with a large search space, such as B2G with exponential complexity. Therefore, we propose an adaptive GA (AGA) that explores more at the early generations and exploits more at the latter generations.

Adaptive Crossover Adaptive crossover involves modifying the crossover rate over generations. For example, the crossover rate might be higher in the early generations to explore diverse solutions and traverse different beams-GW matching. As the generations progress, the crossover rate is adjusted to favor the production of fitter offspring, thereby exploiting the best B2G matching found so far. This dynamic adjustment ensures that the GA maintains an acceptable exploration and exploitation balance throughout the evolutionary process. However, maintaining a tolerable minimum crossover rate rc_{min} even in the latter stages of the GA is crucial to prevent stagnation. The crossover rate r_c is updated over I generations as

Algorithm 8 GA FOR B2G MATCHING

1: **Initialization:**
- Initialize a population $\mathcal{P}$ of size Y with random B2G matching as in (4.44).
- Set initial cross over rate r_c, initial mutation rate r_m, and maximum number of generations $I_{\max}$.
- Initialize generation counter $i = 0$.

2: **for** $k = 1$ to K **do**
3: Solve the convex problem in (4.34) as in (4.35) and (4.36) to get $\hat{f}_b^k$.
4: **while** $i < I_{\max}$ **do**
5: Set an empty population $\mathcal{P}'$ for the next generation.
6: Evaluate the fitness of each chromosome in $\mathcal{P}$ as in (4.45).
7: Update r_c and r_m as in (4.47) and (4.48). {Only for adaptive GA method.}
8: Select the chromosome with the highest fitness from $\mathcal{P}$ and add it to $\mathcal{P}'$.
9: **while** $|\mathcal{P}'| < W$ **do**
10: Select 2 parents from $\mathcal{P}$ for the next generation using *roulette wheel selection*.
11: Perform *crossover* on selected parents with a cross over rate of r_c.
12: Apply *mutation* to offspring with probability r_m.
13: Insert the offspring to $\mathcal{P}'$
14: **end while**
15: Replace old population $\mathcal{P} \leftarrow \mathcal{P}'$.
16: Update $i := i + 1$.
17: **end while**
18: **end for**
19: Return $\vartheta_{g,b}^k$.

follows:

$$r_c(i+1) = r_c(i) - \frac{[r_c(i) - rc_{\min}] \cdot i}{I} \tag{4.47}$$

Adaptive Mutation Adaptive mutation involves modifying the mutation rate over generations. Early in the evolutionary process, a higher mutation rate introduces greater variability, helping the algorithm explore diverse matching configurations and escape local optima. As the algorithm progresses over generations, the mutation rate can be reduced to exploit the best matching and avoid disrupting the best configurations due to mutation. The mutation rate r_m is updated as

$$r_m(i+1) = r_m(i) - [r_m(i) - rm_{\mathsf{min}}]\, i/I. \tag{4.48}$$

The entire process of the AGA for determining B2G matching and LB can be summarized in Algorithm 8, which includes step 7 that is not present in the basic GA.

4.4.4 Solution Approach Summary and Complexity Analysis

Overall Solution Design

As detailed in Section 4.3, our methodology encompasses traffic demand and rain attenuation prediction followed by optimization. Consequently, the comprehensive solution approach of

Algorithm 9 PROPOSED SOLUTION APPROACH

1: **Initialization:** Define W^{fd}, C^{fd}, Q^{QoE}, $\bar{P}_{\mathsf{Blk}}$, $\bar{P}_{\mathsf{QoE}}$ and Q^{max}.
2: **for** $k = 1$ to K **do**
3: Use multi-horizon data-driven prediction to estimate the traffic demand for all time slots in $t \in \Omega_k$ and the rain attenuation for the same period.
4: Solve stage one of the problem in (4.34) as in (4.35) and (4.36).
5: Having the solution from stage one,solve stage two of the problem to find the optimal B2G matching $\vartheta^k_{g,b}$.
6: **end for**
7: Return $f^k_{g,b}$ and $\vartheta^k_{g,b}$.

the proposed method is summarized in Algorithm 9.

Complexity Analysis

The complexity of the LSTM model depends on the number of stacked LSTM layers (L'), the number of units per layer (U), the sequence length (S), and the number of beams (for traffic prediction) or GWs (for rain attenuation prediction). The complexity per LSTM unit is $\mathcal{O}\left(U^2\right)$. Hence, the overall complexity of implementing the LSTM method per cycle is given as

$$X^{\mathsf{LSTM}} = \mathcal{O}\left(L'SBU^3\right). \tag{4.49}$$

Next, the complexity of the GA over I generations and an initial population of size Y is related to the population generation $\mathcal{O}(YB)$, fitness evaluation $\mathcal{O}(YB)$, selection $\mathcal{O}(Y)$, cross over & mutation $\mathcal{O}(YB)$, and generation replacement $\mathcal{O}(I)$. Since these steps repeat over I generations (iterations) per cycle, and over K cycles, the overall complexity of GA is given as

$$X^{\mathsf{GA}} = K(X^{\mathsf{LSTM}} + \mathcal{O}(IYB)). \tag{4.50}$$

On top of the complexity of GA, our proposed AGA method introduces adaptation complexity at each generation, which is linear as described in equations (4.47) and (4.48). Consequently, the overall complexity of the AGA is given by

$$X^{\mathsf{AGA}} = K(X^{\mathsf{LSTM}} + \mathcal{O}(IYB + I\Theta)), \tag{4.51}$$

where $I\Theta$ represents the cumulative adaptation overhead across all generations. Consequently, both the GA and AGA algorithms have polynomial time complexity.

Denote J as the number of ants. The complexity of the ACO algorithm is related to the path construction, that is visiting a beam and making a matching decision $\mathcal{O}(JBG)$, local

Table 4.1: Considered LSTM hyper-parameter values.

Parameters	**Values**
Activation function	tanh
Batch size traffic prediction	256
Batch size attenuation prediction	128
Dropout rate	0.2
Epochs	100
Horizon size traffic prediction	15
Learning rate	0.001
Loss function	MSE
LSTM units per layer	50
Normalization	MinMax scaling
Number of layers	2
Optimizer	Adam
Output Layer	Fully connected dense layer
Sequence length traffic prediction	100
Sequence length attenuation prediction	50

and global pheromone update $\mathcal{O}(JB + BG)$, probabilistic selection $\mathcal{O}(JB)$, and the number of iterations $\mathcal{O}(I)$. Consequently, the overall complexity of the ACO algorithm is given as

$$X^{\mathsf{ACO}} = K(X^{\mathsf{LSTM}} + \mathcal{O}(IJBG)). \tag{4.52}$$

Hence, the complexity of ACO can be easily solved in polynomial time. The complexity of the WLB method is a linear function of the number of beams given as

$$X^{\mathsf{WLB}} = K(X^{\mathsf{LSTM}} + \mathcal{O}(B)). \tag{4.53}$$

4.5 Numerical results and Analysis

This section details the preparation of the data set, presents numerical results, and analyzes the performance of our methods compared to benchmark algorithms.

4.5.1 Traffic Demand and Rain Attenuation Prediction Results

In this section, we evaluate the effectiveness of the proposed models for forecasting rain attenuation and traffic demand. The parameters of the LSTM models are given in Table 4.1.

Fig. 4.8 illustrates actual versus predicted traffic for two randomly selected beams. The figure shows that the LSTM model with multiple outputs and multiple horizons accurately

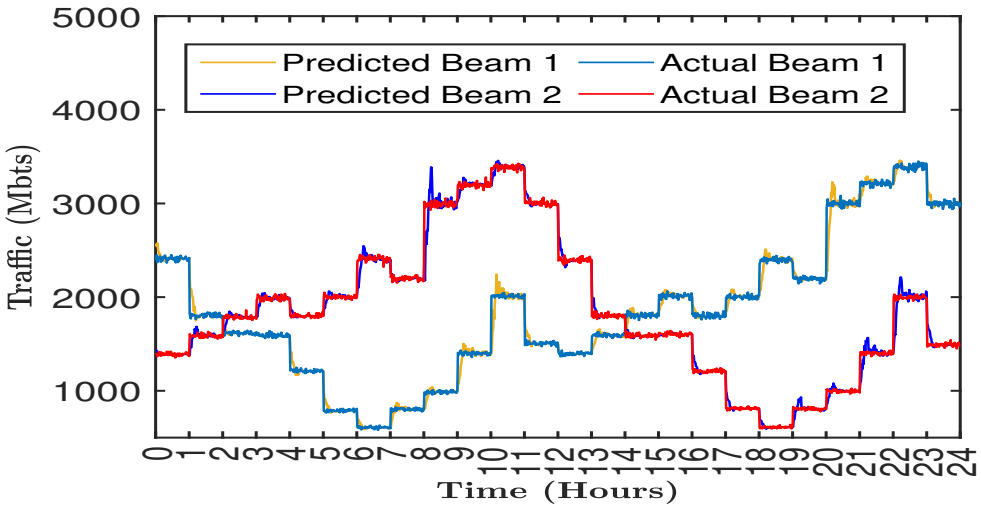

Figure 4.8: Predicted traffic demand for randomly selected beams.

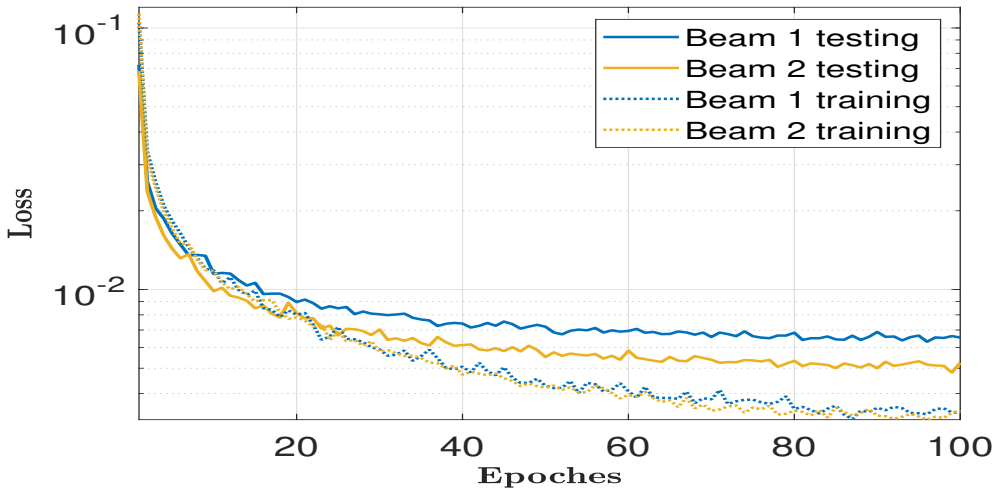

Figure 4.9: Traffic demand prediction loss for randomly selected two beams.

predicts the traffic trends that vary over time, indicating its robustness and reliability. The prediction efficiency of our model is further demonstrated by the lower values of loss of training and testing (validation) in Fig. 4.9. Training loss measures how effectively the model learns from training data, while testing loss evaluates the model's generalization to unseen data.

Similarly, Fig. 4.10 presents the performance of our rain attenuation prediction model, depicting both training and testing loss over the epochs. The plot reveals a consistent decrease in training and testing loss throughout the training process. The small gap between training and testing loss indicates good generalization to new data and no overfitting. The low final loss values further confirm the efficiency and robustness of the proposed model. The relatively

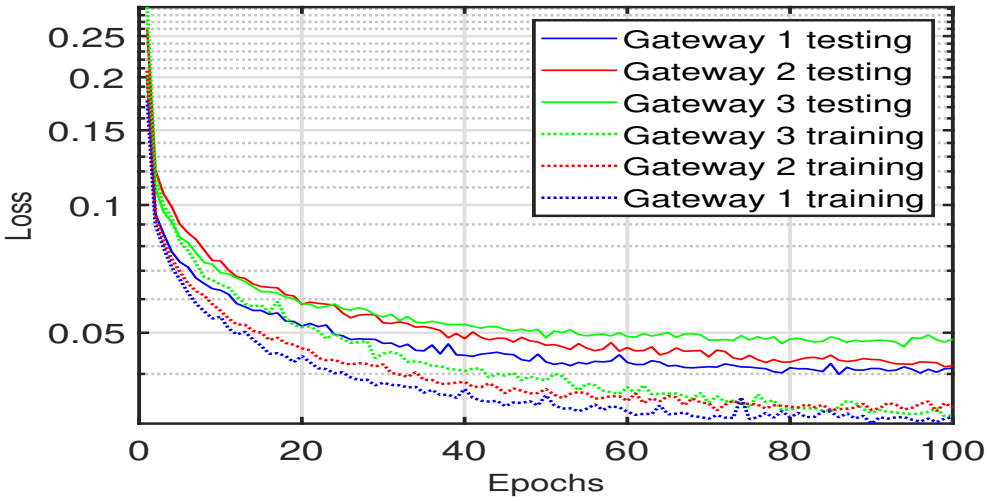

Figure 4.10: Feeder link SNR prediction training and testing loss.

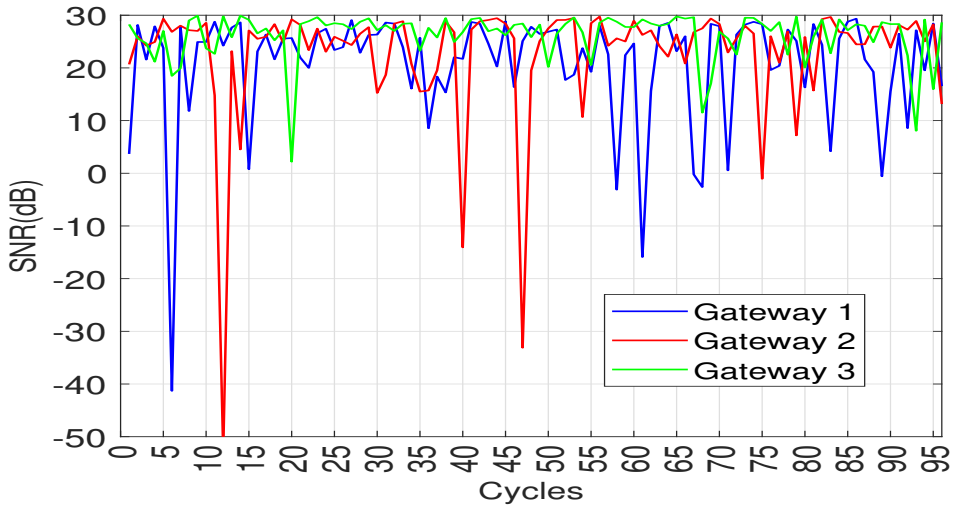

Figure 4.11: Predicted SNR for 1 day with 96 cycles.

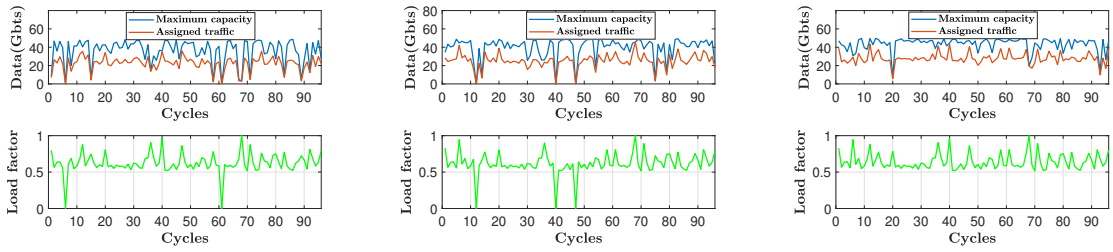

(a) Gateway 1. (b) Gateway 2. (c) Gateway 3.

Figure 4.12: Maximum available capacity, assigned traffic, and maximum load factor.

Table 4.2: Considered parameter values.

Parameters	**Values**
Maximum bandwidth W^{fd}	500 MHz
Number of beams	20
Number of GWs	3
Packet length	15000 (Bytes)
Population size GA & AGA	500 individuals
Period (T)	1 day
P^{fd}	100 Watts
q^{max}	130 (2 MBytes)
q^{QoE}	80 (Packets)
Target BP	0.05
Target QoE violation probability	0.1
Termination criteria	Maximum number of generations
Cycle duration	15 minutes
$[\mathcal{K}, \alpha]$	[0.05, 1.2]
σ^2	0.01 Watts

higher loss for rain attenuation prediction, compared to traffic prediction, is due to the rare extreme points in rain events, which are harder to predict accurately than the fluctuations in traffic data.

Fig. 4.11 illustrates the predicted SNR due to rain attenuation for the FLs connecting the three GWs to a multi-beam satellite over a day, segmented into 96 cycles of 15 minutes each. GWs 1 and 1 show sporadic SNR degradations throughout the day, indicating intermittent weather disturbances. In contrast, GW 3 maintains relatively stable SNR values, indicating reduced atmospheric impact. These observations underscore the importance of adaptive B2G matching.

4.5.2 Numerical Results

In this section, we analyze the running time and the numerical results of our approach and the GA, ACO, and WLB methods. The design parameters for this simulation are given in Table 4.2. For the basic GA, all the parameters are the same as for the AGA except that the mutation rate ($r_m = 0.1$) and the crossover rate $r_c = 0.5$ are kept constant. For the ACO algorithm, 500 ants over 100 iterations, $\beta_{decay} = 0.005$, and a pheromone evaporation rate of 0.1 are considered.

Fig. 4.12 illustrates the maximum per-cycle capacity of each GW after SNR prediction, the total assigned traffic to each GW (i.e., $\sum_{b \in \mathcal{B}} f_{g,b}^{k}$) after solving stages 1 and 2 of the problem,

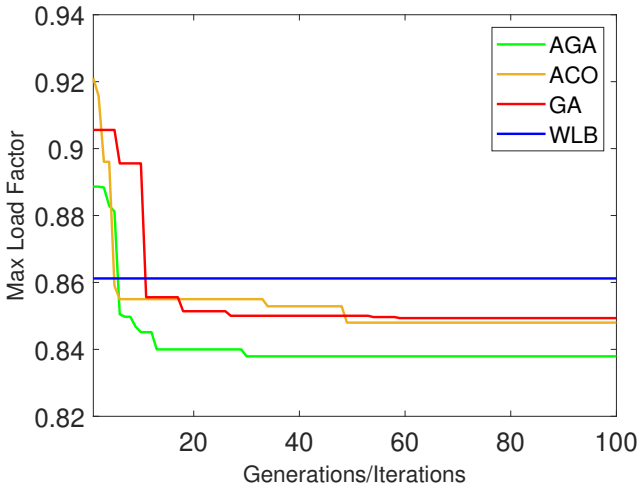

Figure 4.13: Convergence of the maximum load factor $\max \ell_g^k$.

and the resulting load factor ℓ_g^k across 96 cycles over one day using the proposed AGA method. The results reveal that the matched traffic dynamically adjusts according to the varying capacities of the GWs. Notably, the nearly identical load factors observed across the three GWs demonstrate the model's LB efficiency. This consistency indicates that the system can not only mitigate the impact of capacity fluctuations (e.g., due to weather conditions) but also optimally distribute traffic demands across the network, ensuring stable operation and improving overall resource utilization. These findings underscore the robustness of the proposed approach in managing multi-GW satellite systems under dynamic and uncertain conditions.

Fig. 4.13 illustrates the convergence of the maximum load factor towards the minimum ($\min \max \ell_g^k$) for a randomly selected cycle, achieved by the proposed AGA, compared to the benchmark algorithms over generations and iterations. The results indicate that the proposed method outperforms the benchmark algorithms in terms of convergence speed and minimizing the maximum load, which indicates a better load balance. This is attributed to the capability of AGA to dynamically adjust crossover and mutation rates, which enhances the balance between exploration and exploitation, leading to more efficient LB. This adaptability allows the algorithm to quickly converge to optimal solutions, minimizing the maximum load among GWs compared to the benchmark algorithms. The maximum load factor difference between the first and last iterations in the AGA, GA, and ACO algorithms decreases slightly from 0.945 to 0.928. This is because we start with a large initial population (500 for AGA and

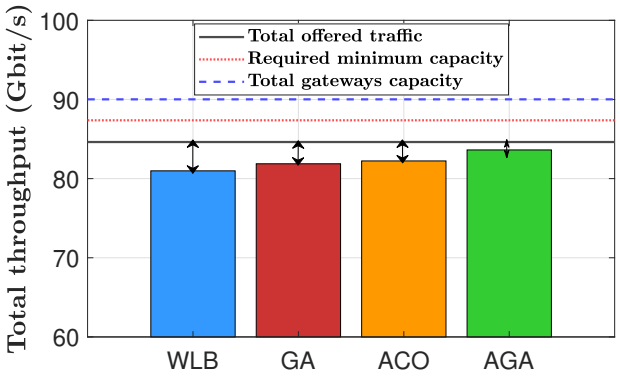

Figure 4.14: Data transmission performance.

GA, and 500 ants for ACO). This large population size allows us to explore a wide range of solutions from the very first iteration. Despite the small numerical difference, this reduction is practically significant for satellite EHF band FLs, which carry tens or even hundreds of gigabits of data. Therefore, going through all iterations until convergence is essential to achieve the best possible solution and to ensure the robustness of the system.

It is important to note that at the cycles where the traffic demand is small and the GWs have sufficient capacity, the QoE requirements of the traffic flows using all the considered B2G matching techniques are almost the same or even the same. This is because all beams receive the minimum capacity needed to satisfy the target QoE requirement, regardless of which GW provides the capacity. The performance difference between the proposed and benchmark algorithms becomes apparent at cycles with peak traffic where the traffic demand begins to approach or exceed the maximum capacity of the GWs. At this point, the efficiency of B2G matching is crucial for reducing packet dropping and optimizing the available capacity of the GWs.

Fig. 4.14 illustrates the total available capacity of the GWs ($\sum_{g\in\mathcal{G}} C^{\mathsf{fd,max}} g(k)$), the minimum capacity required to satisfy the QoE and BP requirements ($\sum_{b\in B} \hat{f}b(k)$), the total offered traffic ($\sum_{b\in B} \lambda_k^b$), and the total throughput ($\sum_{g\in\mathcal{G}} \sum_{b\in B} \vartheta_{g,b}^k f_{g,b}^k$) of the FLs for a randomly selected cycle with peak traffic demand using different B2G matching techniques. The plot indicates that although the total available capacity is sufficient to meet the minimum required capacity to fulfill the QoE and BP requirements, the simulated algorithms perform differently in terms of utilizing the capacity and the transmission throughput of the FLs. The gap between the offered traffic and the total throughput, indicated with double arrows, shows the amount of blocked data. The proposed AGA method outperforms the benchmark

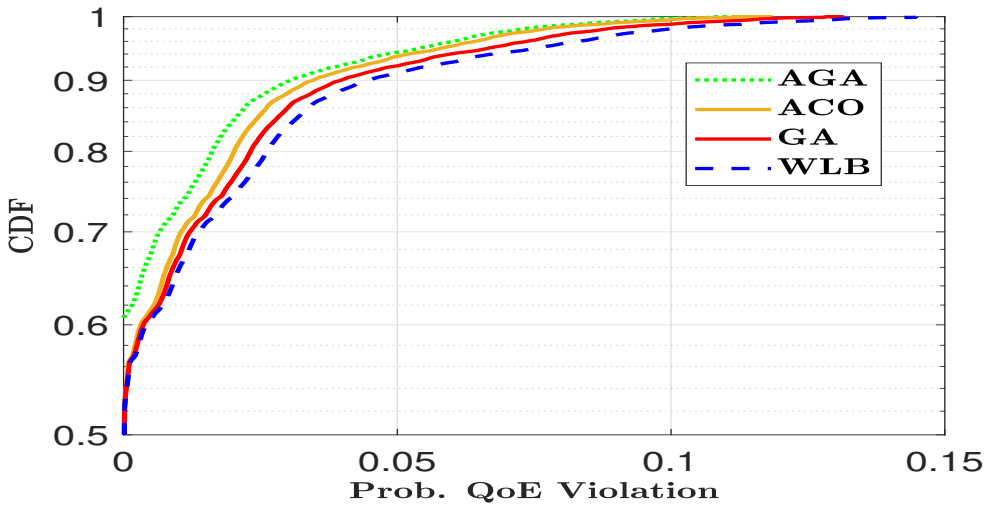

Figure 4.15: CDF of mean Probability of QoE violation.

methods by efficiently transmitting more data, thereby reducing blocked (lost) packets.

Fig. 4.15 shows the CDF of the mean QoE violation probability for traffic flows to all beams, using the proposed and benchmark methods over 96 cycles in one day, experiencing different levels of GW capacity and traffic demand. The results show that the QoE violation probability of the traffic flow with AGA-based B2G matching is generally lower than that of the B2G matching using other benchmark methods. This is because the AGA dynamically adjusts its parameters, leading to more efficient optimization and superior QoE compared to static benchmark methods.

Method	**Prediction model training**		**AGA**	**GA**	**ACO**	**WLB**
	SNR	**Traffic**				
Total running Time (s)	11211	78478	2240.64	2065.92	2395.2	768
Average running time per cycle (s)	116.78	817.5	23.34	21.52	24.95	8.05

Table 4.3: Running time of simulated models.

Table 4.3 summarizes the running times associated with the training of SNR and traffic prediction models, as well as the running time for the simulated AGA, GA, ACO, and WLB methods, including the testing phase of the prediction models. While the WLB and GA

algorithms exhibit shorter execution times compared to AGA and ACO, the AGA algorithm demonstrates a reasonable and acceptable running time. Given its superior performance in terms of load balancing (LB), BP, and QoE given in Figs 4.13, 4.14, and 4.15, AGA is recommended as the preferred solution.

4.6 Conclusion

This chapter addresses the challenge of optimal beam traffic to GW matching with LB among ground GWs, accounting for previously unknown, time-varying rain attenuation and fluctuating traffic demand. The system model integrates QoE and BP requirements. To capture dynamic environmental and traffic conditions, stacked multi-output multi-horizon LSTM Recurrent Neural Network (RNN) is used for traffic demand and rain attenuation prediction. The optimization problem is solved using a low-complexity AGA, enabling efficient resource allocation while meeting service constraints.

Chapter 5

Conclusions and Future Work

5.1 Conclusion

With the rapid advancement of 5G networks, user access to diverse 5G services and the associated traffic demand are evolving dynamically in both volume and QoE expectations. Concurrently, the 5G market is witnessing intensified competition among satellite operators and SPs, leading to increased pressure on satellite operators to efficiently manage resources and meet user demands. In this context, satellite operators must strategically allocate their limited capacity to balance three critical objectives: maximizing revenue, minimizing rental costs of SPs, and satisfying diverse QoE requirements across service types. In Chapter 2 of the thesis, an optimization algorithm for an optimal trade-off among allocated capacity, rental cost, and performance is discussed. This directly addresses Question 1 presented in Chapter 1.

Achieving the optimal balance is increasingly difficult, as traffic demand patterns of multiple services are uncertain and vary significantly in real-time, making traditional optimization methods inadequate. For better adaptability and flexibility in resource allocation, AI and ML techniques offer promising solutions. These models can successfully learn to prioritize services based on QoE sensitivity and traffic characteristics, adapting to dynamic traffic patterns in real time. Chapter 3 of the thesis explored the use of DQN, DDQN, and D3QN techniques to learn the sequence of traffic demand and allocated capacity over time to provide an optimal CA policy to address Question 2.

Furthermore, leveraging EHF bands can provide the additional capacity needed to support growing demand. However, EHF deployment introduces its own challenges, including

severe rain attenuation, variable traffic loads, and link imbalances across feeder links. To mitigate these issues, the development of predictive models is crucial. These models must be capable of accurately forecasting both traffic demand and atmospheric conditions (e.g., rain attenuation), thereby enabling proactive resource management. Additionally, intelligent B2G matching and load balancing mechanisms are essential to maintain service continuity and ensure optimal system performance. This approach not only enhances QoE and system efficiency but also ensures resilient and adaptive service delivery in the face of environmental and demand uncertainties. These methods are explored in detail in Chapter 4 to address Question 3.

5.2 Future Work

This section outlines potential directions for extending the research presented in this thesis. These extensions are motivated by both the limitations of the current modeling framework and the evolving landscape of SatCom technologies. The proposed areas reflect key challenges in next-generation satellite systems and align with emerging trends in QoE-centric network design.

1. Multi-Dimensional QoE Modeling and Optimization: The current work models QoE primarily as a function of queuing delay. In practical scenarios, however, user experience is shaped by multiple performance metrics—such as latency, throughput, jitter, and packet loss. A promising direction for future work is to develop multi-dimensional QoE models that jointly consider these metrics and to investigate dynamic resource allocation strategies that satisfy QoE requirements holistically. This may involve formulating multi-objective optimization frameworks and real-time scheduling algorithms capable of balancing trade-offs among competing QoE indicators.

2. User-Centric Traffic and QoE Modeling: The current work models traffic and QoE at the flow level, aggregating data across multiple users and services for queuing and CA purposes. It assumes uniform QoE requirements among users accessing the same service, which simplifies scheduling decisions. However, in practice, users often have heterogeneous QoE expectations, and satellite systems allocate resources at the individual user level. Capturing this variability requires more fine-grained modeling of user behavior, service preferences, and perceived quality. Future research should explore

dynamic, user-level resource allocation mechanisms that explicitly account for individualized QoE requirements. This becomes even more promising research direction in light of the emerging trend of Direct-to-Device (D2D) SatCom, such as 5G/6G NTN directly serving smartphones and IoT devices.

3. Extension to NGSO Satellite Constellations (MEO/LEO/VLEO/UAV/HAPS): Non-GEO satellite constellations introduce dynamic topologies and frequent handovers, complicating CA and GW assignments. In these networks, the visibility windows between satellites and user terminals or GWs change rapidly, necessitating continuous reassessment of link availability and QoE. Future research should investigate mobility-aware CA frameworks that adapt to changing satellite visibility windows and leverage Inter-Satellite Links (ISLs) for end-to-end traffic coordination.

4. Multi-Orbit Satellite Resource Coordination and Traffic Steering: The future of SatCom lies in heterogeneous orbital architectures, where LEO, MEO, GEO, and VLEO satellites are jointly used to provide global, reliable, and low-latency coverage. Each orbit has distinct characteristics in terms of latency, coverage footprint, link stability, and resource availability. A key research challenge is to design orbit-aware resource allocation strategies that maximize system utility while meeting service-specific QoE constraints.

5. Multi-tenant Resource Orchestration: The current work considered a single satellite service provider offering multiple services. However, real-world scenarios often involve multiple SPs (tenants), each with distinct traffic demands and SLA requirements. In such multi-tenant environments, ensuring QoE becomes considerably more challenging due to competing resource demands, SLA enforcement, and the need for fair resource allocation. Balancing inter-tenant fairness with intra-tenant QoE-aware service differentiation, while adapting to time-varying traffic patterns and capacity constraints, remains a complex task. As a future direction, QoE-aware orchestration frameworks that support dynamic, efficient CA across services and tenants should be explored.

Appendix A

Proof of Proposition 1

Denote $\mu^b(t) = \mu_k^b$ in cycle k-th. We also have $\rho^b(t) = \lambda^b(t)/\mu_k^b$, $\forall t \in \Omega_k$ and $\mu^b(t) = \frac{W^b(t)T_{\mathsf{TS}}}{L}$. Then, constraint (2.16d) can be transferred into the following requirement

$$W_k^b \geq \alpha_{k,1}^b = \max_{t \in \Omega_k} L\lambda^b(t)/T_{\mathsf{TS}}. \tag{1}$$

Similarly, the constraint (2.16b) will be equivalent to

$$W_k^b \geq \alpha_{k,2}^b = \max_{t \in \Omega_k} Lg_{q_{\mathsf{max}}}^{-1}(1 - \bar{P}_{\mathsf{Blk}}, t)/T_{\mathsf{TS}}. \tag{2}$$

The results given in (1) and (2) yield the lower bound of W_k^b as $\alpha_k^b = \max\left(\alpha_{k,1}^b, \alpha_{k,2}^b\right)$, which has completed the proof of Proposition 1.

Appendix B

Proof of Theorem 1

Let $y_{q_{\mathsf{QoE}}}(W_k^b, t) = \sum_{n=0}^{Q_{\mathsf{QoE}}} g_{n,b}(W_k^b, t)$. Taking $Y^b(t) = L\lambda^b(t)/T_{\mathsf{TS}}$, one can express $y_{q_{\mathsf{QoE}}}(W_k^b, t)$ as,

$$y_{q_{\mathsf{QoE}}}(W_k^b, t) = 1 - \left(Y^b(t)/W_k^b\right)^{Q_{\mathsf{QoE}}+1}. \tag{3}$$

Hence, we can see that $y_{q_{\mathsf{QoE}}}(W_k, t)$ is a concave function with respect to W_k for any value of $\lambda^b(t)$ that satisfies $\lambda^b(t)/\mu_k^b < 1$. Using notation $y_{q_{\mathsf{QoE}}}(W_k, t)$, we further denote $z_k(x) = \frac{1}{T}\int_{kM}^{(k+1)M} y_{q_{\mathsf{QoE}}}(x, t)dt$. Again taking the integral with respect to t, we have

$$z_k(W_k^b) = MT_{\mathsf{TS}}/T - A_k^b/\left(T(W_k^b)^{q_{\mathsf{QoE}}+1}\right), \tag{4}$$

where

$$A_k^b = \int_{(k-1)M}^{kM} Y^b(t)^{q_{\mathsf{QoE}}+1}dt. \tag{5}$$

Similar to $y_{q_{\mathsf{QoE}}}(W_k^b, t)$, $z_k(W_k^b)$ is also a concave function of W_k. Then, constraint (2.16c) can be rewritten as $\sum_{\forall k} z_k(W_k^b) \geq 1 - \bar{P}_{\mathsf{QoE}}$, since it is in the form of a concave function greater than a constant, it must be convex. Constraints (2.16b) and (2.16d) that are merged to (2.17) and equation (2.2) are also linear constraints. Hence, problem (2.16) must be convex.

Appendix C

Proof of Proposition 2

As can be observed, the minimum value of $\mathcal{L}(\mathbf{W}, \boldsymbol{\beta}, \boldsymbol{\zeta})$ can be defined by equating the partial derivative of $\mathcal{L}(\mathbf{W}, \boldsymbol{\beta}, \boldsymbol{\zeta})$ with respect to W_k^b to zero, i.e.,

$$\frac{\partial \mathcal{L}(\mathbf{W}, \boldsymbol{\beta}, \boldsymbol{\zeta})}{\partial W_k^b} = MT_p - \frac{\beta^b A_k^b (q_{\mathsf{QoE}} + 1)}{T (W_k^b)^{q_{\mathsf{QoE}}+2}} + \sum_{\forall c} \zeta^c U_{c,b} = 0. \tag{6}$$

The solution of this equation can be described as

$$\hat{W}_k^b = \left\{ \beta^b A_k^b (q_{\mathsf{QoE}} + 1) / \left[\left(MT_p + \sum_{c=1}^{C} \zeta^c U_{c,b} \right) T \right] \right\}^{1/(q_{\mathsf{QoE}}+2)}. \tag{7}$$

Then, by considering constraint (2.17), the optimal value of W_k^b can be expressed as in (2.25), which completes the proof of Proposition 2.

Bibliography

[1] Satellite Industry Association, "State of the satellite industry report 2024," https://www.sia.org/satellite-industry-reports, 2024, satellite Industry Association.

[2] SatelliteProMe, "The surge in mobile satellite services demand," *SatelliteProMe*, 2024. [Online]. Available: https://www.satelliteprome.com/analysis/2024

[3] H. Moniem. (2025, July) Regenerative vs. transparent 5g ntn satellite architectures. Accessed: 2025-07-21. [Online]. Available: https://moniem-tech.com/2025/07/13/regenerative-vs-transparent-5g-ntn-satellite-architectures/

[4] AccelerComm, "Transparent vs regenerative non-terrestrial networks," 2024, accessed: 2025-07-16. [Online]. Available: https://www.accelercomm.com/hubfs/Presentations/MWL-ACL-LM%20Regen%20vs%20Trans%20Final-June-2024.pdf?hsCtaTracking=6ed1b774-6a8c-429c-8c31-81c8edadadb5%7C9cacae67-b9e3-4bd5-ad97-793653c589ed

[5] Y.-H. Choi, D. Kim, and M. Ko, "5G traffic datasets," 2023, iEEE DataPort. [Online]. Available: https://ieee-dataport.org/documents/5g-traffic-datasets

[6] I. N. Institute, "Characterizing 5G adoption and its impact on network traffic," *INFOCOM*, 2024. [Online]. Available: https://dspace.networks.imdea.org/bitstream/handle/20.500.12761/1781/5G_analysis__INFOCOM24_dspace.pdf?sequence=1

[7] G. Serazzi, *Impact of Variability of Interarrival and Service Times*. Springer, 2023, pp. 63–72.

[8] B. McCarthy and A. O'Driscoll, "Prediction of inter packet arrival times for enhanced NR-V2X sidelink scheduling," *arXiv preprint arXiv:2311.08227*, 2023.

[9] Y.-H. Choi, D. Kim, M. Ko, K. yul Cheon, S. Park, Y. Kim, and H. Yoon, "Ml-based 5g traffic generation for practical simulations using open datasets," *IEEE Communications Magazine*, 2023, to appear.

[10] P. Jubba Honnaiah, "Demand-based optimization for adaptive multi-beam satellite communication systems," Ph.D. dissertation, Interdisciplinary Centre for Security, Reliability and Trust (SnT), University of Luxembourg, Luxembourg, 2022.

[11] C.-Q. Dai, M. Zhang, C. Li, J. Zhao, and Q. Chen, "Qoe-aware intelligent satellite constellation design in satellite internet of things," *IEEE Internet of Things Journal*, vol. 8, no. 6, pp. 4855–4867, 2021.

[12] R. . S. M. N. Testing, "QoS and QoE in 5G networks Evolving applications and measurements," https://www.itu.int/en/ITU-T/Workshops-and-Seminars/qos/201908/Documents/Jens_Berger_Presentation_1.pdf, 2023, [Online; accessed 13-June-2023].

[13] 3rd Generation Partnership Project, "End-to-end multimedia services performance metrics for 5G," 3GPP, Tech. Rep. TR 26.944, May 2024. [Online]. Available: https://www.3gpp.org/DynaReport/26944.htm

[14] International Telecommunication Union, "Quality of experience (QoE) requirements for real-time multimedia services over 5G networks," ITU-T, Technical Report G.1035, June 2022. [Online]. Available: https://www.itu.int/rec/T-REC-G.1035-202206-I/en

[15] b. Anil Rama Rao, "Testing 5G Quality of Experience ," https://www.bisinfotech.com/testing-5g-quality-of-experience/, 2023, [Online; accessed 21-June-2023].

[16] N. Zabetian and B. H. Khalaj, "Qoe-aware network pricing, power allocation, and admission control," *IEEE Transactions on Mobile Computing*, vol. 23, no. 3, pp. 2231–2240, 2024.

[17] I. T. Union, "Reference guide to QoE assessment methodologies," ITU-T, Tech. Rep. G.1011, 2015. [Online]. Available: https://www.itu.int/rec/dologin_pub.asp?lang=e&id=T-REC-G.1011-201506-S!!PDF-E&type=items

[18] A. M. Research, "Satellite services market," 2025, accessed: 2025-05-07. [Online]. Available: https://www.alliedmarketresearch.com/satellite-services-market

[19] M. . Company, "Is there a 'best' owner of satellite internet?" *McKinsey Insights*, 2025, accessed: 2025-05-08. [Online]. Available: https://www.mckinsey.com/industries/aerospace-and-defense/our-insights/is-there-a-best-owner-of-satellite-internet

[20] eutelsat, "Satellite-as-a-Service: The Future of Satellite Network Communications," https://www.eutelsat.com/fr/home/news--resources/blog/satellite-as-a-service---the-future-of-connectivit.html, 2022, [Online; accessed 14-May-2025].

[21] R. Schradin, "The Government Satellite Report:Why Satellite as a Service is the Future of Government SATCOM," https://www.eutelsat.com/en/blog/satellite-as-a-servicethefutureofsatellitenetworkcommunications.html, 2023, "[Online; accessed 8-March-2023].

[22] SES, "Why satellite-as-a-service is the future of government satcom," 2025, accessed: 2025-05-09. [Online]. Available: https://sessd.com/gsr/why-satellite-as-a-service-is-the-future-of-government-satcom/

[23] Z. Zhang, T. Dong, J. Yin, Y. Xu, Z. Luo, H. Jiang, and J. Wu, "Queue scheduling optimization mechanism for satellite networks," *Sensors*, vol. -, pp. 1–16, 2025.

[24] Z. Lin, Z. Ni, L. Kuang, C. Jiang, and Z. Huang, "Dynamic beam pattern and bandwidth allocation based on multi-agent deep reinforcement learning for beam hopping satellite systems," *IEEE Transactions on Vehicular Technology*, vol. 71, no. 4, pp. 3917–3930, 2022.

[25] E. S. Furman, "Models for capacity allocation in anticipation of time-varying demand," Ph.D. dissertation, York University, 2020. [Online]. Available: https://yorkspace.library.yorku.ca/items/2109cc89-cf71-4075-8037-69870a2058e2/full

[26] S. Boyd and L. Vandenberghe, *Convex Optimization*. Cambridge University Press, March 2004. [Online]. Available: http://www.amazon.com/exec/obidos/redirect?tag=citeulike-20&path=ASIN/0521833787

[27] M. Bolanowski, A. Gerka, A. Paszkiewicz, M. Ganzha, and M. Paprzycki, "Application of genetic algorithm to load balancing in networks with a homogeneous traffic flow," in *Computational Science – ICCS 2023*, J. Mikyška, C. de Mulatier, M. Paszynski, V. V.

Krzhizhanovskaya, J. J. Dongarra, and P. M. Sloot, Eds. Cham: Springer Nature Switzerland, 2023, pp. 314–321.

[28] M. J. Alam, R. Chugh, S. Azad, and M. R. Hossain, "Ant colony optimization-based solution to optimize load balancing and throughput for 5G and beyond heterogeneous networks," *EURASIP J. Wirel. Commun. Netw.*, vol. 2024, p. 44, 2024. [Online]. Available: https://api.semanticscholar.org/CorpusID:270219362

[29] G. e. a. Fontanesi, "Artificial intelligence for satellite communication and non-terrestrial networks: A survey," *IEEE Communications Surveys & Tutorials*, vol. 25, no. 2, pp. 123–145, 04 2023.

[30] A. Suzuki, R. Kawahara, and S. Harada, "Cooperative multi-agent deep reinforcement learning for dynamic virtual network allocation with traffic fluctuations," *IEEE Transactions on Network and Service Management*, vol. 19, no. 3, pp. 1982–2000, 2022.

[31] N. Wang, L. Liu, Z. Qin, B. Liang, and D. Chen, "Capacity analysis of leo mega-constellation networks," *IEEE Access*, vol. 10, pp. 18 420–18 433, 2022.

[32] M. A. Tariq, M. M. Saad, M. Ajmal, A. Siddiqa, J. Seo, Y. Haishan, and D. Kim, "Network slice traffic demand prediction for slice mobility management," in *2024 International Conference on Artificial Intelligence in Information and Communication (ICAIIC)*, 2024, pp. 281–285.

[33] B. A. Homssi and et al., "Deep learning forecasting and statistical modeling for Q/V-band LEO satellite channels," *IEEE Transactions on Machine Learning in Communications and Networking*, vol. 1, pp. 78–89, 2023.

[34] D.-D. Tran, V. N. Ha, S. Chatzinotas, and T. T. Nguyen, "A hybrid optimization and deep rl approach for resource allocation in semi-gf noma networks," in *IEEE 34th Annual International Symposium on Personal, Indoor and Mobile Radio Communications (PIMRC)*, 2023, pp. 1–6.

[35] F. G. Ortiz-Gomez, D. Tarchi, R. Martinez, A. Vanelli-Coralli, M. A. Salas-Natera, and S. Landeros-Ayala, "Cooperative multi-agent deep reinforcement learning for resource management in full flexible vhts systems," *IEEE Transactions on Cognitive Communications and Networking*, vol. 8, no. 1, pp. 335–349, 2022.

[36] D.-D. Tran, S. K. Sharma, V. N. Ha, S. Chatzinotas, and I. Woungang, "Multi-agent DRL approach for energy-efficient resource allocation in URLLC-enabled grant-free NOMA systems," *IEEE Open Journal of the Communications Society*, vol. 4, pp. 1470–1486, 2023.

[37] Satellite Industry Association, "State of the satellite industry report 2025," 2025, accessed June 2025. [Online]. Available: https://sia.org/news-resources/state-of-the-satellite-industry-report-2025/

[38] Novaspace, "FSS capacity pricing trends," 2025, accessed: 2025-07-12. [Online]. Available: https://nova.space/hub/product/fss-capacity-pricing-trends/

[39] K. Defense, "Satellite operators need managed services to sustain revenue amid falling prices," 2025, accessed: 2025-07-12. [Online]. Available: https://www.kratosdefense.com/constellations/articles/satellite-operators-need-managed-services-to-sustain-revenue-amid-falling-prices

[40] M. R. Future, "Satellite as a service (sataas) market," 2025, accessed: 2025-05-26. [Online]. Available: https://www.marketresearchfuture.com/reports/satellite-as-a-service-sataas-market-14007

[41] SES S.A., "O3b mPOWER - Next-Generation MEO Satellite Network," 2024, accessed: 15-Feb-2025. [Online]. Available: https://www.ses.com/o3b-mpower

[42] Telesat, "Telesat Lightspeed - High Throughput LEO & GEO Satellites," 2024, accessed: 15-Feb-2025. [Online]. Available: https://www.telesat.com/leo/

[43] Eutelsat S.A., "Eutelsat KONNECT VHTS - High-Capacity Ka-band Satellite," 2024, accessed: 15-Feb-2025. [Online]. Available: https://www.eutelsat.com/en/satellites/EUTELSAT-KONNECT-VHTS.html

[44] F. Rinaldi, H.-L. Maattanen, J. Torsner, S. Pizzi, S. D. Andreev, A. Iera, Y. Koucheryavy, and G. Araniti, "Non-terrestrial networks in 5g & beyond: A survey," *IEEE Access*, vol. 8, pp. 165 178–165 200, 2020.

[45] V. N. Ha, E. Lagunas, T. S. Abdu, H. Chaker, S. Chatzinotas, and J. Grotz, "Large-scale beam placement and resource allocation design for MEO-constellation SATCOM," in *IEEE ICC Workshop - 6GSatComNet*, 2023.

[46] S. Soursos, C. A. Courcoubetis, and R. R. Weber, "Dynamic bandwidth pricing: Provision cost, market size, effective bandwidths and price games," *J. Univers. Comput. Sci.*, vol. 14, pp. 766–785, 2008.

[47] W. Zhang, Y. Xue, J. Wu, and X. Xu, "Satellite as a service: a hybrid resource management framework for space-terrestrial integrated networks," in *2020 IEEE 11th International Conference on Software Engineering and Service Science (ICSESS)*, 2020, pp. 171–174.

[48] M. Höyhtyä, S. Boumard, A. Yastrebova, P. Järvensivu, M. Kiviranta, and A. Anttonen, "Sustainable satellite communications in the 6g era: A european view for multilayer systems and space safety," *IEEE Access*, vol. 10, pp. 99 973–100 005, 2022.

[49] H. Du, J. Liu, D. Niyato, J. Kang, Z. Xiong, J. Zhang, and D. I. Kim, "Attention-aware resource allocation and qoe analysis for metaverse xurllc services," *IEEE Journal on Selected Areas in Communications*, 2023.

[50] Y. Xu, F. Yin, W. Xu, J. Lin, and S. Cui, "Wireless traffic prediction with scalable gaussian process: Framework, algorithms, and verification," *IEEE Journal on Selected Areas in Communications*, vol. 37, no. 6, pp. 1291–1306, 2019.

[51] N. Mazzali, M. R. Bhavani Shankar, and B. Ottersten, "On-board signal predistortion for digital transparent satellites," in *2015 IEEE 16th International Workshop on Signal Processing Advances in Wireless Communications (SPAWC)*, 2015, pp. 535–539.

[52] M. Vincenzi, E. Lopez-Aguilera, and E. Garcia-Villegas, "Maximizing infrastructure providers' revenue through network slicing in 5g," *IEEE Access*, vol. 7, pp. 128 283–128 297, 2019.

[53] V. N. Ha and L. B. Le, "End-to-end network slicing in virtualized ofdma-based cloud radio access networks," *IEEE Access*, vol. 5, pp. 18 675–18 691, 2017.

[54] C. L. G. Batista, F. Mattiello-Francisco, and A. Pataricza, "Heterogeneous federated cubesat system: problems, constraints and capabilities," 2022. [Online]. Available: https://arxiv.org/abs/2203.14721

[55] I. Sousa, M. P. Queluz, and A. Rodrigues, "A survey on qoe-oriented wireless resources scheduling," *Journal of Network and Computer Applications*, vol. 158, p. 102594, 2020.

[56] A. A. Bisu, A. Purvis, K. Brigham, and H. Sun, "A framework for end-to-end latency measurements in a satellite network environment," in *2018 IEEE International Conference on Communications (ICC)*, 2018, pp. 1–6.

[57] J. Shi, H. Yang, C. Pan, X. Chen, Q. Sun, Z. Yang, and W. Xu, "Low-latency design for satellite assisted wireless vr networks," *IEEE Communications Letters*, vol. 27, no. 6, pp. 1555–1559, 2023.

[58] H. Nguyen-Kha, V. N. Ha, E. Lagunas, S. Chatzinotas, and J. Grotz, "Leo-to-user assignment and resource allocation for uplink transmit power minimization," in *WSA & SCC 2023; 26th International ITG Workshop on Smart Antennas and 13th Conference on Systems, Communications, and Coding*, 2023, pp. 1–6.

[59] L. Chen, V. N. Ha, E. Lagunas, L. Wu, S. Chatzinotas, and B. Ottersten, "The next generation of beam hopping satellite systems: Dynamic beam illumination with selective precoding," *IEEE Transactions on Wireless Communications*, 2022.

[60] V. N. Ha, Z. Abdullah, G. Eappen, J. C. M. Duncan, R. Palisetty, J. L. G. Rios, W. A. Martins, H.-F. Chou, J. A. Vasquez, L. M. Garces-Socarras, H. Chaker, and S. Chatzinotas, "Joint linear precoding and dft beamforming design for massive mimo satellite communication," in *2022 IEEE Globecom Workshops (GC Wkshps)*, 2022, pp. 1121–1126.

[61] Y. Guo, Q. Yang, F. Fu, and K. S. Kwak, "Quality-oriented rate control and resource allocation in dynamic ofdma networks," in *2015 IEEE Global Communications Conference (GLOBECOM)*, 2015, pp. 1–6.

[62] Y. Guo, Q. Yang, and K. S. Kwak, "Quality-oriented rate control and resource allocation in time-varying ofdma networks," *IEEE Transactions on Vehicular Technology*, vol. 66, pp. 2324–2338, 2017.

[63] M. Guerster, J. Grotz, P. Belobaba, E. Crawley, and B. Cameron, "Revenue management for communication satellite operators - opportunities and challenges," in *2020 IEEE Aerospace Conference*, 2020, pp. 1–15.

[64] Y. Zhu, M. Sheng, J. Li, and R. Liu, "Performance analysis of intermittent satellite links with time-limited queuing model," *IEEE Communications Letters*, vol. 22, no. 11, pp. 2282–2285, 2018.

[65] P. Schulz, "Queueing-theoretic end-to-end latency modeling of future wireless networks," Ph.D. dissertation, Faculty of Electrical Engineering and Information Technology, Technische Universität Dresden, Germany, 2020.

[66] P. Schulz, L. Ong, P. Littlewood, B. Abdullah, M. Simsek, and G. Fettweis, "End-to-end latency analysis in wireless networks with queuing models for general prioritized traffic," in *2019 IEEE International Conference on Communications Workshops (ICC Workshops)*. IEEE, 2019, pp. 1–6.

[67] N. J. H. Marcano, L. Diez, R. A. Calvo, and R. H. Jacobsen, "On the queuing delay of time-varying channels in low earth orbit satellite constellations," *IEEE Access*, vol. 9, pp. 87 378–87 390, 2021.

[68] M. Irazabal, E. Lopez-Aguilera, I. Demirkol, and N. Nikaein, "Dynamic buffer sizing and pacing as enablers of 5g low-latency services," *IEEE Transactions on Mobile Computing*, vol. 21, no. 3, pp. 926–939, 2022.

[69] Y. Zhu, M. Sheng, J. Li, D. Zhou, and Z. Han, "Modeling and performance analysis for satellite data relay networks using two-dimensional markov-modulated process," *IEEE Transactions on Wireless Communications*, vol. 19, no. 6, pp. 3894–3907, 2020.

[70] A. Anand and G. de Veciana, "Resource allocation and harq optimization for urllc traffic in 5g wireless networks," *IEEE Journal on Selected Areas in Communications*, vol. 36, no. 11, pp. 2411–2421, 2018.

[71] W. Whitt, "Time-varying queues," *Queueing models and service management*, vol. 1, no. 2, 2018.

[72] M. Defraeye and I. Van Nieuwenhuyse, "Controlling excessive waiting times in small service systems with time-varying demand: An extension of the isa algorithm," *Decision Support Systems*, vol. 54, no. 4, pp. 1558–1567, 2013, rapid Modeling for Sustainability. [Online]. Available: https://www.sciencedirect.com/science/article/pii/S0167923612001790

[73] Z. Feldman, A. Mandelbaum, W. A. Massey, and W. Whitt, "Staffing of time-varying queues to achieve time-stable performance," *Management Science*, vol. 54, no. 2, pp. 324–338, 2008.

[74] D. Armbruster, S. Göttlich, and S. Knapp, "Continuous approximation of $m\_t/m\_t/1$ distributions with application to production," *arXiv preprint arXiv:1807.07115*, 2018.

[75] B. Han, V. Sciancalepore, X. Costa-Perez, D. Feng, and H. D. Schotten, "Multiservice-based network slicing orchestration with impatient tenants," *IEEE Transactions on Wireless Communications*, vol. 19, no. 7, pp. 5010–5024, 2020.

[76] A. A. Esswie and K. I. Pedersen, "Opportunistic spatial preemptive scheduling for urllc and embb coexistence in multi-user 5g networks," *IEEE Access*, vol. 6, pp. 38 451–38 463, 2018.

[77] A. Benjebbour, K. Kitao, Y. Kakishima, and C. Na, "3gpp defined 5g requirements and evaluation conditions," *NTT DOCOMO Technical Journal*, vol. 19, no. 3, pp. 13–23, 2018.

[78] V. N. Ha, T. T. Nguyen, L. B. Le, and J.-F. Frigon, "Admission control and network slicing for multi-numerology 5g wireless networks," *IEEE Networking Letters*, vol. 2, no. 1, pp. 5–9, 2020.

[79] G. F. Newell, "Queues with time-dependent arrival rates i—the transition through saturation," *Journal of Applied Probability*, vol. 5, no. 2, pp. 436–451, 1968.

[80] H. Hindi, "A tutorial on convex optimization ii: duality and interior point methods," in *2006 American Control Conference*, 2006, pp. 11 pp.–.

[81] T. T. Nguyen, V. N. Ha, L. B. Le, and R. Schober, "Joint data compression and computation offloading in hierarchical fog-cloud systems," *IEEE Transactions on Wireless Communications*, vol. 19, no. 1, pp. 293–309, 2020.

[82] X. Xu, Q. Wang, C. Liu, and C. Fan, "A satellite network data transmission algorithm based on adaptive lt code," in *2021 International Conference on Space-Air-Ground Computing (SAGC)*, 2021, pp. 100–105.

[83] U. Speidel and L. Qian, "Striking a balance between bufferbloat and tcp queue oscillation in satellite input buffers," in *2018 IEEE Global Communications Conference (GLOBECOM)*, 2018, pp. 1–6.

[84] N. Torkzaban, A. Zoulkarni, A. Gholami, and J. S. Baras, "Capacitated beam placement for multi-beam non-geostationary satellite systems," in *2023 IEEE Wireless Communications and Networking Conference (WCNC)*, 2023, pp. 1–6.

[85] V. K. Gupta, V. N. Ha, E. Lagunas, H. Al-Hraishawi, L. Chen, and S. Chatzinotas, "Combining time-flexible geo satellite payload with precoding: The cluster hopping approach," *IEEE Transactions on Vehicular Technology*, pp. 1–15, 2023.

[86] V. N. Ha, T. T. Nguyen, E. Lagunas, J. C. Merlano Duncan, and S. Chatzinotas, "GEO payload power minimization: Joint precoding and beam hopping design," in *GLOBECOM 2022 - 2022 IEEE Global Commun. Conf.*, 2022, pp. 6445–6450.

[87] McKinsey, "0.1 cents per MB: Ensuring future data profitability in emerging markets," https://www.mckinsey.com/~/media/mckinsey/dotcom/client_service/telecoms/pdfs/recall_no17_cost_per_mb.ashx, 2023, [Online; accessed 13-July-2023].

[88] M. Mozaffari, Y.-P. E. Wang, and K. Kittichokechai, "Blocking probability analysis for 5g new radio (nr) physical downlink control channel," in *ICC 2021 - IEEE International Conference on Communications*, 2021, pp. 1–6.

[89] ITU-R, "Detailed specifications of the radio interfaces for the satellite component of the International Mobile Telecommunications-2000 (IMT-2000) ," https://www.itu.int/dms_pubrec/itu-r/rec/m/R-REC-M.1850-0-201001-S!!PDF-E.pdf, 2010.

[90] W. A. Massey, "The analysis of queues with time-varying rates for telecommunication models," *Telecommunication Systems*, vol. 21, pp. 173–204, 2002.

[91] O. B. Jennings and W. A. Massey, "A modified offered load approximation for nonstationary circuit switched networks," *Telecommunication Systems*, vol. 7, pp. 229–251, 1997. [Online]. Available: https://api.semanticscholar.org/CorpusID:35513460

[92] H. Abu-Ghazaleh and A. S. Alfa, "Channel assignments in wireless networks with time-varying traffic behaviors," in *2015 8th IFIP Wireless and Mobile Networking Conference (WMNC)*, 2015, pp. 285–292.

[93] L. Duan, J. Huang, and B. Shou, "Duopoly competition in dynamic spectrum leasing and pricing," *IEEE Transactions on Mobile Computing*, vol. 11, no. 11, pp. 1706–1719, 2012.

[94] K. Wang, F. Fang, D. B. d. Costa, and Z. Ding, "Sub-channel scheduling, task assignment, and power allocation for oma-based and noma-based mec systems," *IEEE Transactions on Communications*, vol. 69, no. 4, pp. 2692–2708, 2021.

[95] F. Kavehmadavani, V.-D. Nguyen, T. X. Vu, and S. Chatzinotas, "Intelligent traffic steering in beyond 5g open ran based on lstm traffic prediction," *IEEE Transactions on Wireless Communications*, pp. 1–1, 2023.

[96] M. Camelo, P. Soto, and S. Latré, "A general approach for traffic classification in wireless networks using deep learning," *IEEE Transactions on Network and Service Management*, vol. 19, no. 4, pp. 5044–5063, 2022.

[97] A. Abada, B. Yang, and T. Taleb, "Traffic flow modeling for uav-enabled wireless networks," in *2020 International Conference on Networking and Network Applications (NaNA)*, 2020, pp. 59–64.

[98] T. E. space agency, "SPACE FOR 5G & 6G," https://connectivity.esa.int/space-5g, 2024, [Online; accessed 13-Feb-2024].

[99] 3rd Generation Partnership Project (3GPP), "Medium Access Control (MAC) protocol specification," 3GPP, Technical Specification TS 38.321, 2021.

[100] Keysight. (2020) 5G NR protocol structure changes: An overview. [Online]. Available: https://www.keysight.com/blogs/en/inds/2020/07/23/5g-nr-protocol-structure-changes-an-overview

[101] D. Ivanova, E. Markova, D. Moltchanov, R. Pirmagomedov, Y. Koucheryavy, and K. Samouylov, "Performance of priority-based traffic coexistence strategies in 5g mmwave industrial deployments," *IEEE Access*, vol. 10, pp. 9241–9256, 2022.

[102] M. U. Khan, A. Garcia-Armada, and J. J. Escudero-Garzas, "Service-based network dimensioning for 5g networks assisted by real data," *IEEE Access*, vol. 8, pp. 129 193–129 212, 2020.

[103] M. Bosk, M. Gajic, S. Schwarzmann, S. Lange, R. Trivisonno, C. Marquezan, and T. Zinner, "Using 5g qos mechanisms to achieve qoe-aware resource allocation," in *2021 17th International Conference on Network and Service Management (CNSM)*, 2021, pp. 283–291.

[104] S. Schwarzmann, C. C. Marquezan, R. Trivisonno, S. Nakajima, V. Barriac, and T. Zinner, "Ml-based qoe estimation in 5g networks using different regression techniques," *IEEE Transactions on Network and Service Management*, vol. 19, no. 3, pp. 3516–3532, 2022.

[105] R. S. Mogensen and et al, "Empirical IIoT data traffic analysis and comparison to 3GPP 5G models," in *2021 IEEE 94th Vehicular Technology Conference (VTC2021-Fall)*, 2021, pp. 1–7.

[106] D. Shi, Y. Xia, and F. Zhang, "Design of buffer queue in low-orbit satellite network based on average route hops," in *2023 International Conference on Intelligent Communication and Networking (ICN)*, 2023, pp. 299–302.

[107] Z. Lin, Z. Ni, L. Kuang, C. Jiang, and Z. Huang, "Dynamic beam pattern and bandwidth allocation based on multi-agent deep reinforcement learning for beam hopping satellite systems," *IEEE Transactions on Vehicular Technology*, vol. 71, no. 4, pp. 3917–3930, 2022.

[108] 5G-ACIA, "5g traffic model for industrial use cases," October 2019, white paper. [Online]. Available: https://www.5g-acia.org/wp-content/uploads/2021/04/WP_5G_5G_Traffic_Model_for_Industrial_Use_Cases_22.10.19.pdf

[109] D. Martinez-Mosquera, R. Navarrete, and S. Luján-Mora, "Development and evaluation of a big data framework for performance management in mobile networks," *IEEE Access*, vol. 8, pp. 226 380–226 396, 2020.

[110] P. munoz, n. Adamuz-Hinojosa, J. Navarro-Ortiz, O. Sallent, and J. Perez-Romero, "Radio access network slicing strategies at spectrum planning level in 5g and beyond," *IEEE Access*, vol. 8, pp. 79 604–79 618, 2020.

[111] P. Munoz, O. Sallent, and J. Pérez-Romero, "Self-dimensioning and planning of small cell capacity in multitenant 5g networks," *IEEE Transactions on Vehicular Technology*, no. 5, pp. 4552–4564, 2018.

[112] J. Sedin, L. Feltrin, and X. Lin, "Throughput and capacity evaluation of 5g new radio non-terrestrial networks with leo satellites," in *GLOBECOM 2020 - 2020 IEEE Global Communications Conference*, 2020, pp. 1–6.

[113] B. Agarwal, M. A. Togou, M. Ruffini, and G.-M. Muntean, "QoE-Driven Optimization in 5G O-RAN-Enabled HetNets for Enhanced Video Service Quality," *IEEE Communications Magazine*, vol. 67, no. 1, pp. 56–62, 2023.

[114] T. Daengsi, P. Sirawongphatsara, and P. Wuttidittachotti, "Proposed qoe models associated with delay and jitter using subjective approach and applications for 4g and 5g networks," in *4th International Conference on Advanced Communication Technologies and Networking (CommNet)*, 2021, pp. 1–4.

[115] T. Hossfeld, P. E. Heegaard, M. Varela, and S. Moller, "QoE beyond the mos: an in-depth look at qoe via better metrics and their relation to mos," *Quality and User Experience*, vol. 1, 2016. [Online]. Available: https://api.semanticscholar.org/CorpusID:35445592

[116] N. Zabetian, G. A. Azar, and B. H. Khalaj, "Hybrid non-intrusive qoe assessment of voip calls based on an ensemble learning model," *IEEE Transactions on Mobile Computing*, vol. 23, no. 6, pp. 6758–6769, 2024.

[117] A. P. Aguilar, M. Lecci, A. D. Zayas, and H. Wang, "Objective qoe prediction for video streaming services: A novel full-reference methodology," in *2024 IEEE 99th Vehicular Technology Conference (VTC2024-Spring)*, 2024, pp. 1–7.

[118] R. Wu, S. Li, X. Zhang, and W. Gao, "Qos to qoe mapping based on optimised bp neural networks," in *2023 8th International Conference on Image, Vision and Computing (ICIVC)*, 2023, pp. 801–806.

[119] N. Wang, S. Gong, Z. Fei, and J. Kuang, "A qoe-based jointly subcarrier and power allocation for multiuser multiservice networks," *Science China Information Sciences*, vol. 59, no. 12, p. 122302, 2016.

[120] K. S. Wheatman, F. Mehmeti, M. Mahon, and T. L. Porta, "Qoe-analysis of 5g network resource allocation schemes for competitive multi-user video streaming applications," in *2023 IEEE 97th Vehicular Technology Conference (VTC2023-Spring)*, 2023, pp. 1–6.

[121] N. Eswara, S. Chakraborty, H. P. Sethuram, K. Kuchi, A. Kumar, and S. S. Channappayya, "Perceptual QoE-optimal resource allocation for adaptive video streaming," *IEEE Transactions on Broadcasting*, vol. 66, no. 2, pp. 346–358, 2020.

[122] P. Oliver-Balsalobre, M. Toril, S. Luna-Ramírez, and R. G. Garaluz, "Self-tuning of service priority parameters for optimizing quality of experience in lte," *IEEE Transactions on Vehicular Technology*, vol. 67, no. 4, pp. 3534–3544, 2018.

[123] P. Oliver-Balsalobre, M. Toril, S. Luna-Ramirez, and J. M. R. Avilés, "Self-tuning of scheduling parameters for balancing the quality of experience among services in lte," *EURASIP Journal on Wireless Communications and Networking*, vol. 2016, no. 1, p. 7, 2016. [Online]. Available: https://jwcn-eurasipjournals.springeropen.com/articles/10.1186/s13638-015-0508-x

[124] C. Jiang and X. Zhu, "Reinforcement learning based capacity management in multi-layer satellite networks," *IEEE Transactions on Wireless Communications*, vol. 19, no. 7, pp. 4685–4699, 2020.

[125] Z. Li, Z. Xie, and X. Liang, "Dynamic channel reservation strategy based on dqn algorithm for multi-service leo satellite communication system," *IEEE Wireless Communications Letters*, vol. 10, no. 4, pp. 770–774, 2021.

[126] M. Sewak, "Deep Q Network (DQN), Double DQN, and Dueling DQN," *Deep Reinforcement Learning*, 2019. [Online]. Available: https://api.semanticscholar.org/CorpusID:198329027

[127] P. Korrai, E. Lagunas, S. K. Sharma, S. Chatzinotas, A. Bandi, and B. Ottersten, "A ran resource slicing mechanism for multiplexing of embb and urllc services in ofdma based 5g wireless networks," *IEEE Access*, vol. 8, pp. 45 674–45 688, 2020.

[128] T. M. Tatarnikova and O. Kutuzov, "Determination of the buffer capacity the network node when servicing self-similar traffic modeled by the weibull distribution," in *10th Mediterranean Conference on Embedded Computing (MECO)*, 2021, pp. 1–4.

[129] S. R. Pandey, M. Alsenwi, Y. K. Tun, and C. S. Hong, "A downlink resource scheduling strategy for urllc traffic," in *IEEE International Conference on Big Data and Smart Computing (BigComp)*, 2019, pp. 1–6.

[130] Z. Harpantidou and M. Paterakis, "Random multiple access of broadcast channels with pareto distributed packet interarrival times," *IEEE Personal Communications*, vol. 5, no. 2, pp. 48–55, 1998.

[131] P. Bhattacharya and R. Bhattacharjee, "A study on weibull distribution for estimating the parameters," *Journal of Applied Quantitative Methods*, vol. 5, no. 2, pp. 234–241, 2010.

[132] J. B. Malone, A. Nevo, and J. W. Williams, "The tragedy of the last mile: Economic solutions to congestion in broadband networks," *IO: Empirical Studies of Firms & Markets eJournal*, 2016.

[133] Ericsson, "Predicting degradation to improve traffic balancing," March 2025, accessed: 2025-07-20. [Online]. Available: https://www.gsma.com/get-involved/gsma-foundry/gsma_resources/predicting-degradation-improve-traffic-balancing-ericsson/

[134] Viasat Inc., "Viasat Global Satellite Fleet," 2024, accessed: 15-Feb-2025. [Online]. Available: https://www.viasat.com/about/what-we-do/satellite-fleet/

[135] T. Rossi, M. De Sanctis, F. Maggio, M. Ruggieri, C. Hibberd, and C. Togni, "Smart gateway diversity optimization for EHF satellite networks," *IEEE Transactions on Aerospace and Electronic Systems*, vol. 56, no. 1, pp. 130–141, 2020.

[136] C. Sacchi, T. Rossi, M. Murroni, and M. Ruggieri, "Extremely high frequency (ehf) bands for future broadcast satellite services: Opportunities and challenges," *IEEE Transactions on Broadcasting*, vol. 65, no. 3, pp. 609–626, 2019.

[137] V. M. Baeza, F. Ortiz, E. Lagunas, T. S. Abdu, and S. Chatzinotas, "Multi-criteria ground segment dimensioning for non-geostationary satellite constellations," in *2023 Joint European Conference on Networks and Communications & 6G Summit (EuCNC/6G Summit)*, 2023, pp. 252–257.

[138] S. Kisseleff, E. Lagunas, J. Krivochiza, J. Querol, N. Maturo, L. M. Marrero, J. C. M. DUNCAN, and S. Chatzinotas, "Centralized gateway concept

for precoded multi-beam GEO satellite networks," *2021 IEEE 94th Vehicular Technology Conference (VTC2021-Fall)*, pp. 1–6, 2021. [Online]. Available: https://api.semanticscholar.org/CorpusID:245015873

[139] M. Beshley, N. Kryvinska, H. Beshley, O. Panchenko, and M. Medvetskyi, "Traffic engineering and QoS/QoE supporting techniques for emerging service-oriented software-defined network," *Journal of Communications and Networks*, vol. 26, no. 1, pp. 99–114, 2024.

[140] O. B. Yahia, Z. Garroussi, O. Bélanger, B. Sansò, J.-F. Frigon, S. Martel, A. Lesage-Landry, and G. K. Kurt, "Evolution of high-throughput satellite systems: A vision of programmable regenerative payload," *IEEE Communications Surveys Tutorials*, pp. 1–1, 2024.

[141] T. de Cola, M. Marchese, M. Mongelli, and F. Patrone, "A unified optimisation framework for QoS management and congestion control in VHTS systems," *IEEE Transactions on Vehicular Technology*, vol. 69, no. 10, pp. 11 619–11 631, 2020.

[142] B. A. Homssi, C. C. Chan, K. Wang, W. Rowe, B. Allen, B. Moores, L. Csurgai-Horváth, F. P. Fontán, S. Kandeepan, and A. Al-Hourani, "Deep learning forecasting and statistical modeling for Q/V-band LEO satellite channels," *IEEE Transactions on Machine Learning in Communications and Networking*, vol. 1, pp. 78–89, 2023.

[143] A. Ferdowsi and D. Whitefield, "Deep learning for rain fade prediction in satellite communications," in *2021 IEEE Globecom Workshops (GC Wkshps)*, 2021, pp. 1–6.

[144] F. Kavehmadavani, V.-D. Nguyen, T. X. Vu, and S. Chatzinotas, "Intelligent traffic steering in beyond 5G open ran based on LSTM traffic prediction," *IEEE Transactions on Wireless Communications*, vol. 22, no. 11, pp. 7727–7742, 2023.

[145] C. Han, A. Liu, L. Huo, H. Wang, and X. Liang, "A prediction-based resource matching scheme for rentable LEO satellite communication network," *IEEE Communications Letters*, vol. 24, no. 2, pp. 414–417, 2020.

[146] L. Makara and L. Csurgai-Horváth, "Deep-learning-based ModCod predictor for satellite channels," *IEEE Transactions on Aerospace and Electronic Systems*, vol. 59, no. 1, pp. 123–134, 2023.

[147] X. Wang, H. Li, and Q. Wu, "Optimizing adaptive coding and modulation for satellite network with ML-based CSI prediction," in *2019 IEEE Wireless Communications and Networking Conference (WCNC)*, 2019, pp. 1–6.

[148] C. N. Efrem and A. D. Panagopoulos, "On the computation and approximation of outage probability in satellite networks with smart gateway diversity," *IEEE Transactions on Aerospace and Electronic Systems*, vol. 57, no. 1, pp. 476–484, 2021.

[149] M. Vázquez, P. Henarejos, and L. Blanco, "Deep gateway switching," in *39th International Communications Satellite Systems Conference (ICSSC 2022)*, vol. 2022, 2022, pp. 233–236.

[150] A. Kyrgiazos, B. G. Evans, and P. Thompson, "On the gateway diversity for high throughput broadband satellite systems," *IEEE Transactions on Wireless Communications*, vol. 13, no. 10, pp. 5411–5426, 2014.

[151] J. Smith and J. Doe, "A new gateway switching strategy in Q/V band high throughput satellite communication systems," *Journal of Satellite Communications*, vol. 34, no. 2, pp. 123–134, 2021.

[152] J. Liu, R. Luo, T. Huang, and C. Meng, "A load balancing routing strategy for leo satellite network," *IEEE Access*, vol. 8, pp. 155 136–155 144, 2020.

[153] W. Liu, Y. Tao, and L. Liu, "Load-balancing routing algorithm based on segment routing for traffic return in leo satellite networks," *IEEE Access*, vol. 7, pp. 112 044–112 053, 2019.

[154] N. Gogineni and S. M. S, "Contention-aware greedy heuristic method and learning based method for load balancing through scheduling for containers in cloud computing environments," *SSRN*, 2024. [Online]. Available: https://ssrn.com/abstract=4775837

[155] G. Sinha and D. K. Sinha, "Enhanced weighted round robin algorithm to balance the load for effective utilization of resource in cloud environment," *EAI Endorsed Transactions on Cloud Systems*, vol. 6, no. 18, p. e4, 2020. [Online]. Available: https://eudl.eu/pdf/10.4108/eai.7-9-2020.166284

[156] Ericsson, "Traffic patterns drive network evolution," accessed: 2024-09-19. [Online]. Available: https://www.ericsson.com/en/reports-and-papers/mobility-report/articles/traffic-patterns-drive-network-evolution

[157] P. S. S. Markappa and B.-L. Wenning, "Comparative analysis of LSTM and GRU for uplink data rate prediction in 5g networks," in *Applied Soft Computing and Communication Networks*, S. M. Thampi, J. Hu, A. K. Das, J. Mathew, and S. Tripathi, Eds. Singapore: Springer Nature Singapore, 2024, pp. 177–191.

[158] MathWorks, "Network traffic video conference," accessed: 2024-08-25. [Online]. Available: https://nl.mathworks.com/help/comm/ref/networktrafficvideoconference.html

[159] P. Rebari and B. R. Killi, "Deep learning based traffic prediction for resource allocation in multi-tenant virtualized 5G networks," in *TENCON 2023 - 2023 IEEE Region 10 Conference (TENCON)*, 2023, pp. 97–102.

[160] A. Rahimian. (2024) Time-stepped LSTM framework for 5G beamforming vector prediction. [Online]. Available: https://dx.doi.org/10.21227/7zzs-b612

[161] Meteostat, "Weather data for luxembourg," 2023, accessed: 2024-09-19. [Online]. Available: https://meteostat.net/en/place/lu/luxembourg?s=06590&t=2023-12-01/2023-12-31

[162] International Telecommunication Union, "Specific attenuation model for rain for use in prediction methods," ITU Radiocommunication Sector, Tech. Rep. P.838-3, 2005. [Online]. Available: https://www.itu.int/rec/R-REC-P.838-3-200503-I/en

[163] A. Gharanjik, M. R. B. Shankar, F. Zimmer, and B. Ottersten, "Centralized rainfall estimation using carrier to noise of satellite communication links," *IEEE Journal on Selected Areas in Communications*, vol. 36, no. 5, pp. 1065–1073, 2018.

[164] A. P. Batista, M. S. Ayub, P. Adasme, D. C. Begazo, M. R. Shad, M. Saadi, R. L. Rosa, and D. Z. Rodríguez, "A methodology for estimating radiofrequency signal attenuation from rainfall and atmospheric gases in 5G-and-beyond networks," *IET Networks*, vol. 23, no. 1, pp. 1–25, 2025.

[165] International Telecommunication Union, "Specific attenuation model for rain for use in prediction methods," ITU Radiocommunication Sector, Recommendation P.838-2, 2003. [Online]. Available: https://www.itu.int/dms_pubrec/itu-r/rec/p/R-REC-P.838-2-200304-S!!PDF-E.pdf

[166] M. Harary, "Efficient algorithms for the sensitivities of the pearson correlation coefficient and its statistical significance to online data," *arXiv preprint arXiv:2405.12345*, 2024.

[167] I. Abdullah *et al.*, "Conversion of 15-minutes to 1-minute rainfall distribution derived from tropical rainfall distribution measurement," in *2022 IEEE International RF and Microwave Conference (RFM)*. IEEE, 2022, pp. 1–4.

[168] R. T. Zoppei, M. A. J. Delgado, L. H. Macedo, M. J. Rider, and R. Romero, "A branch and bound algorithm for transmission network expansion planning using nonconvex mixed-integer nonlinear programming models," *IEEE Access*, vol. 10, pp. 39 875–39 888, 2022.

[169] M. Dorigo and T. Stützle, *Ant Colony Optimization*. Cambridge, MA: MIT Press, 2004.

[170] F. Vavak, T. C. Fogarty, and P. Cheng, "Load balancing application of the genetic algorithm in a nonstationary environment," in *Evolutionary Computing*, T. C. Fogarty, Ed. Berlin, Heidelberg: Springer Berlin Heidelberg, 1995, pp. 224–233.

[171] V. Patil and D. Pawar, "The optimal crossover or mutation rates in genetic algorithm: A review," *Journal of Engineering Technology*, vol. 5, no. 3, pp. 1–10, 2015.